UNIVERSIDADE DE LISBOA
FACULDADE DE CIÊNCIAS
DEPARTAMENTO DE QUÍMICA E BIOQUÍMICA

Epithelial Differentiation: From Organoids to Cells in Cystic Fibrosis Patients

André Miguel Carapinha Gomes

Mestrado em Bioquímica
Especialização em Bioquímica Médica

Dissertação orientada por:
Professora Dr.ª Margarida D. Amaral
Dr.ª Iris Silva

2019

This page is intentionally left blank

Acknowledgements

First of all, I would like to thank my supervisors. Prof. Margarida Amaral, for giving me the opportunity of joining her lab and starting my career in science in a very demanding but rewarding work environment, where I learnt not just many techniques but also to think by myself and solve problems. Also, for the mentorship and the corrections for this thesis. And Iris Silva, for all the teachings and guidance throughout the year and the major help in putting this thesis together, as well as the corrections and suggestions to improve it.

Second, I would like to thank all my lab colleagues who helped, in any way, the conclusion of this thesis and to grow as a person and a scientist. In particular, Susana for patiently helping me with all my PCRs and dealing with my frustrations. But also, for all the helpful advice, for all the conversations and the good mood and laughter that always changed my mood for the best. Sofia Ramalho, for teaching me to work with the worst samples ever (yes you can still do it) and all the helpful conversations, the constant bickering and funny comebacks. Margarida Quaresma, for the "pro-level" WBs, for being a person that is always ready to teach, for all the fruitful scientific discussions that always made me think and for the amazing straightforward "no-nonsense" personality that always lead to hilarious conversations and even political fights. Madalena Pinto, who has a great knowledge of her work and the field, and can do anything except maybe infect organoids (that remains to be seen); I just hope I never get your tone. Filipa Simões, with whom I could always discuss my work and would always have great scientific advice and suggestions that would help get pass any obstacle and not be stressed. Aires Duarte, for all the pivot tables, macros and troubleshooting, and all the patience in explaining and helping me with my weakest subject; this thesis wouldn't be the same without your help. Sofia Correia, our "labinha" and the backbone of our lab; thanks for putting up with all the "Sofia where is this?" and "Sofia, where can I find that?". Arthur, you came near the end of this work but you helped a lot with my electrophysiology experiments, thank you for teaching me more about these techniques. Ines Pankonien, for all the suggestions and conversations. Luis e Daniel, thanks for the all the help and for introducing me to CS:GO; sorry Daniel for any pain I caused in the gym, but I'm glad I got a new gym buddy. Raquel Centeio, shame you weren't here longer but you helped during my first months in the lab; thanks for all the funny conversations. Violeta, for helping me with so many things during this year. And Prof. Margarida Ramos, for always being available to discuss and help me interpret my Ussing chamber experiments.

Last but not least, I want to thank my family and all my friends for being present and for supporting me through this journey that is now over. All your help and the conversation at all dinners and coffees will not be forgotten.

Summary

Cystic Fibrosis (CF) is the most common lethal recessive genetic disorder in the Caucasian population, affecting about 90,000 people worldwide. CF is caused by mutations in the *Cystic Fibrosis Transmembrane Conductance Regulator* (*CFTR*) gene which encodes a chloride (Cl^-) and bicarbonate (HCO_3^-) anion channel that is located in the apical side of epithelial cells. The lack of function of mutant CFTR leads to an impairment of anion transport and, consequently, of fluid secretion, resulting in a dysregulation of fluid homeostasis and osmolarity across several epithelia. This means that CF causes several symptoms that include chronic inflammation and infection of the airways, gastrointestinal tract perturbations, pancreatic insufficiency and infertility. It also affects tissue regeneration and epithelial differentiation, resulting in tracheal malformations, delayed wound healing, altered gland secretion and compromised barrier function of several epithelia. However, it is the airways disease, characterized by low height of the airway-surface liquid (ASL) and thick mucus that impairs mucociliary clearance leading to chronic inflammation and infections progressively deteriorating lung function, which remains the major cause of morbidity and mortality among individuals with CF.

Since the discovery of the *CFTR* gene, over 2,000 different mutations have been reported and most presumed to be CF-causing, so a classification system was created, consisting of seven classes (I-VII) into which CFTR mutations are grouped according to the molecular/cellular defect they elicit. This classification also evolved to assist in drug discovery. Indeed, since mutations in the same class share the same basic molecular defect, a common therapeutic strategy should rescue all mutations in the same class. In the past few years, small-molecule drugs were approved which (alone or combined) rescue mutant CFTR with specific mutations. The first, VX-770 (Ivacaftor), is used as a potentiator of the CFTR channel, and thus applies to individuals with CF who have gating or conductance mutations (classes III and IV). When in combination with a CFTR corrector, VX-809 (Lumacaftor) or VX-661 (Tezacaftor), that rescue the defective traffic of CFTR with the most prevalent CF-causing mutation (F508del), it applies to individuals with CF who are F508del-homozygous. However, individuals with CF who do not carry any of these mutations may still get clinical benefit from their administration. Moreover, there are also individuals with CF who have the mutations for which the drugs were designed but who do not benefit from them, probably due to other factors, such as modifier genes and environmental factors. Thus, a personalized medicine approach, termed theranostics (**thera**peutic diag**nostics**) is becoming an important approach to bring the right drugs to the individuals who can benefit from them. To this end, several *ex vivo* models have been used to assist in the laboratory testing of these drugs, including primary human nasal and bronchial epithelial (HNE/HBE) cells as well as intestinal crypts that are used to create 3D-intestinal organoids. More recently, another model was developed through the culturing of 2D-monolayers of intestinal epithelial cells derived from these 3D-organoids, hereby opening a vast array of possibilities for CFTR function assessment. Indeed, if shown to recapitulate *in vivo* CFTR function, these organoid-derived 2D-monolayers hold promise for replacing or complementing 3D-intestinal organoids and fresh biopsies. The latter in particular are used for CF diagnosis/prognosis but, in centres where immediate electrophysiological analysis of biopsies is not possible, to ship them to reference centres is impossible due to their short-term viability for electrophysiology (~6h). Nevertheless, fresh biopsies maintain their feasibility to generate 3D-organoids over a 24-h period and thus can be shipped to reference centres which

can then generate 3D- and 2D monolayers and analyze the latter in direct Ussing chamber measurements. Notwithstanding, because 2D-monolayers are a new model system, it is still poorly characterized as well as their usage in CF diagnosis/prognosis and in determining responsiveness to drugs.

The main goals of this MSc project were:

1) to characterize the novel 2D-intestinal cellular system by assessing:
    a. The expression levels of plasma membrane (PM) proteins and ion channels present in the native tissue which are essential for Cl^- secretion;
    b. The differentiation status and progress of the 2D-intestinal epithelial monolayers by differentiation and proliferation markers under differentiation and non- differentiation conditions.
2) to compare CFTR function in native tissues and primary cultures derived from individuals with CF and non-CF controls by:
    a. Ussing chamber measurements of CFTR-mediated Cl^- secretion in fresh rectal biopsies;
    b. Forskolin-induced swelling (FIS) assay of intestinal 3D-organoids derived from rectal biopsies;
    c. Ussing chamber measurements of 2D-intestinal monolayers.
3) To establish correlations between:
    a. Values obtained in 2a, 2b and 2c for the same individuals as well as with other CF biomarkers from these individuals, in order to assess if 2D-intestinal monolayers recapitulate the properties of the more established models in predicting disease severity so as to validate them as good personalized cell models for CFTR function and thus for CF diagnosis/prognosis;
    b. Values obtained in 2b and 2c for the same individuals to determine whether 2D-intestinal monolayers recapitulate the CFTR modulator drugs found in 3D-organoids and thus assess whether they constitute a good model to predict individuals' drug responses.

Our results on the differentiation of the 2D-monolayers showed a low expression of CFTR protein in the late differentiation stages and high levels of CFTR expression and function in the less differentiated monolayers. This finding has led us to use the less differentiated monolayers in our subsequent measurements of Cl^- secretion. Moreover, we established good correlations among function parameters measured in the 2D-monolayers, the 3D-organoids and the fresh rectal biopsies, showing that 2D-monolayers are good models to assess CFTR function *in vivo*. Importantly, our results also showed good correlations between measurements of CFTR function in 2D-monolayers and other CF biomarkers such as fecal elastase. The assays used to analyze rescue of CFTR function with modulators showed significant rescue in 4 out of 7 individuals analyzed.

Overall, these results show that the 2D-monolayers seem to be a good model to replace or complement the 3D-organoids and rectal biopsies to assess CFTR function. However, they should be further studied in more individuals with different mutations. Additionally, this 2D-model could assist in providing a precision medicine approach to individuals with CF, in order to give the right drug to the right individual because, in contrast to fresh rectal biopsies, they evidence responses to CFTR modulators.

Keywords: Cystic Fibrosis; CFTR; CFTR modulators; 2D intestinal monolayers; Epithelial differentiation.

Resumo

A Fibrose Quística (FQ) é a doença genética recessiva mais comum na população caucasiana, afetando cerca de 90,00 pessoas em todo o mundo. A FQ é causada por mutações no gene que codifica a proteína CFTR (do inglês, *Cystic Fibrosis Transmembrane Conductance Regulator)*), que é um canal de aniões cloreto (Cl^-) e bicarbonato (HCO_3^-) e que está presente na membrana apical das células epiteliais. A perda de função da CFTR mutada leva à ausência de secreção de aniões e, consequentemente, da secreção de fluido, resultando numa desregulação da homeostase do fluido e da osmolaridade nos diferentes epitélios. Assim, a FQ é uma doença que afecta múltiplos sistemas e causa várias manifestações clínicas tais como, infeções pulmonares recorrentes, insuficiência do pâncreas exócrino, diabetes relacionada com a FQ, distúrbios gastrointestinais, doença hepática, doença renal crónica e infertilidade masculina. Também é uma doença que afeta a reconstituição dos tecidos e a diferenciação epitelial e por isso indivíduos com FQ apresentam malformações na traqueia, alterações na regeneração celular, secreções glandulares anómalas e alterações na permeabilidade de vários tecidos epiteliais. No entanto, a doença das vias respiratórias, caracterizada pelo aumento da viscosidade do muco que dificulta a *clearance* muco-ciliar e ao aumento da incidência das infeções respiratórias graves e processos inflamatórios que progressivamente reduzem a função respiratória, permanece a principal causa de mortalidade dos indivíduos com FQ.

Desde a descoberta do gene *CFTR* em 1989, mais de 2,000 mutações foram descritas, a maioria das quais presumivelmente causadora de FQ. Assim, para melhor as caracterizar, foi proposto um sistema de classificação, consistindo em sete classes (I-VII), onde as mutações da CFTR são agrupadas de acordo com o defeito molecular/celular que provocam. A classe I consiste em mutações que geram codões stop prematuros levando à produção de proteínas truncadas que são degradadas pelo proteassoma. As mutações de classe II causam um defeito de *folding* da proteína CFTR e a sua subsequente retenção no retículo endoplasmático e degradação, impedindo o seu tráfego para a membrana plasmática (MP). A mutação F508del, a mais comum na FQ, faz parte desta classe. As mutações de classe III afectam a regulação do canal CFTR diminuindo a sua probabilidade de abertura. Mutações de classe IV provocam constrangimentos no poro da CFTR e, por conseguinte, uma redução drástica na condutância do canal. Mutações de classe V levam a uma redução nos níveis de CFTR, normalmente provocada por mecanismos de *splicing* alternativo que dão origem a transcritos normais e aberrantes em proporções diferentes. Mutações de classe VI reduzem a estabilidade da CFTR na MP, levando à sua internalização e degradação. Por fim, mutações de classe VII levam à perda por completo da expressão do gene *CFTR* geralmente devido a grandes deleções e, por isso, são chamadas de "irrecuperáveis" pois não podem ser tratadas farmacologicamente para recuperação da função da CFTR. Este sistema de classificação foi evoluindo no sentido de auxiliar no desenvolvimento de fármacos. Com efeito, já que mutações da mesma classe causam o mesmo defeito molecular, uma mesma estratégia terapêutica deverá tratar todas as mutações da mesma classe. Recentemente, foram aprovados fármacos consistindo em pequenas moléculas que (sozinhas ou em combinação) fazem o resgate da proteína CFTR com mutações específicas. O primeiro, VX-770 (Ivacaftor), é usado como potenciador do canal CFTR e está aprovado para mutações de classe III e algumas mutações de classe IV. Atualmente, é utilizado também em combinação com corretores da CFTR, como o VX-809 (Lumacaftor) ou o VX-661 (Tezacaftor), que corrigem o defeito de tráfego para a MP. Estes corretores foram desenvolvidos para a mutação mais comum - F508del-CFTR.

No entanto, indivíduos que não possuem as mutações para as quais se aplicam os moduladores podem também ter benefício clinico da sua administração. Além disso, existem indivíduos que têm as mutações para as quais estes fármacos se aplicam, mas que não demonstram benefício após administração dos mesmos. Tal é devido a outros fatores, tais como genes modificadores e fatores ambientais. Logo, uma abordagem de medicina personalizada designada teranóstico (do inglês, ***thera****peutic diag****nostics***) torna-se cada vez mais importante para trazer o fármaco certo para os indivíduos que dele podem receber benefício. Para tal, têm sido criados modelos celulares *ex vivo* para auxiliarem em ensaios laboratoriais de previsão de eficácia destes fármacos. Estes modelos, gerados a partir de materiais biológicos derivados dos indivíduos, incluem células dos epitélios nasal ou brônquico (de lavagens bronquiais ou de pulmões transplantados) ou células intestinais obtidas de biopsias rectais. Estas últimas têm sido utilizadas para gerar organóides intestinais tridimensionais (3D) usados para testar o efeito dos moduladores da CFTR. No entanto, mais recentemente, foi criado um novo modelo através do cultivo de monocamadas bidimensionais (2D) de células epiteliais intestinais obtidas a partir dos organóides 3D. Estes sistemas celulares 2D abrem novas possibilidades para o teste de moduladores da CFTR. Com efeito, se se demonstrar que recapitulam a função basal da CFTR *in vivo* em medições de secreção de Cl^- em microcâmaras de Ussing, estes sistemas celulares 2D têm elevado potencial para substituir ou complementar os organóides intestinais 3D e as biopsias rectais frescas. Estas últimas em particular são usadas para diagnóstico/prognóstico da FQ, mas em centros onde não é possível a sua análise imediata por eletrofisiologia, não é possível o seu envio para centros de referência, dado o curto espaço de tempo em que se mantêm viáveis para eletrofisiologia (~6h). Porém, as biopsias frescas mantêm a sua viabilidade para gerar organóides 3D durante 24h, sendo assim possível o seu envio para centros de referência onde se pode produzir organóides 3D e monocamadas 2D, estas últimas para análise direta em camara de Ussing. No entanto, uma vez que as monocamadas 2D são sistema modelo novo, estão pouco caracterizadas, não tendo sido ainda demonstrada a sua aplicabilidade para diagnóstico/prognóstico da FQ ou para testar o efeito e eficácia dos fármacos moduladores CFTR.

Os principais objetivos deste projeto de mestrado eram:

1) A caracterização do novo modelo em estudo, as monocamadas 2D, avaliando:
    a. A expressão de proteínas de membrana e canais iónicos presentes no tecido nativo e essenciais para a secreção de Cl^-;
    b. A diferenciação das células epiteliais intestinais por marcadores de diferenciação e proliferação, em condições de não diferenciação e de diferenciação.
2) A análise da função da CFTR em tecidos nativos e em culturas de células primárias de indivíduos com FQ, comparando com controlos normais através de:
    a. Medição em microcâmaras de Ussing da secreção de Cl^- mediada pela CFTR em biopsias rectais frescas;
    b. Ensaios de inchamento mediado por Forscolina (FIS) em organóides intestinais provenientes das biopsias rectais;
    c. Medição em microcâmaras de Ussing da função da CFTR em monocamadas 2D de células epiteliais intestinais derivadas dos organóides 3D;
3) Estabelecer correlações entre:
    a. Os valores obtidos em 2.a, 2b e 2c para os mesmos indivíduos e com os outros biomarcadores da FQ destes indivíduos, com o intuito de validar as monocamadas 2D de

células epiteliais intestinais como um bom modelo celular personalizado para a medição da função da CFTR e consequentemente para diagnóstico/prognóstico da FQ.

b. Os valores obtidos em 2b e 2c para os mesmos indivíduos para avaliar se as últimas recapitulam as respostas aos fármacos moduladores CFTR observadas em organóides 3D e assim determinar se as monocamadas 2D são um bom modelo para a previsão da resposta a estes fármacos.

Os resultados do estudo da diferenciação das monocamadas 2D mostraram que existe uma perda de expressão de CFTR nas células diferenciadas e uma elevada expressão e função de CFTR nas monocamadas 2D não diferenciadas. Por isso, ao longo to trabalho, usámos as monocamadas 2D não diferenciadas nas medições de secreção de Cl^- em microcâmaras de Ussing.

Estabelecemos boas correlações entre a função de CFTR medida nas monocamadas 2D, nos organóides 3D e nas biopsias retais. Os nossos resultados mostraram que a função basal máxima da CFTR medida nas monocamadas 2D (2D $\Delta I_{sc\text{-}eq}$ (max)) se correlaciona com a mesma ativação máxima medida nas biopsias rectais (Biopsy $\Delta I_{sc\text{-}eq}$ (max)) e com as medições de inchamento 'basal' dos organóides 3D, i.e., só com forscolina (AUC [Fsk] = 0.8). Por fim, ainda estabelecemos correlações entre medições de função de CFTR em monocamadas 2D e outros biomarcadores de FQ, nomeadamente mostrámos que existe uma correlação entre a secreção de Cl^- ativada pelo cAMP e co-ativada colinergicamente nas monocamadas 2D (2D $\Delta I_{sc\text{-}eq}$ (max)) com o valor de elastase fecal E1 nos indivíduos com FQ.

Os ensaios de FIS permitiram-nos concluir que existe função residual da CFTR em 3 dos 6 indivíduos em que os organóides foram estudados e foi possível prever benefício clínico em 5 desses 6 indivíduos com pelo menos um fármaco modulador da CFTR testado. Os nossos ensaios de resgate de função de CFTR com moduladores da CFTR em monocamadas 2D permitiram-nos encontrar resposta significativa em 4 dos 7 indivíduos testados.

Em suma, estes resultados aqui apresentados demonstram que há um potencial na aplicação do modelo de células intestinais 2D para substituir ou complementar os ensaios realizados nos organóides 3D e nas biopsias rectais frescas. Uma aplicação muito importante deste novo modelo será na "medicina personlizada", ou teranóstico no qual as monocamadas 2D seriam usadas para prever qual a terapia mais adequada para um determinado indivíduo com FQ. Para uma validação mais profunda deste modelo, no futuro, mais ensaios deveriam ser realizados com monocamadas 2D de maior número de indivíduos com FQ com diferentes mutações.

Palavras-chave: Fibrose Quística; CFTR; Moduladores da CFTR; Monocamadas intestinais 2D; Diferenciação epitelial.

Table of Contents

Index of Figures and Tables

List of Acronyms and Abbreviations

2D	Two-dimensional
3D	Three-dimensional
ABC	ATP-binding cassette
Amil	Amiloride
ANOVA	Analysis of variance
APS	Ammonium persulfate
AUC	Area under the curve
BK	Large conductance
cAMP	Cyclic adenosine monophosphate
CCH	Carbachol
CF	Cystic Fibrosis
CFTR	Cystic Fibrosis Transmembrane Conductance Regulator
$CFTR_{inh}$-172	CFTR-specific inhibitor 172
CK18	Cytokeratin 18
DMSO	Dimethyl sulfoxide
E-cad	E-cadherin
ENaC	Epithelial sodium channel
ER	Endoplasmic reticulum
ERAD	ER associated degradation
$F12^{ghp}$	Advanced DMEM/F12 + 1% Pen/Strep + 1% Glutamax + 1% HEPES
FEE	Fecal elastase E1
FIS	Forskolin-induced swelling
Fsk	Forskolin
HBEC	Human bronchial epithelial cell
HNEC	Human nasal epithelial cell
HRP	Horse-radish peroxidase
IBMX	3-isobutyl-1-methylxanthine
I_{eq-sc}	Equivalent short-circuit current
IF	IBMX/Fsk
IK	Intermediate conductance
Indo	Indomethacin
IRT	Immunoreactive trypsin assay
LGR5	Leucine rich repeat-containing G protein coupled receptor 5
MCC	Mucociliary Clearance
N-cad	N-cadherin
NBD	Nucleotide binding domain

NKCC1	$Na^+ K^+ 2Cl^-$ Cotransporter 1
NPD	Nasal potential difference
PAGE	Polyacrilamide gel electrophoresis
PBS	Phosphate-buffered saline
Pen/Strep	Penicilline/Streptomycin
PI	Pancreatic insufficiency
PKA	Protein kinase A
PM	Plasma membrane
PTC	Premature stop codon
RD	Regulatory domain
R_{te}	Resistance
RT-PCR	Reverse transcriptase polimerase chain reaction
SD	Standard deviation
SDS	Sodium dodecyl sulfate
SLC	Solute-linked Carrier
TMD	Transmembrane domain
TBS	Tris-buffered saline
TEER	Transepithelial electrical resistance
TEMED	Tetramethylethylenediamine
V_{te}	Voltage
WB	Western blot
WT	Wild-Type

1. Introduction

1.1 Cystic Fibrosis

Cystic Fibrosis (CF) is the most common recessive genetic disorder, affecting around 45,000 individuals in Europe and about 90,000 worldwide[1–3]. It is caused by mutations in the CF transmembrane conductance regulator (*CFTR*) gene, which encodes a cAMP-regulated chloride (Cl^-) and bicarbonate (HCO_3^-) anion channel located in the apical side of epithelial cells[4,5]. Since its discovery and sequencing in 1989[6], over 2,000 different mutations have been identified so far (http://genet.sickkids.on.ca/StatisticsPage.html), most of which presumed to be CF-causing (www.cftr2.org). The most frequent mutation – F508del – is present in ~80% of individuals worldwide in, at least, one allele[2].

CF is a multisystem disease, affecting different organs and tissues, which causes several clinical manifestations, such as recurrent pulmonary infections and inflammation, exocrine pancreas insufficiency, CF-related diabetes, gastrointestinal disorders (including meconium ileus in the neonatal period), liver disease, chronic kidney disease and infertility in both male and female individuals[2,7]. However, irreversible lung damage caused by chronic obstructive lung disease is still the main cause of morbidity and cause of death of 85% of individuals with CF[8].

For the pathophysiology of the lung disease, CFTR interactions with other proteins, such as the epithelial sodium channel (ENaC)[9], may have a major role (Figure 1.1). CFTR mutations hinder the transport of Cl^- and HCO_3^- ions which leads to an increase in ENaC function and, thus, sodium (Na^+) hyper-absorption. Ultimately, this leads to severe epithelial dehydration in the airways and impedes mucociliary clearance (MCC)[10–12]. However, besides osmotic regulation, CFTR regulates the pH of the airway surface liquid by HCO_3^- ion transport[13–15]. Impairment of HCO_3^- transport lowers the pH of the mucosa, which leads to a more viscous mucus[16,17] and contributes negatively to the function of anti-microbial peptides, contributing to an increase in infections prevalence[18]. As lung disease progresses, bronchiectasis settles and individuals with CF experience several infections from Gram negative bacteria, in which *Pseudomonas aeruginosa* is the most predominant[19].

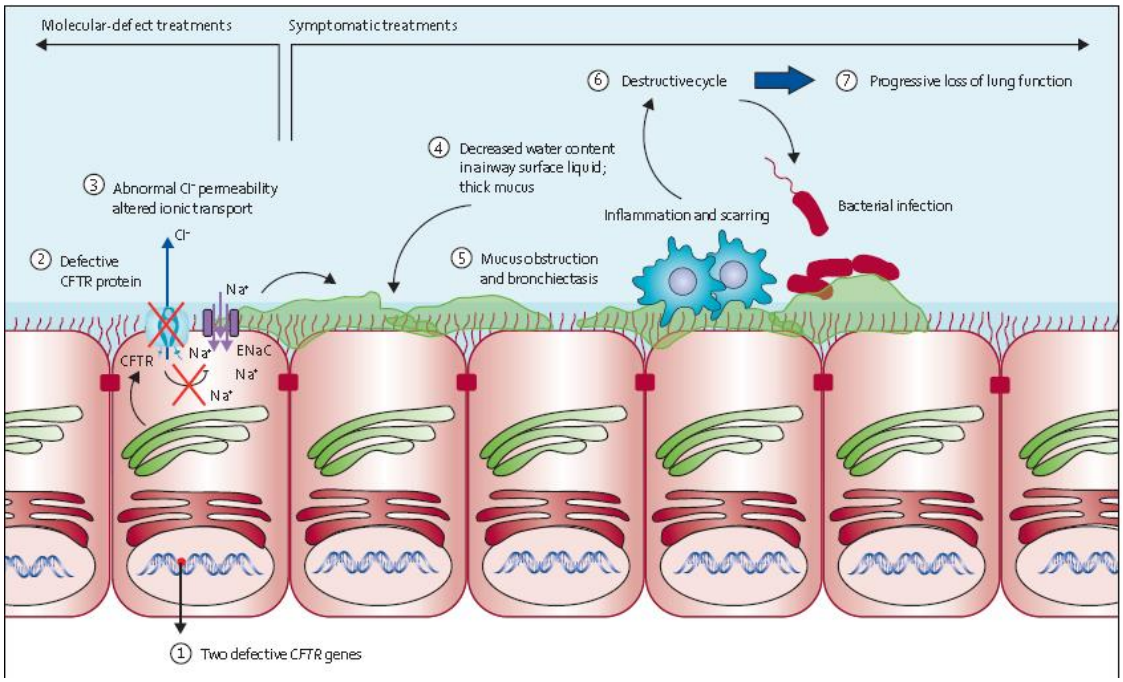

Figure 1.1 - Effects of CFTR functional deficiency in the airway epithelium. Reduced or absent Cl^-/HCO_3^- transport leads to hyper-absorption of Na^+ reducing airway-surface liquid hydration, mucociliary clearance, and pH dysregulation, which leads to an increase in mucous viscosity and impairs innate immunity. This contributes to chronic inflammation and lung injury, which is the main cause of death among CF patients. Retrieved from De Boeck, K. & Amaral, M.D. (2016).

Apart from the airways, defective Cl^- and HCO_3^- anion secretion also affects the epithelial cells of the pancreas and the biliary duct. Mucus plugging affects the secretion of the digestive enzymes by the acinar cells to the small intestine. The enzymes remain clogged in the pancreatic ducts and start to damage the pancreatic tissue[20,21]. The obstruction occurs early in uterus, so individuals with classical CF develop pancreatic insufficiency (PI) at birth or soon after, while individuals with some CFTR residual function develop PI later in life[22,23]. This PI can be surpassed with the help of pancreatic enzyme replacement therapy[21,24]. Apart from that, the lack of HCO_3^--rich fluid secreted by the pancreas combined with CFTR deficiency in the proximal intestine causes poor digestive function in the intestine due to the ineffective neutralization of gastric fluids[25]. There is a strong correlation of deterioration of lung function and poor nutritional status[26,27], so increased care in nutrition means more longevity for individuals with CF. Defective transport of Cl^- and HCO_3^- ions to the intestinal lumen leads to thick mucus which can cause obstructions in the distal small intestine (meconium ileus for infants and distal intestinal obstructive system for older individuals) that can result in rupture and sepsis, and ultimately death. Inflammation is also a hallmark of the CF intestine, in which the defective mucus clearance allow abnormal bacterial colonization that alters the immune system behavior which, in turn, leads to an increase in mucus production[25].

CF was initially described in 1938[28] and, at the time, it was fatal in infancy. Currently, with symptomatic therapies such as digestive enzyme supplementation, mucolytic and hydrator therapies, airway clearance and frequent courses of antibiotics, the disease stopped being a childhood disease

and more than 50% of individuals with CF reach adulthood, as indicated being the median age of survival ~40 years[29]. However, this heavy therapeutic 'load' and the progressive loss of lung function still pose a high burden for the individuals with CF and the healthcare system[2]. Ultimately, all of these therapies work downstream of the disease and only treat the upcoming symptoms. If we want a more permanent solution for CF, it is essential to understand the *CFTR* gene and its role in the cell.

1.2 CFTR

1.2.1 Structure and Regulation of CFTR Protein

CFTR is a 1480-residue long membrane protein that is a member of the ATP-binding cassette (ABC) superfamily, although it is the only ABC protein that functions as an ion channel[30,31]. Moreover, unlike other ABC transporters that pump substrates against their electrochemical gradient, CFTR conducts anions down their electrochemical gradient[32]. Also, besides the sequence of two transmembrane domains (TMDs) that form the translocation pathway and two cytoplasmic nucleotide-binding domains (NBDs) which hydrolyze ATP that all typical ABC transporter have, CFTR has an additional regulatory domain (RD) that must be phosphorylated to allow the open channel conformation[33,34]. Recently, the human CFTR structure was determined by cryo-EM[32], which was important to understand the RD regulation and the ATP dependent channel gating.

The RD rests in a position that inhibits NBD dimerization and, thus, channel opening[32]. So, only upon phosphorylation of this domain by protein kinase A (PKA), ATP can bind to the NBDs, forming a dimer that changes the conformation of the TMDs opening the channel and allowing Cl^- efflux (Figure 1.3). Hydrolysis of ATP and release of inorganic phosphate causes the channel to close but it can rapidly open again upon the addition of another ATP molecule (Figure 1.3)[35]. At rest, the R region is kept dephosphorylated by phosphatase activity[36], which is important to conserve ATP levels[37].

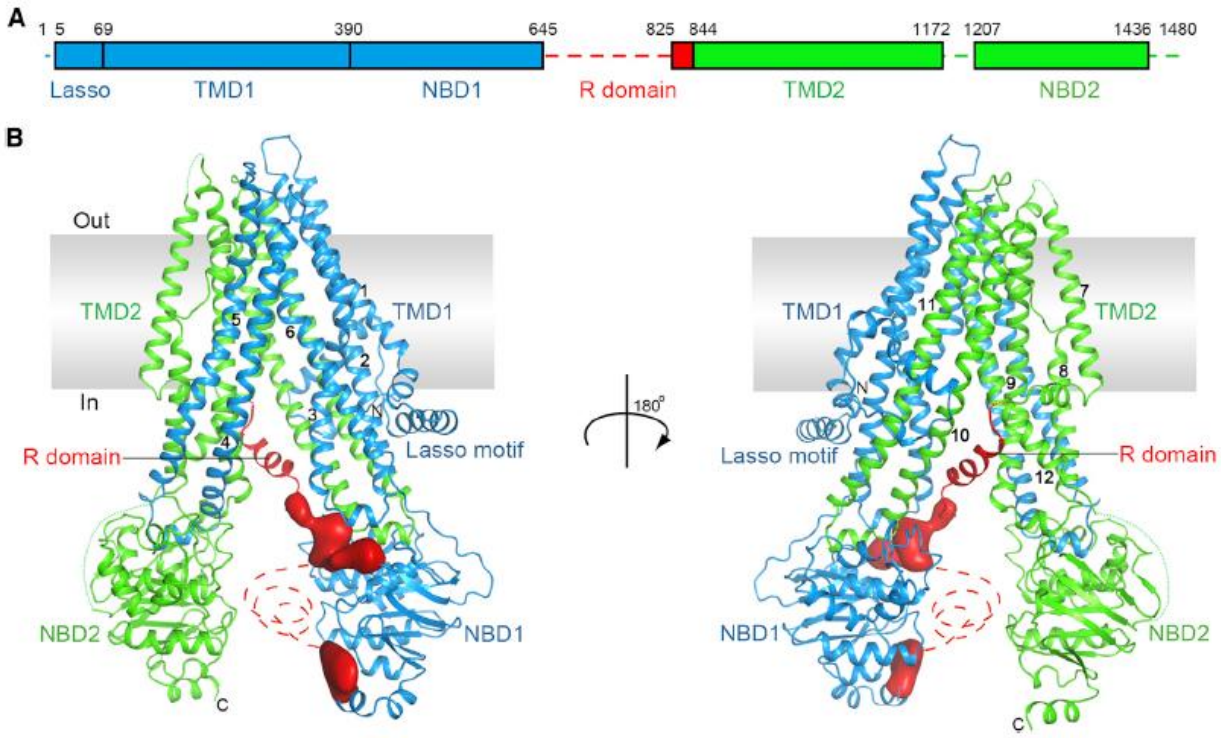

Figure 1.2 - Structure of the human CFTR in the dephosphorylated, ATP free conformation. A. The domain organization of CFTR protein, starting in the N-terminus with the Lasso motif, followed by the TMD1 and NBD1, R domain towards the middle of the sequence, and TMD2 and NBD1 in the C-terminus. **B.** Ribbon diagram of the CFTR protein. Out is the outside of the cell and In is the cytoplasm. TMD1 and TMD2 are the transmembrane domains of CFTR, NBD1 and NBD2 the nucleotide binding domains and R is the regulatory domain. Numbers 1 to 12 identify the 12 transmembrane helices. The EM densities in red correspond to the unstructured regions of R domain and R domain association with NBD1. Dashed lines are unresolved regions. Retrieved from Liu, F. *et al* (2017).

CFTR biogenesis occurs at the endoplasmic reticulum (ER), which provides the first steps in the protein folding quality control[38]. Protein chaperones, such as calnexin, evaluate the folding state of CFTR and target misfolded proteins for ER associated degradation (ERAD) by the 26S proteasome[39,40]. Folded CFTR leaves the ER and goes to the Golgi network for final maturation before trafficking to the plasma membrane, by the endosome network[41]. The most common CFTR mutation F508del, a deletion in phenylalanine 508, affects protein trafficking. This mutation destabilizes CFTR structure and folding, making it a target for the ERAD pathway, with low amounts of mature proteins reaching the cell membrane[42]. As more mutations were discovered, causing different defects on the CFTR protein, it began to be relevant to group the mutations based on the functional defects they elicit.

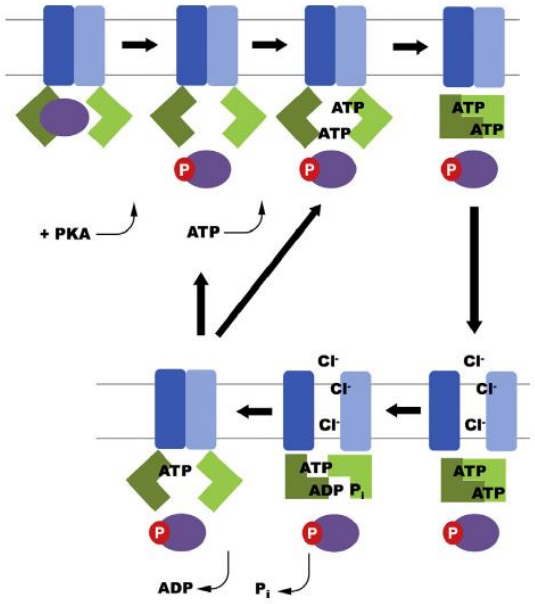

Figure 1.3 – Scheme of CFTR molecular mechanism. Grey lines are the lipid bilayer; the cytosolic part is at the bottom and the extracellular part at the top. The dark blue rectangle is TMD1 and the light blue is TMD2, the light green L shaped box is NBD2 and the dark green is NBD1, and the purple oval is the R region. For CFTR activation, the R region is phosphorylated by PKA, allowing ATP binding to both NBDs. This changes TMDs conformation which allows the pore to open and the efflux of chloride and bicarbonate. Hydrolysis of ATP at the catalytically active site closes the channel, although it can be rapidly reopened by the addition of another ATP molecule. Retrieved from Cant, N. *et al* (2014).

1.2.2 Functional Classification of CFTR Mutations and Theratypes

The approximately 2200 described *CFTR* gene mutations consist in missense (39.6%), frameshift (15.6%), splicing (11.4%), and nonsense (8.3%) mutations; large (2.6%) and in-frame (2.0%) deletions or insertions; promoter mutations (0.7%); and non-pathological variants[1]. These mutations cause different cellular and molecular effects. Therefore, in order to facilitate the discovery of mutation-specific therapies, they can be grouped into seven classes according to the functional defect they elicit.

Class I mutations are mostly nonsense mutations, causing the production of truncated proteins and, often, nonsense-mediated mRNA decay. Class II mutations contribute to protein misfolding and retention at the ER with subsequent degradation, thus impairing protein traffic to the cell membrane. F508del mutation is included in this class. Class III mutations impair gating of the CFTR channel. Class IV mutations significantly diminish CFTR channel conductance. Class V mutations lead to a decrease in normal CFTR protein levels, usually due to alternative splicing that generates both normal and altered mRNA transcripts. Class VI mutations destabilize CFTR at the plasma membrane, either by increasing CFTR endocytosis or decreasing its recycling back to the membrane. Lastly, class VII mutations include large deletions and are called “non-rescuable” mutations because they cannot be pharmacologically rescued, and therefore there is the need to target alternative chloride channels or develop mutation agnostic therapies (Figure 1.4)[1].

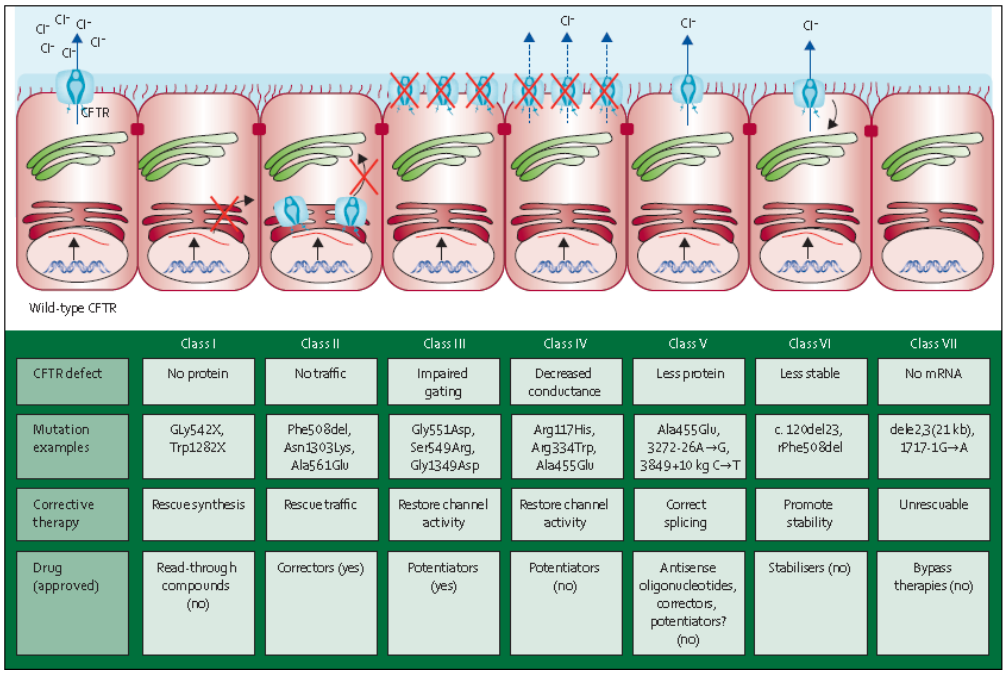

	Class I	Class II	Class III	Class IV	Class V	Class VI	Class VII
CFTR defect	No protein	No traffic	Impaired gating	Decreased conductance	Less protein	Less stable	No mRNA
Mutation examples	Gly542X, Trp1282X	Phe508del, Asn1303Lys, Ala561Glu	Gly551Asp, Ser549Arg, Gly1349Asp	Arg117His, Arg334Trp, Ala455Glu	Ala455Glu, 3272-26A→G, 3849+10 kg C→T	c. 120del23, rPhe508del	dele2,3(21 kb), 1717-1G→A
Corrective therapy	Rescue synthesis	Rescue traffic	Restore channel activity	Restore channel activity	Correct splicing	Promote stability	Unrescuable
Drug (approved)	Read-through compounds (no)	Correctors (yes)	Potentiators (yes)	Potentiators (no)	Antisense oligonucleotides, correctors, potentiators? (no)	Stabilisers (no)	Bypass therapies (no)

Figure 1.4 – Summary of all seven CFTR functional mutation classes and respective therapeutic strategies. It is expected that each mutation from the same class responds to the same type of therapeutic strategy. However, class VII mutations cannot be rescued by any modulator and, thus, it is necessary to pursue other strategies. Retrieved from De Boeck, K. & Amaral, M.D. (2016).

There are some CFTR modulator drugs that have been approved recently: VX-770 (Ivacaftor®) is a potentiator that is indicated for the treatment of class III mutations but has been shown to work in other mutations from class IV or V[43–45]; VX-809 (Lumacaftor®) is a corrector, which means that it assists in the correct protein folding and trafficking to the plasma membrane, which benefits individuals with the homozygous F508del mutation or other class II mutations and in the clinic it is combined with Ivacaftor® for an increase in benefit[46]; and VX-661 (Tezacaftor®), that corrects the same molecular defect as Lumacaftor® but in combination with Ivacaftor® it has been shown to have higher rescue effects for F508del homozygous individuals[47]. This last combination, known as Symkevi® in Europe, has also been approved for individuals with one F508del allele and one mutation with residual function[48,49].

1.2.3 CFTR and Epithelial Differentiation

Besides its major role in chloride and bicarbonate secretion, fluid secretion and regulation of osmolarity, CFTR is also an important protein regarding epithelial differentiation. In the lung, its cellular distribution was found to change with the degree of differentiation of the epithelial cells, evolving from diffused expression (in nonpolarized cells) to a predominantly apical distribution (in differentiated and polarized cells) and it was observed that mutated CFTR impairs the proliferation of predominantly undifferentiated cell types (e.g. Club cells) and its expression is necessary for their

further differentiation[50]. Moreover, it was established that CF epithelia has impaired differentiation[51]. Experiments in epithelial differentiation with cell lines expressing WT-CFTR and F508del-CFTR have shown that the WT cells develop a larger transepithelial electrical resistance (a measure of epithelial tightness) than mutant cells[52]. This is also evidenced in the epithelia of tubular organs where protein interactions with CFTR are crucial in cell junction formation. Therefore, lack of CFTR compromises barrier function and normal function of epithelial tissue by affecting tight junctions and gap junctions formation[53,54]. In addition to differentiation, lack of CFTR also affects wound healing and normal airway epithelial regeneration. The delay in this process may even start fibrotic responses in the lung tissue[55]. In addition to its role in the epithelial differentiation process, CFTR is actually necessary to maintain the differentiated and polarized state of the differentiated cells. Epithelial-mesenchymal transition is a process whereby fully differentiated polarized epithelial cells transition into a mesenchymal phenotype, giving rise to apolar fibroblastoid cells, such as fibroblasts and myofibroblasts[56]. Lack of CFTR activity and the inflammation processes in the lung linked with CF can induce Transforming Growth Factor – β1 – driven epithelial-mesenchymal transition, where the increase in proliferative cells causes an increased tissue remodeling and repair in the CF lung[57]. In summary, CFTR has a clear role in epithelial differentiation and epithelial tissue homeostasis that is yet poorly understood and should be further explored.

1.3 Current Diagnosis Methods for CF

Usually, CF suspicion in an individual may arise from the presentation of typical clinical symptoms, having a CF case in the family or if there was a positive result in a newborn screening program. Then, the clinician needs to perform laboratory tests, classically sweat Cl^- concentration, nasal potential difference (NPD), genetic testing or other complementary methods (e.g. Cl^- current measurements using rectal biopsies in Ussing chambers)[58,59].

1.3.1 Sweat Chloride Concentration Test

The sweat test was first described in 1959 and it remains to this day the gold standard of CF diagnosis[59]. The standard sweat test (the Gibson and Cooke technique) needs to be performed with care and high skill, and consists in stimulating localized sweating by the iontophoresis of pilocarpine into the skin. Sweat is then collected on filter paper, gauze, or in microbore tubing[60] over a controlled period of time. The test is considered positive when it presents a Cl^- concentration of more than 60 mmol/L, and levels below 30 mmol/L are considered normal for all age groups[61,62]. Individuals with values in the intermediate range (30-60 mmol/L) probably have a CFTR mutation with a mild effect[63]. Also, some adults may have values in the intermediate range, so sweat Cl^- levels alone may be insufficient to diagnose CF in the older adolescent[64]. Nevertheless, it is still a widely used test for the diagnosis of CF.

1.3.2 Nasal Potential Difference (NPD)

The impairment of Cl^- conductance and subsequent Na^+ hyper-absorption in individuals with CF can be detected by NPD measurements, which assess the voltage created by the movement of these ions through the epithelia. These measurements can be performed in the mucosa or the inferior turbinate by placing an exploring electrode on the respiratory epithelium and a reference electrode into the subcutaneous tissue of the forearm. Baseline potential difference (PD) is more negative in individuals with CF. Diagnostic is made by evaluating the bioelectrical profile change (in reference to the baseline) when amiloride (Amil), an ENaC inhibitor, is applied (becomes less negative in CF) following the addition of a Cl^--free solution and isoproterenol, that lowers the potential difference in an healthy individual and has little or no response in CF[65,66] (see figure 1.5). Test results can be influenced by several factors such as recent viral infections, electrode position and the genotype, and are technically difficult, so only specialized centers perform this technique[67].

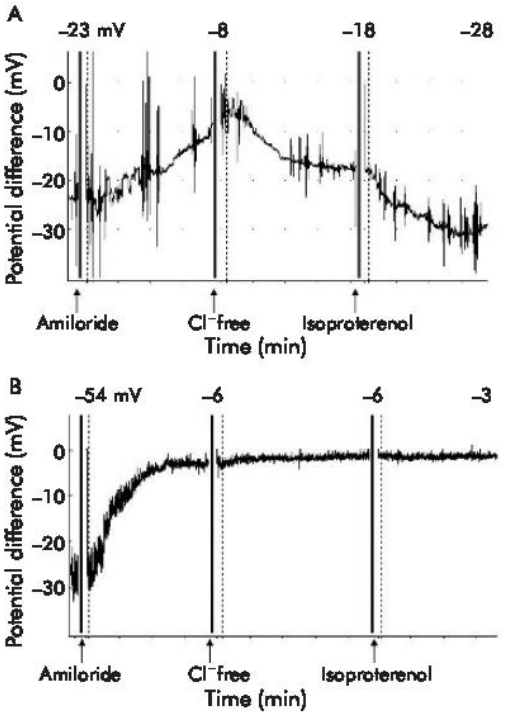

Figure 1.5 – Nasal potential difference measurement in (A) a healthy individual and (B) a person with classic CF. In a healthy individual the basal PD is negative, then rises (approaching zero) after the addition of Amil and decreases with the addition of a Cl^-free solution and isoproterol. The individual with classic CF has a more negative baseline and has a faster rise in PD after the application of Amil. There is no alteration after the application of a Cl^-free solution and isoproterol. Retrieved from De Boeck, K. et al (2005).

1.3.3 CFTR Genotyping

Although the *CFTR* gene was discovered in 1989, since then the diagnosis of CF cannot be based simply on gene sequencing and mutation analysis. Of the 2200 mutations already described, not all of them are yet characterized, meaning that some of them may not be "CF causing" or may not lead to a "classic CF" phenotype. Moreover, there are mutations that may not be confined to the gene but may be located in the promoter region or in other regulatory regions, so they would probably not be identified by the normal sequencing tests. Albeit two CF causing mutations should imply CF diagnosis, the diagnosis should be made regarding the clinical symptoms and laboratory tests, with the possibility of additional genetic analysis to confirm a CF genotype[59].

1.3.4 Newborn Screening Programs

As newborn screening programs are being widely used, they have become the most common route of CF diagnosis, as opposed to the traditional way of analyzing the symptoms as they emerge. So far, many screening algorithms have already been developed[68]. The first step to neonatal screening is based on the immunoreactive trypsinogen assay (IRT), which is simple and inexpensive to perform on the newborn heel prick sample (Guthrie Test)[69]. In case of the CF newborns, the IRT levels remain elevated for weeks to months in both pancreatic sufficient and insufficient individuals, being repeated 2 weeks after birth to increase the specificity[70]. These children proceed to further testing, which may include genetic testing for a panel of CFTR mutations that are more frequent in the population, as well as a sweat test[71]. Nevertheless, this screening is designed to pick up cases of classical CF, who will benefit from early therapy, and to exclude healthy carriers. There are sometimes equivocal diagnoses: infants that do not meet the diagnostic criteria for CF, that have a mutation that is not CF-causing or do not have clinical symptoms but, later in life, may develop organ changes that require intervention. The term CFTR-related metabolic disease was created to describe these cases in order to provide the specific care that they require[72].

1.3.5 Cl^- current measurements using rectal biopsies in Ussing chambers

The measurement of Cl^- ion secretion in human native colonic tissue have already been established as a robust *ex vivo* biomarker for the evaluation of CFTR function, which additionally can correlate with the CF individual genotype and clinical parameters such as sweat chloride concentration and fecal elastase E1 (FEE) levels[73–75]. To perform this test, a series of pharmacological stimuli are applied to directly and indirectly stimulate CFTR conductance and then the results can be divided into three groups (Figure 1.6).

At the start of the experiment, Amil is added to inhibit ENaC-generated Na^+ currents. Then, application of carbachol (CCH), a cholinergic receptor agonist, raises intracellular [Calcium (Ca^{2+})], activating Ca^{2+}-gated potassium (K^+) channels. This generates a driving force for Cl^- secretion through CFTR and elicits lumen-positive responses in tissues from individuals with CF and lumen-negative in non-CF tissues (Figure 1.6, first peak). Thus, when CCH is applied a second time, now in the presence of indomethacin (Indo) to inhibit endogenous cAMP production, there is no cAMP and CFTR-mediated Cl^- secretion, so we get lumen-positive responses from K^+ secretion (Figure 1.6, second peak). Shortly after, when 3-isobutyl-1-methylxantine (IBMX) and Forskolin (Fsk) are added to elicit cAMP-dependent CFTR-mediated Cl^- secretion, lumen-negative responses are observed in non-CF individuals (Figure 1.6A, third peak) and "non-classic CF" individuals (Figure 1.6B, third peak) but no response is observed from the "classic CF" subgroup (Figure 1.6C). Lastly, still in the presence of the last reagents, CCH stimulation creates three different responses on the subgroups: monophasic lumen-negative in tissues from "normal" individuals (Figure 1.6A, fourth peak); biphasic responses in the "non-classic CF" individuals (Figure 1.6B, fourth peak); and monophasic lumen-positive in tissues from the "classic CF" individuals (Figure 1.6C, fourth peak)[75].

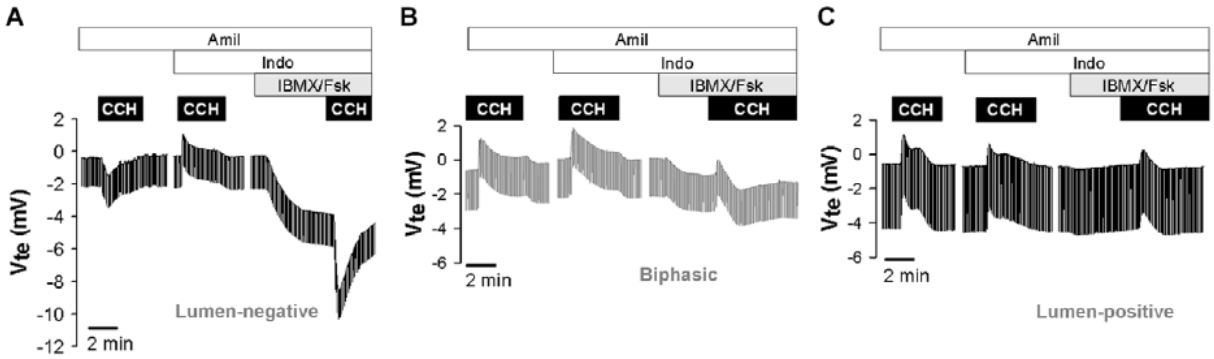

Figure 1.6 – Three possible micro-Ussing chamber readouts for the assessment of CFTR function and the distinction between subtypes of individuals. A This is the normal CFTR function readout, with lumen-negative response to carbachol (CCH) and lumen-positive response in the presence of indomethacin (Indo) and amiloride (Amil). There is CFTR-mediated Cl^- secretion after the stimulation with IBMX/Fsk and CCH on top, as evidenced by the lumen-negative responses. B Two lumen-positive responses to CCH (with and without Indo) followed by a smaller (compared to the normal) lumen-negative response to IBMX/Fsk. When CCH is added, there is a biphasic response consisting in a lumen positive response due to K^+ secretion followed by a lumen-negative response due to CFTR activity and Cl^- transport. **C** This is a classic CF readout, with three lumen-positive responses to CCH due to lack of CFTR activity and no response to IBMX/Fsk. Adapted from Sousa, M. *et al* (2012).

1.4 CF Personalized Therapies

In recent years, the emergence of CF modulator drugs gave a chance of therapy to individuals with CF. Nevertheless, the CF modulators are only approved for certain mutations. Since mutations from the same class may benefit from the same therapies and there are factors other than *CFTR* genotype that influence drug response, individuals with *CFTR* genotypes other than the approved ones can benefit from the same CFTR modulators and not all individuals with CF will benefit from the approved therapies. Thus, over the years, *in vitro* models have been developed to predict each individual's drug response in a precision medicine approach. In this way, care for individuals with CF can be done with a more personalized medicine approach, where one drug does not fit all, but there may be a right drug for each individual with CF.

1.4.1 Primary Human Bronchial/Nasal Epithelial Cells

Recently, primary cultures of human bronchial epithelial cells (HBEC) and human nasal epithelial cells (HNEC) have been developed to replicate *in vitro* the physiological and pathophysiological conditions occurring *in vivo*, as closely as possible. These cells can be collected from individuals with CF and non-CF controls and, with the appropriated culturing conditions, can be differentiated in to the main cell types present in the airways and acquire the normal *in vivo* morphology and key cellular and physiological processes[76]. Both models can be used for drug response assessment in individuals with CF in a personalized medicine approach by using, for instance, electrophysiological approaches in Ussing chambers and other molecular techniques[77,78].

1.4.2 Nasospheroids

HNECs are easily accessible by nasal brushings (which are less invasive than rectal biopsies) and are a good model to study CFTR *ex vivo*. Thus, recently, this allowed using differentiated HNECs to form spheroids *in vitro* that maintain the normal tissue morphology and differentiated state (ciliated cells are present and there is mucus production), and replicate better the physiological transport events than a cell monolayer[79,80]. There are nasospheroids developed that maintain a "lumen out" configuration (cilia are in contact with the culture medium) in which there is an increased accessibility of the drugs (e.g. VX-770) to the luminal side and an increase in CFTR function causes the organoid to shrink[79]. Conversely, there are also nasospheroids that retain a "lumen in" configuration and, in this case, CFTR rescue can be assessed by the level of spheroid swelling[80]. Both of these models can be used to study pharmacological manipulation of CFTR and drug rescue in a personalized medicine approach. Nevertheless, these kinds of 3D models have their limitations, such as a big variability in spheroid diameter and spheroid swelling that difficult analysis and quantification, and a short lifetime in culture.

1.4.3 3D Intestinal Organoids

Another model recently developed is the use of intestinal 3D organoids, which are formed from intestinal crypts, to assess CFTR function[81]. The intestinal crypts can be isolated from rectal biopsy tissue and contain at their base LGR5+ stem cells[82] that allow the generation of the intestinal organoids (Figure 1.7).

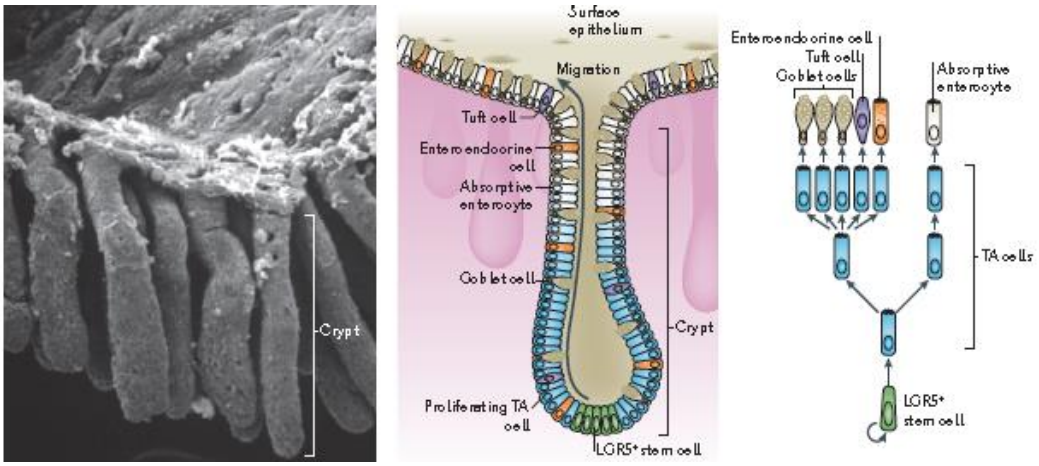

Figure 1.7 – Crypt structure, cell composition and distribution in the colon crypts. Structure of the colonic crypts seen by a scanning electron micrograph (left panel). LGR5^{+} stem cells at the crypt base generate rapidly proliferating transit-amplifying cells in the lower half of the crypt (middle panel). These cells subsequently differentiate into the mature lineages of the epithelium (Absorptive enterocytes, goblet cells, Tuft cells and enteroendocrine cells) as shown in the lineage tree (right panel). Adapted from Barker, Nick (2013).

These organoids are made from cells expressing high levels of CFTR and are a good tool for the indirect assessment of CFTR function using the forskolin-induced swelling assay (FIS)[81]. In this assay the organoids swell in presence of forskolin, a compound that activates the adenylyl cyclase enzyme and raises intracellular cAMP levels, activating CFTR. When CFTR is active, there is Cl^- exit through CFTR and Na^+ ions follow through the paracellular space resulting in fluid secretion to the lumen[83]. This swelling can be observed by using confocal microscopy and depends uniquely on CFTR activity, as shown by the use of CFTR inhibitors and modulators (Figure 1.8). Moreover, this assay can be used for the analysis of CFTR rescue after the use of modulators and even for drug development purposes[84–87]. These organoids can be expanded indefinitely in culture and can be selected to be roughly the same size, which are clear advantages when compared to the nasospheroids, and provide a more high-throuput analysis when compared with the HBECs/HNECs, the gold standard for *ex vivo* CFTR functional analysis[88].

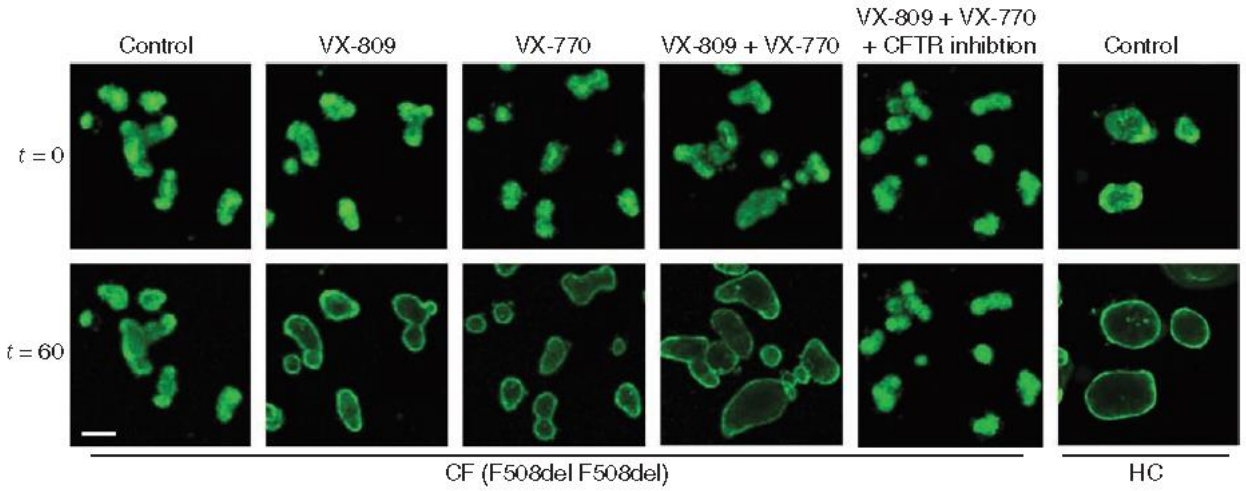

Figure 1.8 – Forskolin-induced swelling assay. At t=60 a visible swelling can be observed in CF individual (F508del homozygous) derived intestinal organoids treated with VX-809, VX-770 and even greater with the combination (VX-809/VX-770) when compared with the control. Using a CFTR inhibitor we can see no visible swelling from the organoids treated with the combination therapy, meaning that the swelling observed is CFTR-dependent. On the far right is represented the swelling of non-CF organoids. Retrieved from Dekkers, J. *et al* (2013).

1.4.4 2D Intestinal Monolayers

There is a disadvantage in using the FIS assay with the 3D organoids. In the case of WT and residual function genotypes, there is pre-swelling of the organoids which may undervalue the swelling of those organoids in response to CFTR modulators. Thus, one attractive alternative would be to split the 3D organoids and seed the cells in porous membrane supports to generate a monolayer of undifferentiated intestinal epithelial cells (Figure 1.9) that maintain CFTR activity and can be further differentiated into the several differentiated cell types found in the colon[89] (See Figure 1.7). Thus, this apparently versatile model could potentially be used to evaluate ion transport through CFTR or CFTR functional rescue by CFTR modulators in a personalized medicine approach using, for instance,

micro-Ussing chambers, as it is currently being done with the HBECs/HNECs. In these assays, ion flow can be measured directly as opposed to fluid secretion like in the 3D-organoids. Moreover, this model could be used to study intestinal epithelial differentiation and its effect on CFTR and other related ion channels, and how mutated CFTR can affect this differentiation process.

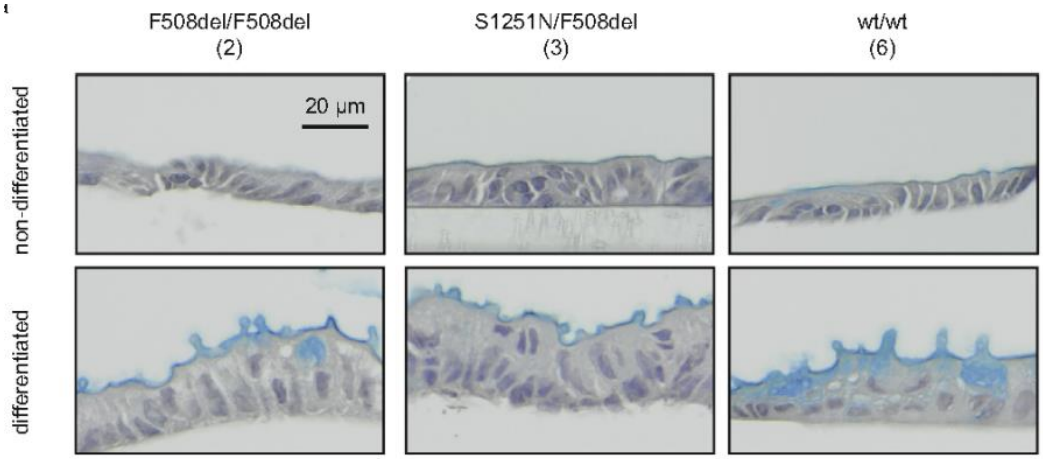

Figure 1.9 – Histological section of the 2D intestinal monolayers derived from 3D intestinal organoids. A monolayer of cells can be generated both with WT cells and CF patient derived cells and with differentiation increase in size, present villus-like structures and test positive for mucins and other glycoproteins with the Alcian Blue/Periodic Acid-Schiff staining. Adapted from Zomer-van Ommen, D.D. *et al* (2018).

2. Objectives

The main goals of this MSc project were:

1) **To characterize the novel 2D-intestinal cellular system by assessing:**

    a. The expression levels of plasma membrane (PM) proteins and ion channels present in the native tissue which are essential for Cl^- secretion;
    b. The differentiation status and progress of the 2D-intestinal epithelial monolayers by differentiation and proliferation markers under differentiation and non- differentiation conditions.

2) **To compare CFTR function in native tissues and primary cultures derived from individuals with CF and non-CF controls by:**

    a. Ussing chamber measurements of CFTR-mediated Cl^- secretion in fresh rectal biopsies;
    b. Forskolin-induced swelling (FIS) assay of intestinal 3D-organoids derived from rectal biopsies;
    c. Ussing chamber measurements of 2D-intestinal monolayers.

3) **To establish correlations between:**

    a. Values obtained in 2a, 2b and 2c for the same individuals as well as with other CF phenotypes from these individuals, in order to assess if 2D-intestinal monolayers recapitulate the properties of the more established models in predicting disease severity so as to validate them as good personalized cell models for CFTR function and thus for CF diagnosis/prognosis;
    b. Values obtained in 2b and 2c for the same individuals to determine whether 2D-intestinal monolayers recapitulate the CFTR modulator drugs found in 3D-organoids and thus assess whether they constitute a good model to predict individuals' drug responses.

3. Materials and Methods

Experiments described in this thesis were performed at the lab of Professor Dr. Margarida Amaral's group (FunGP, BioISI, Faculty of Sciences, University of Lisboa, Portugal) over the work period of one year.

3.1 Cell Culture

All cells were grown at 37 ºC in a 5% CO_2 and 95% air-humidified water saturated atmosphere. All cell culture was performed according to standard conditions.

3.1.1 Culture conditions of the human intestinal organoids

The crypts were isolated from human rectal biopsies and intestinal organoids were cultured as previously described[90] by Beekman's lab, Utrecht, The Netherlands. Briefly, biopsies were washed with PBS (Corning, USA) and then treated with 10 mM EDTA (Invitrogen, USA) in PBS for 90 min at 4ºC with continuous rocking. Later, the crypts containing the $LGR5^+$ positive stem cells were disrupted from the tissue by vigorously washing with PBS and saving the supernatant. Supernatant was centrifuged (230g, 5 min, 4 ºC), and pelleted crypts were re-suspended in 50% (v/v) Matrigel Matrix (Corning, USA), diluted in complete culture medium consisting of 20% (v/v) $F12^{ghp}$, 2% (v/v) B27 (Invitrogen, USA), 1.25 mM N-acetylcysteine (Sigma-Aldrich, USA), 50 ng/mL mouse epidermal growth factor (Invitrogen, USA), 50% (v/v) Wnt-3a-conditioned medium (lab-made), 10% (v/v) Noggin-conditioned medium (lab-made), 30% (v/v) R-spondin-conditioned medium (lab-made), 10 mM nicotinamide (Sigma-Aldrich, USA), 50 nM TGF-β inhibitor A83-01 (Tocris Bioscience, Germany), 10 µM P38 MAPK inhibitor SB202190 (Sigma-Aldrich, USA) and 0.2% Primocin antibiotic (InvivoGen, USA). Crypts were seeded in matrigel with a density of around 10-30 crypts per 10 µL matrigel droplet. The matrigel was polymerized for approximately 15 min at 37 ºC 5% CO_2 and the complete culture medium was then added. 0.1% Gentamicin (Sigma-Aldrich, USA) was added to culture medium for the first week of culture since passage 0 is more susceptible to contamination. Medium was refreshed every 2-3 days. Crypts rapidly close and bud into intestinal organoids after 7-10 days after which they were passaged (Figure 3.1). Culture medium was refreshed every 2-3 days and 3D organoids were passaged every 7-10 days.

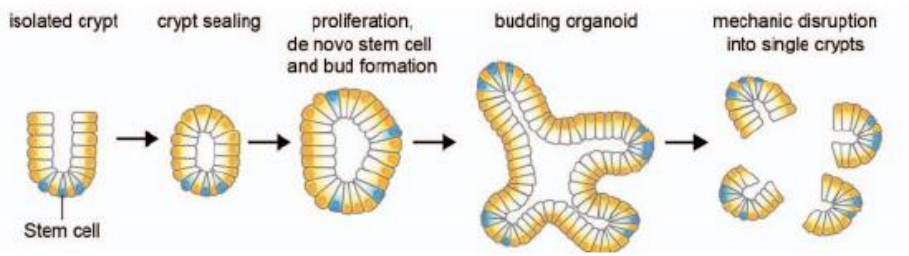

Figure 3.1 – Schematic representation of organoid generation from plated intestinal crypts from rectal biopsies. The plated crypts in matrigel matrix will start to close and proliferate. After 7-10 days they can be mechanically disrupted into smaller individual organoids that are further expanded. Retrieved from Dekkers, van der Ent & Beekman (2013).

3.1.2 Culture conditions of the 2D intestinal monolayers

The generation of the 2D intestinal epithelial cell monolayer in porous membrane filters was performed as already described by the Beekman's lab, Utrecht, The Netherlands[89]. The matrigel droplets containing the 3D organoids are disrupted and the organoids are pooled in $F12^{ghp}$ and spun down (230g, 5 min, 4ºC), after which the medium is removed. To the organoid pellet 500-700 µL of TrypLE Express 1X (Gibco, USA) is added and it is re-suspended with an F12 pre-coated p200 tip. The cells are incubated twice at 37 ºC for 2 min and disrupted with an F12 pre-coated tip after each incubation. The percentage of single cells is then checked (at least 90%) and the tube is put directly on ice and inactivated with the TrypLE inactivation solution (10% FBS in $F12^{ghp}$). The cells are centrifuged (282g, 5 min, 4 ºC, medium removed) and pooled, after which they are counted in a Neubauer counting chamber (the amount needed is 250,000 cells per filter). The cells are re-suspended in the first day culture medium (complete organoid medium (see section 3.1.1)) with the addition of 10 µM ROCK inhibitor Y-27632 (Selleck Chemicals, USA) and transferred to the apical side of Transwell® 6.5mm polyester 0.4 µm pore membrane inserts (Corning, USA). 600 µL of culture medium is added in the basolateral side. The next day, the filters are refreshed with complete organoid culture medium without ROCK inhibitor. On the fifth day, TEER is measured with a Millicell-ERS voltmeter with a chopstick electrode (Millipore, USA) and it should be at least $100\Omega xcm^2$. If so, Ussing chamber experiments can be performed on the undifferentiated monolayer (see section 3.2.2) or the filters can be switched to the differentiation medium. To differentiate the intestinal epithelial monolayer, filters are refreshed with the differentiation medium, which is the organoid culture medium without the Wnt-3a-conditioned medium, nicotinamide and the P38 MAPK inhibitor SB202190. Medium is refreshed every 2 days until the TEER values are, at least, $800\Omega xcm^2$, making the filters suitable for Ussing chamber experiments and indicating that a tighter cell monolayer is formed.

To test for the CFTR functional rescue, the undifferentiated monolayers are treated with CFTR correctors (3 µM VX-661 (Selleck Chemicals, USA) (dissolved in DMSO) or 0.05% DMSO (control condition)) for 24h and then analyzed in the Ussing chamber (see section 3.2.2).

3.2 Functional CFTR analysis

3.2.1 Measurement of CFTR Mediated Cl^- Secretion in Rectal Biopsies

Biopsies from individuals with CF were obtained in Hospital de Dona Estefânia (Lisbon, Portugal), Hospital Santa Maria (Lisbon, Portugal), Centro Hospitalar e Universitário de Coimbra and Motol University Hospital (Prague, Czech Republic). The colon preparation was performed by applying an enema of saline solution and superficial rectal mucosa biopsies (2.8 mm in diameter) were obtained by rectoscopy and forceps biopsy. The tissues were mounted in Ussing chamber inserts under a stereomicroscope using dissection forceps. The inserts were the fixed between the two half cells of the Micro-Ussing chambers, separating the apical from the basolateral bath solutions.

Transepithelial measurements were performed under open-circuit conditions in micro-Ussing chambers as described previously[73,75]. The tissue was perfused continuously with Ringer buffer (NaCl 145 mM, KH_2PO_4 0.4 mM, $K_2HPO_4 \bullet 3H_20$ 1.6 mM, D-glucose 5 mM, $MgCl_2 \bullet 6H_20$ 1 mM, Ca-gluconate$\bullet H_20$ 1.3 mM, pH 7.4, 280 mOsm/Kg) until a baseline is achieved, followed by the experimental solutions. Voltage (V_{te}) values were recorded at all times with Power Lab software (AD Instruments Inc., New Zealand). Values for V_{te} were referred to the basolateral side of the epithelium and resistance (R_{te}) was determined by applying short intermittent pulses (0.5 µA/s), measuring pulsated deviations in V_{te} and accounting for the area of the inserts. An empty insert was previously recorded to correct the measured values. Equivalent short-circuit currents ($I_{eq\text{-}sc}$) were calculated using Ohm's law ($I_{eq\text{-}sc} = V_{te}/ R_{te}$).

After a baseline is achieved, amiloride (Amil, 20 µM, apical) (Sigma-Aldrich, USA) was applied to block electrogenic Na^+ absorption through ENaC. Next, carbachol (CCH, 100 µM, basolateral) (Sigma-Aldrich, USA) was added to induce a cholinergic response which results in the activation of Ca^{2+}-activated basolateral K^+ ion channels, eliciting a driving force for Cl^- secretion. Indomethacin (Indo, 10 µM, basolateral) (Sigma-Aldrich) was then applied for 20 min to inhibit prostaglandin production and abolish endogenous cAMP production and thus CFTR-mediated Cl^- secretion. After this, CCH was applied again in the presence of Indo to induce only K^+ secretion. Following a new washout with Indo, an IBMX/Forskolin (IBMX/Fsk, 100 µM/2 µM, basolateral) (Sigma-Aldrich, USA) solution is added (in the presence of Indo) to stimulate cAMP production through the activation of the adenylyl cyclase enzyme and inhibit cAMP degradation through phosphodiesterase, thus activating CFTR-mediated Cl^- secretion. Lastly, CCH was added on top of the previous solutions for a cholinergic co-activation of CFTR.

3.2.2 Measurement of CFTR Mediated Cl^- Secretion in 2D Intestinal Monolayers

Intestinal epithelial 2D-monolayers grown in porous membrane supports (see section 2.1.2) were mounted between two round half-inserts with central open areas of 0.33 cm^2 and fixed in the middle of the two-half cells of the micro-Ussing chambers. To assess CFTR basal function, transepithelial

measurements were performed as described previously (see Section 3.2.1). After the addition of the solution containing Indo, IBMX, Fsk and CCH (10 µM, 100 µM, 2µM and 100 µM, basolateral), a solution of CFTR-specific inhibitor 172 ($CFTR_{inh}$-172, 30 µM, apical) (Cystic Fibrosis Foundation Therapeutics, USA) was applied to inhibit CFTR-mediated Cl^- secretion.

To evaluate CFTR functional rescue with the correctors and potentiators, the 2D monolayers were treated as described above (see section 3.2.1) and also mounted on the micro-Ussing chambers. Briefly, the cells were bathed in Ringer solution on both sides and, after a baseline is achieved, a solution of Amil (20µM, apical) was applied to block ENaC, as before. Next, IBMX/Fsk (100µM, 0.8µM, apical) was added to stimulate CFTR-mediated Cl^- secretion. To assess if it is possible to further potentiate CFTR activity, a solution of VX-770 (3µM, apical) (Selleck Chemicals, USA) was added. Lastly, $CFTR_{inh}$-172 (30 µM, apical) was added to assess the specificity of the cAMP-dependent activation. Three replicates of both conditions (VX-661 and DMSO) were tested and CFTR functional rescue was assessed by comparison of $\Delta_{Isc\text{-}IBMX/Fsk}$ values between control and treatment.

3.2.3 Forskolin-induced swelling assay

The FIS assay was performed as previously described[81]. The organoids from each individual with CF were seeded in matrigel in a pre-warmed 96-well culture plate and treated with the corrector VX-661 (3 µM) for 24h. Before the assay, serial dilutions of 0.02, 0.128, 0.8 and 5 µM solutions of Fsk alone or in combination with VX-770 (3 µM) were prepared. After the 24h incubation period, calcein green (3µM) (Invitrogen, USA) was added to the organoids and live cell imaging was carried out in a confocal microscope (Leica TCS SP8 Falcon, Leica Microsystems, Germany), at 37 ºC 5% CO_2 and two sets of images (fluorescence and bright field) were taken for 60 min with 10 min intervals (7 time points in total).

Using the set of fluorescence images, the organoid swelling was quantified using Cell Profiler software (Broad Institute's Imaging Platform, USA) and a pipeline developed by a lab member (Hugo Botelho). The results were plotted using Graph Pad Prism v6 software, in which the quantification of the surface area increase relative to t = 0 (normalized area, Figure 3.2) at different Fsk concentrations per treatment was averaged from two independent wells per assay. The results were then expressed as the absolute area under the curve (AUC) calculated from the normalized area (baseline = 100%, t = 60 min), averaged from a minimum of n=3 independent assays. Control organoids (CF114, F508del/S1251N) were also plated in each independent assay and the concentration of Fsk in which they respond (seen by the increase in AUC) to the potentiator VX-770, was the concentration used to evaluate treatment response and CFTR functional rescue. So, CFTR rescue was assessed by comparison of average AUC values between the control column (Fsk only) and the treatment columns (Fsk + VX-770, Fsk + VX-661, Fsk + VX-661/VX-770) for [Fsk] = 0.8 µM. Comparison with the control organoids was used to predict clinical benefit.

3.3 Expression Analysis

3.3.1 Gene Expression Analysis

3.3.1.1 RNA Purification

When the 3D-organoids were confluent and the filters reached the appropriate resistance, the RNA was collected from the cells and purified using the NZY Total RNA Isolation Kit (Nzytech, USA), according to manufacturer's instructions. RNA concentrations, as well as sample purity, were evaluated using a Nanodrop ND1000.

3.3.1.2 cDNA Synthesis

In order to perform RT-PCR assays, purified RNA was used to generate cDNA. This was performed with NZY M-MuLV Reverse Transcriptase (Nzytech, MB08301), according to manufacturer's instructions. Briefly, to 1µg of purified RNA a mix of 0.2 µg of random hexamers and a 0.5 mM mix of dNTPs (mix of dATP, dGTP, dCTP and dTTP, Nzytech, MB08701) were added. Next, the tubes were heated to 65ºC for 5 min and rapidly put on ice. Finally, 100 U of the reverse transcriptase, RNase inhibitor (Nzytech, MB08402) and 1x reaction buffer were added, and the reaction was performed in a thermocycler with the following conditions: 10 min at 25ºC, 50 min at 37ºC and 15 min at 70ºC.

3.3.1.3 RT-PCR

The reagents of the PCR reaction are described in table 3.1 and the reaction was carried out as described in table 3.2. The reaction conditions were optimized for each primer used (see table 3.3).

After the reaction, the PCR products were analyzed in a 2% agarose (SeaKem LE Agarose, Lonza) gel using a RedSafe nucleic acid staining solution (Intron Biotechnology). For size determination, the NZYDNA Ladder VI (Nzytech, MB089) was used.

Table 3.1 – Reagents used in the PCR reactions.

Reagent	Volume (µL)
H_20	until 25
Buffer 10x	2.5
$MgCl_2$ (50 mM)	0.75
dNTPs (0.5 mM)	0.08
Taq Polimerase (5U/µL)	0.1
Forward Primer (10 µM)	0.5
Reverse Primer (10 µM)	0.5
cDNA (50 ng/µL)	1

Table 3.2 – PCR programme used in the PCR reactions.

Step	Duration (min)	Temperature (ºC)
Initial Denaturation	5	95
Cycle - Denaturation	1	95
Cycle - Annealing	1	60/64
Cycle - Elongation	1	72
Final Elongation	5	72
Total of 40 Cycles		

Table 3.3 – Primer sequences used for each gene studied in this work and annealing temperature of each primer.

Gene	Forward Sequence 5'>3'	Reverse Sequence 5'>3'	Temperature of annealing (ºC)
CK18	CACAGTCTGCTGAGGTTGGA	GAGCTGCTCCATCTGTAGGG	60
CFTR	GCAAACTTGACTGAACTGGA	GGTGCTGGTGATAATCACTG	60
DRA	GAGAGCACAGGAGGCAAAAC	CAGCAAACTGCATCAGCATT	60
IK	CGGGAACAAGTGAACTCCAT	ACTGGGGAAAGTAGCCTGGT	60
BK	TAAGGACACCAGGAGGGTTG	GCTCTGAGACTTGGGGAGTG	64
E-cad	CGAGAGCTACACGTTCACGG	GGGTGTCGAGGGAAAAATAGG	64
NKCC1	CCAGAATTTGGTGGTGCAATT	TTTGGGTATGGCTGACTGAGG	60
LGR5	GAATCCCCTGCCCAGTCTC	ATTGAAGGCTTCGCAAATTCT	64
ENaC	TCCTACCCTCGTCCCTACCT	CCAGGAAGGAGAAAACCACA	64
SLC26A9	AGGTCACAGAGCCTCAGGAA	CTGAGCCTCAACTCCAGGTC	64
GAPDH	ATGGGGAAGGTGAAGGTCG	GGGGTCATTGATGGCAACAATA	64

3.3.2 Western Blot

When the 3D-intestinal organoids were confluent, matrigel was re-suspended and the organoids were pooled in $F12^{ghp}$ and centrifuged (230g, 5 min, 4ºC). The medium was removed and cold PBS was added to re-suspend the pellet, following another spin down (230g, 5 min, 4ºC). In order to obtain the lysates, the appropriate amount of lysis buffer (31.25 mM Tris HCl (Sigma-Aldrich, USA) pH 6.8; sodium dodecyl sulfate (SDS) 1.5% (v/v) (Gibco, USA); glycerol 5% (v/v) (Sigma-Aldrich, USA); bromophenol blue 0.02% (w/v) (Sigma-Aldrich, USA); dithiotreitol 50 mM (Sigma-Aldrich, USA); 1% Protease inhibitor cocktail (Roche, Germany)) was added to the pellet. Also, benzonase (Sigma-Aldrich, E1014) 25U/ml, in the presence of 3 mM $MgCl_2$, was added to shear the DNA. For the confluent 2D-monolayers, filters were washed with cold PBS on the apical side and 40 µL of lysis buffer was added to the apical side. The surface of the filters was scraped to collect protein lysates.

Both samples were then separated by SDS-PAGE using a 7% (w/v) separating gel (Tris-HCl 375 mM pH 8.8; acrylamide:bisacrylamide 7% (v/v) (Bio-Rad, USA); glycerol 0.1% (v/v); SDS 0.1% (v/v); ammonium persulfate (APS) 0.075% (v/v) (Bio-Rad, USA); tetramethylethylenediamine (TEMED) 0.06% (v/v) (Sigma-Aldrich, USA)) and a 4% stacking gel (Tris-HCL 125 mM pH 6.8; acrylamide:bisacrylamide 4% (v/v); SDS 0.1% (v/v); APS 0.075% (v/v); TEMED 0.08% (v/v)). The electrophoresis was run on a Tris-Glycine-SDS buffer (Bio-Rad, USA) at 60-100V until the migration front reached the end of the gel. The separating gel was transferred to a polivinylidene difluoride membrane (Merck Millipore, USA) using a Tris-Glycine buffer (Bio-Rad, USA), at 400 mV for 1h30min. The membranes (except for CFTR analysis) were blocked for, at least 30 min with 5% (w/v) skimmed milk (Nestlé, Molico, Switzerland) in PBS supplemented with Tween 20 0.1% (v/v) (PBS-T) and then incubated overnight at 4ºC with primary antibodies (Table 3.4) diluted in 5% milk in PBS-T. After washing 3 times for 10 min each with PBS-T, the membranes were incubated with the horseradish peroxidase (HRP)-conjugated secondary antibody (Table 3.5) 1h at room temperature. For the CFTR analysis, the previous steps were made using TBS-T and a 1% (w/v) skimmed milk in TBS-T. To reveal the bands, a chemiluminescent reaction was made with a mixture of peroxide:luminol/enhancer solution 1:1 (Bio-Rad, USA) and it was detected through a Chemidoc XRS plus analyzer (Bio-Rad, USA). Quantification of the intensity of the bands was performed using the ImageLab software (Bio-Rad, USA).

Table 3.4 – Primary antibodies used in this work.

Primary Antibodies				
Target	**Dilution**	**Host**	**Company**	**Reference**
CFTR	1:500	Mouse	CFF	596
N-cadherin	1:500	Mouse	BD Biosciences	610920
E-cadherin	1:5000	Mouse	BD Transduction Lab	610181
Cytokeratin-18	1:1000	Mouse	Santa Cruz	sc-32329
KI-67	1:500	Rabbit	Abcam	ab16667
Na^+K^+ ATPase α	1:1000	Mouse	Santa Cruz	sc-48345
GAPDH	1:10000	Mouse	Abcam	ab8245

Table 3.5 – Secondary antibodies used in this work.

Secondary Antibodies					
Antibody	**Target**	**Dilution**	**Host**	**Company**	**Reference**
(H+L)-HRP Conjugate	Mouse IgG	1:3000	Goat	Bio-Rad	170-6515
(H+L)-HRP Conjugate	Rabbit IgG	1:3000	Goat	Bio-Rad	170-6516

3.4 Statistical Analyses

Statistical differences were calculated using Student's t-test or analysis of variance (ANOVA) as suitable. Data are expressed as mean ± standard deviation (SD). Pearson coefficients (*r*, for normal samples) and Spearman coefficients (ρ, for not normal samples) were used to find correlations and partial correlations amongst patients' clinical data and laboratory assessed CFTR function parameters. *P*-values of <0.05 were considered significant.

4. Results and Discussion

4.1 Description of Phenotypes of Individuals with CF

For this project, samples were collected from individuals with CF at several centers, namely individuals CFL54/59/61/65 are from Motol University Hospital (Prague, Czech Republic), CFL70 is from Hospital de Dona Estefânia (Lisboa, Portugal), CFL75 is from Centro Hospitalar e Universitário de Coimbra (Coimbra, Portugal) and CFL80 is from Hospital de Santa Maria (Lisboa, Portugal). An overview of laboratory, clinical data and biologic material analyzed from these individuals with CF is presented in table 4.1.

Table 4.1 – Overview of data from individuals with CF: Individual's codes; *CFTR* genotypes; sex (M = male, F = female); age at study; age at diagnosis (NBS = newborn screening); fecal elastase E1 values (FEE, µg/g stool); exocrine pancreatic function (PS = pancreatic sufficient, PI = pancreatic insufficient); forced expiratory volume in 1 sec in percentage predicted (FEV_1, %) and sweat [Cl^-] (mmol/L) at time of samples collection; samples analyzed (rectal biopsies (B), intestinal organoids (3D), and 2D intestinal monolayers (2D)). Clinical/laboratory data was obtained at the hospital of samples collection.

Individual Code	CFTR Genotype	Sex	Age at Study	Age at Diagnosis	FEE	Exocrine pancreatic function	FEV_1	Sweat [Cl^-]	Samples analyzed
CFL54	F508del/R347P	F	18	1	351.0	PS	64	84.6	B, 3D, 2D
CFL59	F508del/S955P	M	7	0 (NBS)	500.0	PS	95	56.5	B, 3D, 2D
CFL61	F508del/G542X	M	8	0 (NBS)	1.0	PI	95	82.7	B, 2D
CFL65	F508del/F508del	M	13	2	1.0	PI	89	117.0	B, 3D, 2D
CFL70	F508del/A561E	M	1	0	30	PI	101	112	B, 3D, 2D
CFL75	F508del/R334W	F	8	0	500	PS	124	91.0	B, 3D, 2D
CFL80	F508del/F508del	F	13	2	1	PI	61	125.0	B, 3D, 2D

4.2 Characterization of the 2D Intestinal Monolayers

In order to understand whether this novel cellular model can be used for further functional studies in addition or replacement of the models currently used to analyze CFTR function (sections 4.3 and 4.4), a series of gene and protein expression analysis were made by using RT-PCR and WB. Since the 2D-monolayers can be cultured in both non-differentiating and differentiating conditions, the objective was to understand if the same ion channels were expressed in the 2D-monolayers grown under these two different conditions/ differentiation states and to compare their expression patterns with those of the 3D-intestinal organoid model already in use. Another goal was to compare CFTR gene and protein levels among the three models analyzed. The overall results can be observed in the next subsections.

4.2.1 Gene Expression Analysis Comparison Among Models

As mentioned before, ENaC function is related with CFTR and, in case of CFTR functional loss, ENaC is upregulated in the airways, which leads to Na^+ hyper-absorption. ENaC consists in three subunits (α, β e γ) which assemble in a 1:1:1 heterotrimers[91]. In the colon, ENaC is upregulated and the insertion of its β-subunit promotes ENaC activity[92]. Therefore, for these analyses ENaC β-subunit was targeted. Several other ion channels and transporters are involved in Cl^- secretion. Cl^- entry across the basolateral membrane of secretory epithelia is mediated mainly by the $Na^+/K^+/2Cl^-$ cotransporter 1 (NKCC1) and, ultimately, the rate of basolateral Cl^- entry via NKCC1 determines the overall rate of Cl^- secretion[93]. The activity of K^+ channels is also necessary for Cl^- secretion. Ion flux studies under voltage clamp conditions show that K^+ channels localized on the basolateral membranes provide the driving force for active Cl^- secretion in trachea and colon[94]. The intermediate conductance (IK) K^+ channel (encoded by the *KCNN4* gene) is a Ca^{2+}-activated K^+ channel located in both apical and basolateral membranes of the human colonic epithelial cells. The large conductance (BK) K^+ channel is also a Ca^{2+}-activated K^+ channel but is located mainly in the apical membrane of epithelial cells[95,96]. Solute-linked carrier(SLC)26A9 is a cell membrane transporter that interacts with CFTR by its STAS domain[97], and its presence results in an increased agonist-stimulated anion conductance in airway cells in a CFTR-dependent way[98]. This member of the SLC family has also been reported as a strong modifier gene in CF intestinal and pancreatic disease[99,100]. SLC26A3 (DRA) is a $2Cl^-/HCO_3^-$ exchanger in epithelial cells and is potently activated by CFTR[101]. These channels were also analyzed by RT-PCR. Finally, to check for the differentiation status of the cells, LGR5 was used in addition to CK18 and E-cad. LGR5 is a stem cell marker that is found in the crypt base columnar cells but not in the more differentiated cell types of the colon[82], making it a good marker to assess the differentiation of the 2D monolayers.

Firstly, in order to characterize the presence of *CFTR*, CFTR-related ion channels, other channels that are essential for Cl^- secretion and some differentiation markers, gene expression analyses were made using the fresh tissue (rectal biopsies), 3D intestinal organoids and 2D intestinal monolayers (both undifferentiated and differentiated). The overall results can be seen in Figure 4.1.

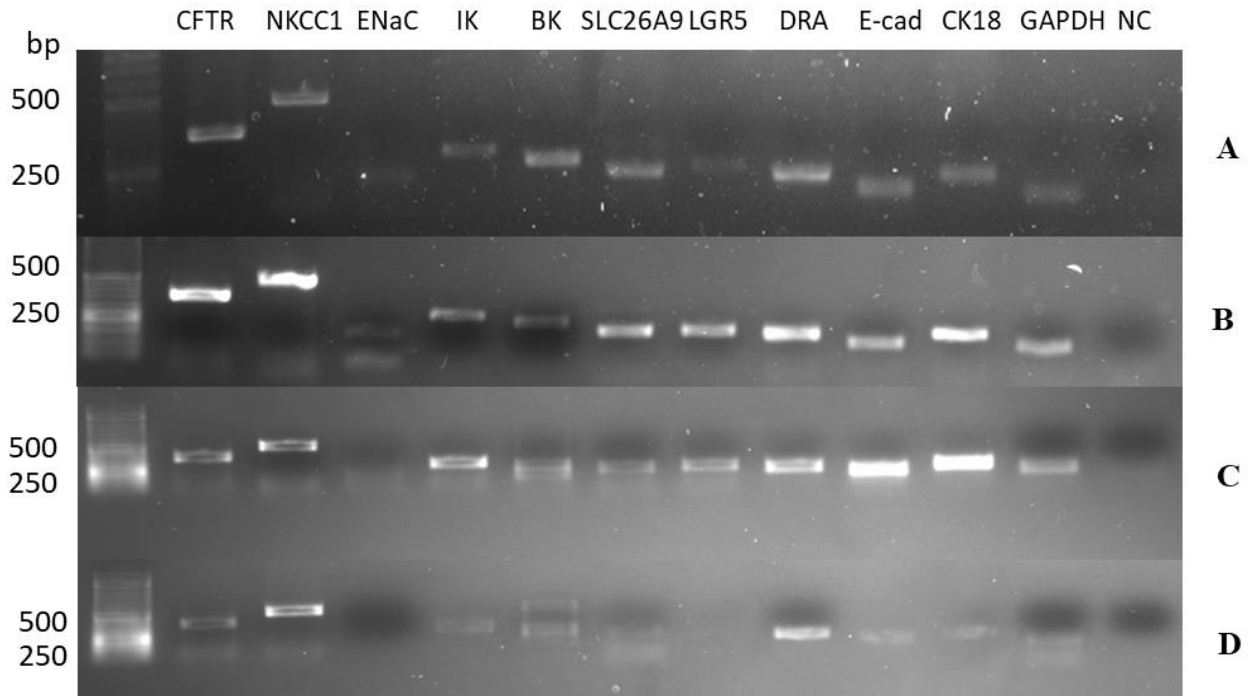

Figure 4.1 - Gene expression analysis of CFTR and related membrane proteins and ion channels, and differentiation markers. Gene expression was analyzed for a WT donor: **A** - rectal biopsy; **B** – 3D-organoids; **C** - Undifferentiated 2D-monolayers; **D** – Differentiated 2D-monolayers. The expression of Cl^- channels and proteins essential for Cl^- secretion, such as *CFTR*, *NKCC1*, *IK*, *BK* and *SLC26A9* were analyzed. *ENaC* expression was also analyzed as well as *DRA*, which is related with HCO_3^- secretion. Differentiation markers like *LGR5*, *E-cad* and *CK18* were analyzed. *GAPDH* levels were used as a control. NC – Negative Control.

By comparison of the gene expression results from the fresh biopsies and the 3D-organoids, we can observe that all genes analyzed are expressed in both samples. Since the biopsies are composed by several cell types of the mucosa (stem cells of the crypts and differentiated cells of the *villi*) and the 3D-organoids are composed by several crypt cells, it was expected that the gene expression on both samples would be different. However, the results show that for example *CFTR* and *NKCC1* are both expressed in the biopsies and in the 3D-organoids, as well as LGR5, which is in agreement with the existence of stem crypt cells in the native tissue. *ENaC* seems to be very low expressed in both models, which is in agreement with the lack of amiloride-sensitive currents observed in the WT rectal biopsies analysis in the Ussing chamber (see section 4.2.3). Both *IK* and *BK* channels are expressed in the biopsies and 3D-organoids, which are crucial for the CFTR function analysis in the rectal biopsies, generating CCH-stimulated positive currents in individuals with CF (see section 4.4). Moreover, *SLC26A9* is expressed, making the 3D organoids a possible tool for the analysis of this alternative Cl^- transporter. Analyzing the undifferentiated intestinal 2D-monolayers, we can observe that the genes that are expressed are the same as those expressed in the 3D organoids. This is expected since these monolayers are derived from the individual's 3D organoids. In this case, the change in culture conditions to permeable membrane supports does not alter gene expression. In the differentiated intestinal 2D-monolayers, however, there is one striking difference which is the loss of the stem cell marker of the crypt-base cells *LGR5*. This result indicates that the differentiation process has occurred as expected and that the stem cells present in the fresh biopsies, 3D intestinal organoids and undifferentiated 2D-monolayers are no longer present in the

differentiated intestinal 2D-monolayers. The potassium channels *IK* and *BK* are still expressed in both monolayers, so there should be K^+ secretion in both undifferentiated and differentiated conditions. As observed in the rectal biopsies and 3D-organoids, *ENaC* expression is still very low and *CFTR* and *NKCC1* genes are still expressed in both monolayers. Nevertheless, CFTR, CK18 and E-cad protein levels were assessed to further characterize these new models.

4.2.2 Biochemical Characterization During Differentiation of the 2D Intestinal Epithelial Monolayer

To characterize the differentiation and/or proliferative state of the 2D-monolayers, which can be cultured in non-differentiating and differentiating conditions, several analyses to assess the expression of a series of proteins were made by WB. The variation of CFTR protein levels among the three models was also analyzed.

In order to assess the differentiation state and infer the epithelial polarization, levels of E-cadherin (E-cad), N-cadherin (N-cad) and Cytokeratin 18 (CK18) were assessed (Figure 4.2). E-cad and N-cad are cell adhesion molecules that are present in adherens junctions, characteristic of polarized epithelial cells. N-cad is mostly expressed in mesenchymal-type cells while E-cad is expressed in highly differentiated epithelial cells, which means that after differentiation there is an increase in expression of E-cad and a decrease in N-cad[102]. CK18 is a cytoskeleton protein of the intermediate filament family. It is mainly a structural protein and is largely expressed in polarized and highly differentiated epithelial cells[103]. To assess the proliferative state of these cells, Ki-67 protein was analyzed. This protein was first identified in Hodgkin lymphoma cell nuclei as an antigen that is highly expressed in proliferative cells and strongly downregulated in quiescent and resting cells in the G0-phase[104,105]. Since then, Ki-67 has become a widely used cell proliferation marker.

WB analysis (Figure 4.2) showed that there is a decrease in Ki-67 protein levels in the differentiated 2D-monolayers when compared with the 3D-organoids and the undifferentiated 2D-monolayers (grown in expansion media, i.e., non-differentiating conditions). Therefore, we can conclude that the 3D-organoids and the undifferentiated 2D-monolayers are cells in highly proliferative states. When we switch the 2D-monolayers to the differentiation media for 6 days, the cells lose their proliferative status, as shown by the decrease in the levels of Ki-67. We can also see that E-cad and CK18 are elevated in the 2D-differentiated cells and N-cad is diminished. This is in agreement with the fact that the stem-like cells present in the bottom of the crypts (that are able to form the 3D-organoids) undergo differentiation until they reach the more differentiated cell types of the *villi*, such as enterocytes or goblet cells. Thus, our results show that the 2D-undifferentiated monolayers seem to be composed of crypt-base stem cells and transit-amplifying progenitor cells, and the 2D-differentiated monolayers of mainly enterocytes and other differentiated cells, such as goblet cells.

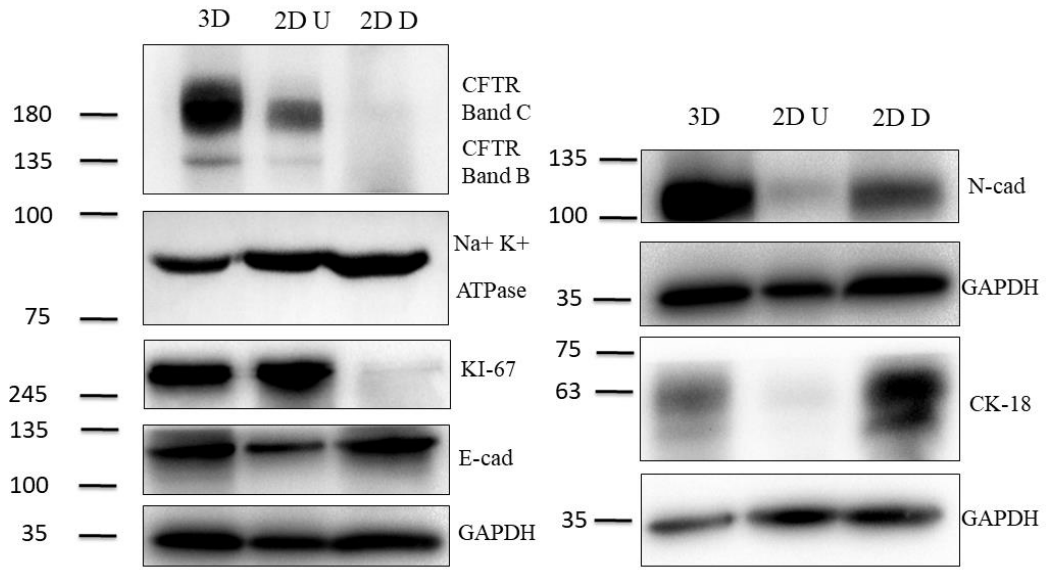

Figure 4.2 – WB analysis of WT 2D undifferentiated and differentiated monolayers and 3D-organoids. For the assessment of the differentiation state amongst the 3 models, the levels of E-cad, N-cad and CK-18 were analyzed. The proliferation state of the cells was assessed by the protein levels of Ki-67. Also, CFTR protein levels were analyzed amongst the 3 models. GAPDH and Na^+ K^+ ATPase were used as loading controls. 3D – 3D organoids; 2D U – 2D undifferentiated monolayers; 2D D – 2D differentiated monolayers.

To characterize CFTR protein expression in this novel model we also analyzed CFTR protein expression by WB. Typically, WT-CFTR originates 2 bands in WB that depend on the glycosylation state of the protein. A more prominent band with 170-180 kDa corresponding to the fully glycosylated, mature CFTR (band C) and a fainter band of 150 kDa which is the ER core-glycosylated form of the protein (band B)[106]. Both the 3D-organoids and 2D-undifferentiated monolayers present an extensive CFTR band C and a fainter band B, suggesting high levels of processing efficiency and mature CFTR protein in the membrane. In the differentiated 2D-intestinal monolayers we can see a significant decrease in CFTR protein levels. It was described that CFTR expression in the large intestine is mainly found in the base of the crypts[107–110], where the cells are essentially enrolled in fluid secretion whereas the enterocytes in the intestinal *villi* are responsible for absorptive processes and CFTR expression decreases[111]. Here, the 3D-organoids and 2D-undifferentiated monolayers (mainly composed of $LGR5^+$ stem cells) are representative of the crypt cells of the colon that express high levels of CFTR. Therefore, the 2D-differentiated monolayers consist of the differentiated cells of the colon in which CFTR expression is much lower. Thus, based on this information, for functional studies of CFTR activity and CFTR-mediated fluid secretion the 2D-undifferentiated monolayer seems to be the most adequate model, along with the already used 3D-intestinal organoids. Therefore, we have used these cells throughout our subsequent studies.

4.2.3 Analysis of WT CFTR Basal Activity Using Ussing Chamber Experiments in 2D Intestinal Cell Cultures

After confirming CFTR expression in the 2D-monolayers, CFTR function was assessed by Ussing chamber measurements, where samples from several individuals with CF with different mutations and non-CF controls were analyzed. Before the assessment of drug response in these intestinal 2D-cell cultures (see section 4.3), here we aimed to assess the basal CFTR activity of the 2D-monolayers in the Ussing chamber. For this, we used undifferentiated and differentiated monolayers from a WT donor, so as to compare the respective levels of CFTR function. The results are depicted in Figure 4.3.

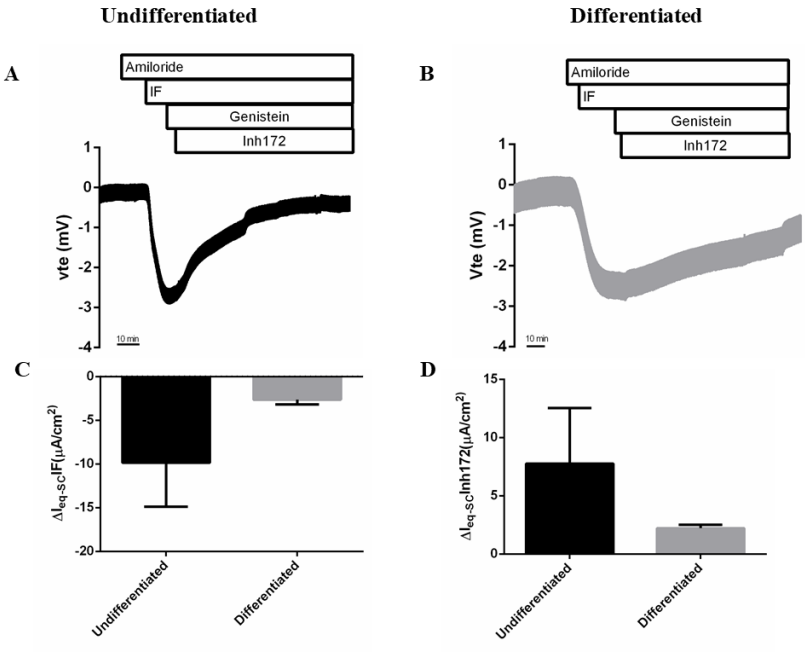

Figure 4.3 – Results from Ussing chamber measurements for basal activity in 2D-intestinal monolayers from a WT donor. Representative original recordings of the effects of cAMP-dependent (IBMX/Fsk (IF), 100μM/2μM, apical) activation, CFTR potentiation (Genistein, 25 μM, apical) and CFTR-specific inhibition (CFTRinh-172 (Inh172), 30μM, apical) on transepithelial voltage (Vte) in 2D intestinal epithelial monolayers from a WT donor. Experiments were performed in the presence of Amiloride (20 μM, apical) for: (A) undifferentiated monolayers; (B) differentiated monolayers (after 6 days of culture in differentiation media). Summary of activated equivalent short-circuit currents (ΔIeq-sc) upon: (C) IF addition for the two models; (D) Inh172 addition for the two models. Data represent the mean of measurements on 4 replicates per condition ± SD. The comparisons in (C) and (D) are not significant according to an unpaired T-test.

After adding Amil, we can immediately see that there is no change in voltage (Figure 4.3A,B), which is not surprising given the low amount of ENaC mRNA observed (Figure 4.3). Combined, these results indicate that ENaC expression is very low and thus we could not measure any function. When IBMX/Fsk (IF) is added in both conditions, in order to raise the levels of intracellular cAMP and elicit CFTR-mediated Cl^- secretion, we see a negative deflection, as expected when using a WT donor sample due to active CFTR (Figure 4.3A,B). However, looking at the amount of current produced by IF stimulation on both conditions, we do see a decrease in CFTR-dependent current in the differentiated 2D-monolayers, although not significant (Figure 4.3C). This effect is also seen in the CFTRinh-172 response

(Figure 4.3D). This can be explained by the lower levels of CFTR protein expression observed upon differentiation as discussed in section 4.2.1, which is also in agreement with what is known about CFTR expression and function in the crypt-base stem cells vs. differentiated villi cells. Nevertheless, the currents measured are not as low as would be suggested by the low expression levels of CFTR protein in the differentiated 2D-monolayers. This could be due to differences in differentiation of the 2D-monolayers analyzed in the Ussing chamber vs. the ones analyzed in the WB or, more likely the fact that even low expression of WT CFTRs may be enough to produce a considerable CFTR-generated current.

As this chapter's goal was to characterize the 2D-monolayers derived from 3D-organoids, we can reach several conclusions from these preliminary experiments:

1) We can observe from the differentiation markers analysis that these 2D-monolayers differentiate quickly, as after only 6 days in differentiation media we observed a significant decrease in cell proliferation and an increase in proteins characteristic of polarized epithelial cells, namely E-cad and CK18;
2) Upon intestinal epithelial differentiation, CFTR protein levels decrease, which is also expected due to the change in CFTR expression in the colon crypts/*villi*.
3) From the functional analyses, we determined that the CFTR-mediated Cl^- currents are diminished in the differentiated vs non-differentiated monolayers.

Therefore, for the subsequent experiments, we used undifferentiated 2D-intestinal monolayers for further assessment of CFTR function and rescue in 2D-monolayers with different *CFTR* genotypes.

4.3 Comparison of CFTR Function Assessment Between Rectal Biopsies and 2D Intestinal Monolayers

Our aim here was to compare the basal CFTR function assessment (with no drugs) in the rectal biopsies from individuals with CF with the basal function that can be assessed in the 2D-intestinal monolayers of the same individuals. The potential use of these 2D-monolayers for the same purpose of the fresh tissue would bring certain advantages. We would not be dependent on tissue quality of the biopsy and also would not be restrained by the short-time limitations of tissue viability, preventing the need to collect the biopsies as close as possible to the laboratory where the analysis will be performed. This is of particular interest for centres which do not have electrophysiological tests in place, as they could benefit from shipping the samples to others which have. Moreover, given these limitations, using the 2D-monolayers would avoid the need to repeat the biopsies upon failure of the analysis, ruling out the necessity of exposing the individual to a second invasive and uncomfortable procedure.

4.3.1 WT

To first compare CFTR function in the 2D-monolayers of intestinal cells derived from a non-CF (wt/wt) donor with that in the rectal biopsies, CFTR function was measured in the Ussing chamber using the same protocol (Figure 4.4).

Ussing chamber recordings of transepithelial voltage of the wt/wt donor rectal biopsies (Figure 4.4A) show a transient negative deflection upon basolateral cholinergic stimulation with CCH, evidencing a predominance of CFTR-mediated Cl^- currents. Sequentially, the second CCH stimulation (now in the presence of indomethacin, Indo) shows a transient positive voltage deflection due to global luminal K^+ secretion, since in this case, Cl^- secretion is inhibited due to the abolishment of intracellular cAMP production by Indo. This effect has been demonstrated to be a valid approach to assess CFTR-mediated Cl^- secretion[75]. Subsequently, and still in the presence of Indo, IBMX/Fsk was added to elicit an increase in intracellular cAMP concentration, thus stimulating CFTR and generating a negative voltage due to CFTR activity. Finally, a third CCH stimulation was performed in the presence of the previous *stimuli* (Fsk/IBMX) and provoked a very large and transient negative peak, demonstrative of CFTR maximal activation. These results evidence the typical response of a wt-CFTR using this protocol[75].

Transepithelial voltage of the wt 2D-intestinal monolayers was also recorded in the Ussing chamber in the exact same conditions (Figure 4.4B). The first CCH stimulation in the 2D-monolayers produced the same type of response as in the fresh tissue, despite with some delay. However, the effect of the second CCH stimulation in the 2D-monolayers was different from that in the fresh tissue. In the rectal biopsies, the second CCH stimulation activates Ca^{2+}-gated K^+ channels that are present in the apical and basolateral membranes of colonic epithelial cells[112]. As the response observed in the rectal biopsies is a positive voltage deflection, we can conclude that the luminal K^+ secretion is larger than the basolateral absorption, so the net current elicited by K^+ exit is positive. In the case of the 2D-monolayers, we observed a negative voltage deflection. This could eventually be due to larger K^+ currents corresponding to exit at the basolateral side, causing the net current to be negative. Further experiments are necessary to confirm this hypothesis. Upon stimulation with IBMX/Fsk, a negative deflection was observed in the monolayers, as expected, confirming CFTR function, and this was larger than that observed in the rectal biopsies. Finally, CCH elicited in the 2D-intestinal monolayers a large and brief negative voltage peak as observed in the rectal biopsies. Overall, we can confirm that the effects seen in the 2D-intestinal monolayers are similar to those observed in the fresh tissue, despite the discrepancy observed in the CCH stimulation in the presence of Indo.

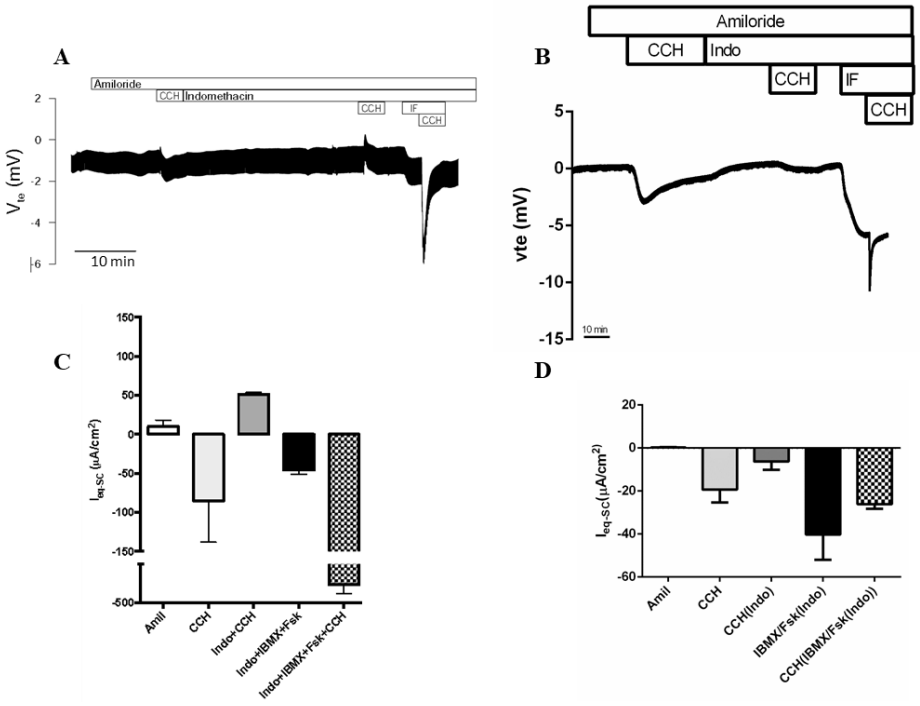

Figure 4.4 – Results from Ussing chamber measurements in rectal biopsies and 2D-monolayers from a WT donor. Representative original recording of the effects of cholinergic (CCH, 100 µM, basolateral) and cAMP-dependent (IBMX/Fsk, 100µM/2µM, basolateral) activation on transepithelial voltage (Vte) in a WT donor: (A) Rectal biopsies; (B) Undifferentiated 2D intestinal monolayers. Experiments were performed in the presence of Amiloride (Amil, 20 µM, apical) and/or Amiloride + Indomethacin (Indo, 10 µM, basolateral), as indicated in the figure. (C) and (D) Summary of activated equivalent short-circuit currents (ΔIeq-sc) for Amil (ΔIeq-sc,Amil), basal CCH (ΔIeq-sc,CCH), CCH + Indo (ΔIeq-sc,CCH(Indo)), IBMX/Fsk + Indo (ΔIeq-sc,IBMX/Fsk(Indo)) and CCH following IBMX/Fsk application (ΔIeq-sc,CCH(IBMX/Fsk(Indo))); data represent the mean of measurements of 3 replicates ± SD.

Following the Ussing chamber experiments with the undifferentiated 2D-monolayers, we applied the same protocol used in the biopsies to the differentiated 2D-intestinal monolayers to assess how the reduced protein levels of CFTR (as described early in section 4.2.2) affect the Ussing chamber readout (Figure 4.5).

If we compare the undifferentiated 2D-monolayer tracing (Figure 4.5B) with that of the differentiated 2D-monolayer tracing (Figure 4.5A), we can observe that for the first CCH stimulation the responses are quite similar, albeit smaller but faster in the differentiated 2D-monolayers. This may be due to the lower levels of CFTR and, consequently, the lack of the CFTR characteristic kinetics. However, when we observe the second stimulation of CCH (in the presence of Indo to ablate the intracellular levels of cAMP), the negative deflection produced in the 2D-differentiated monolayers is both larger and faster when compared with the that in the 2D-undifferentiated monolayers, which may be CFTR-related or influenced by the presence of different K^+ channels or still due to differences in the expression levels of these (or other) channels. Accordingly, and because we still do not know if the same ion channels, namely K^+ channels, are equally present in the 2D-differentiated and 2D-undifferentiated monolayers, as well as their distribution, we cannot yet attribute the difference observed in this CCH stimulation to reduced levels of CFTR only. Moreover, the first and second CCH responses in the differentiated 2D-monolayers (Figure 4.5B) produce very similar currents, further supporting the lack of role of cAMP stimulation in these responses. Then, when we stimulate both types of 2D-monolayers with IBMX/Fsk, still in the

presence of Indo, we can observe that the voltage change is much smaller in the 2D-differentiated monolayers, reinforcing that the reduced cAMP-stimulated CFTR-mediated Cl^- secretion in these is consistent with the decreased protein expression (see section 4.2.2). Next, when the 2D-monolayers were further stimulated with CCH under IBMX/Fsk, we can observe a negative peak in voltage that is bigger in the 2D-differentiated cells than in the 2D-undifferentiated cells. This can be due to the fact that the IBMX/Fsk stimulation in the 2D-undifferentiated monolayers already induces near-maximal activation of the CFTR protein. Moreover, as the IBMX/Fsk response is smaller in the differentiated monolayers, then the cells are not so depolarized and CCH further depolarizes the cells, in a transient response that is rapidly restored to the levels of Indo + IBMX/Fsk stimulation. However, the fact that in the 2D-differentiated monolayer experiment, the final addition of $CFTR_{inh}$-172 ablates the IF-specific current, suggests that this response is CFTR-specific, unless, as some authors report, the $CFTR_{inh}$-172 is not entirely specific for the CFTR ion channel[113].

Overall, these results can assist in the further characterization of undifferentiated and differentiated 2D-monolayers, although more experiments testing other conditions should be performed in order to understand the physiology and corresponding bioelectrical properties of these 3D-organoid derived cells.

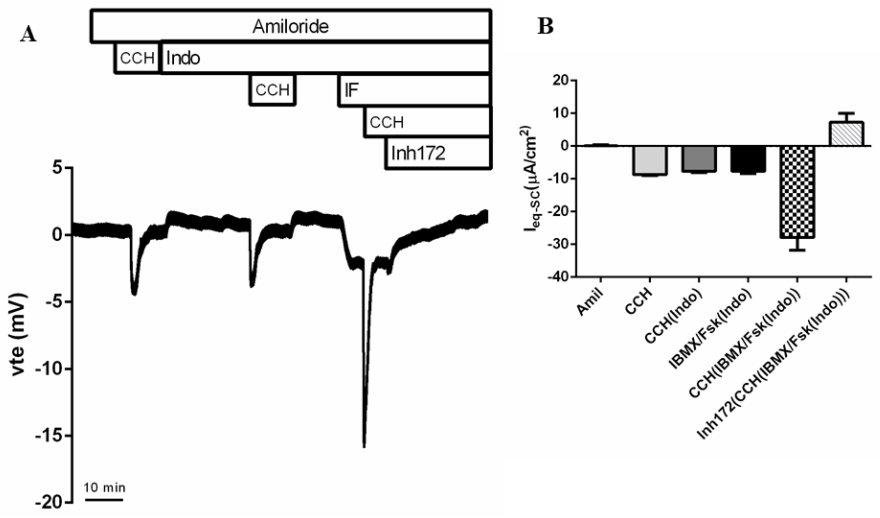

Figure 4.5 - Results from Ussing chamber measurements in differentiated 2D-monolayers from a WT donor. Representative original recording of the effects of cholinergic (CCH, 100 µM, basolateral) and cAMP-dependent (IBMX/Fsk, 100µM/2µM, basolateral) activation on transepithelial voltage (Vte) in the WT donor: (A) differentiated intestinal epithelial monolayers. Experiments were performed in the presence of Amiloride (Amil, 20 µM, apical) and/or Amiloride + Indomethacin (Indo, 10 µM, basolateral), as indicated in the figure. (B) Summary of activated equivalent short-circuit currents (ΔIeq-sc) for Amil (ΔIeq-sc,Amil), basal CCH (ΔIeq-sc,CCH), CCH + Indo (ΔIeq-sc,CCH(Indo)), IBMX/Fsk + Indo (ΔIeq-sc,IBMX/Fsk(Indo)), CCH following IBMX/Fsk application (ΔIeq-sc,CCH(IBMX/Fsk(Indo))) and Inh172 following CCH/IBMX/Fsk (ΔIeq-sc, Inh172 (CCH(IBMX/Fsk(Indo))) application; data represent the mean of measurements of 3 replicates ± SD.

4.3.2 Residual CFTR Function Mutations

4.3.2.1 F508del/S955P

To confirm whether the results seen in the previous section were not restricted to wt/wt samples and how mutations in CFTR affect the Ussing chamber readouts of 2D-monolayers derived from 3D-organoids, 2D-monolayers from an individual (CFL59) with a high residual function mutation (F508del/S955P genotype) were analyzed and the tracings were compared with those of rectal biopsies from the same individual (Figure 4.6).

Analysis of the Ussing chamber recordings of voltage measurements in rectal biopsies (Figure 4.6A) shows a positive K^+ secretory response after basal cholinergic stimulation by CCH, already indicating a lack of Cl^- secretion through CFTR. After IBMX/Fsk addition to stimulate cAMP-dependent Cl^- secretion, there is a negative deflection in voltage meaning that there is residual CFTR activity that is further increased by the basal stimulation with CCH. This last CCH stimulation is presented in a monophasic manner, much like a wt-CFTR response (see figure 1.6A). However, the overall current is ~7.5% of that in wt/wt CFTR biopsies. This means that this individual has a relatively high CFTR residual activity for an individual with CF.

In the analysis of the CFL59 2D-monolayers, unlike the rectal biopsies, in the first two basal CCH stimulations we observe two negative deflections instead of two positive responses (Figure 4.6B). The second CCH negative deflection (in the presence of Indo) is smaller than the first CCH, and this might be explained by the fact that, in the first stimulation, there could be the combination of currents from CFTR-mediated Cl^- secretion and a larger basolateral K^+ currents corresponding to K^+ exit, while in the second CCH stimulation only the basolateral K^+ exit is producing those smaller currents. The stimulation with IBMX/Fsk shows a clear CFTR activation and the final CCH increased the current only slightly, perhaps due to "near-to-maximal" activation with just IBMX/Fsk. Still, when compared with the ones in the rectal biopsies, the overall currents calculated for the 2D-monolayers are smaller. These last currents were abolished by the use of $CFTR_{inh}$-172, which indicates that they were generated due to CFTR-mediated Cl^- secretion, suggesting residual CFTR activity. Overall, both tracings from the biopsies and the 2D-monolayers indicate that there is residual CFTR activity, highlighted by the extent of the negative voltage deflection upon IBMX/Fsk and IBMX/Fsk+CCH stimulation and, in the case of the 2D-monolayers, the use of $CFTR_{inh}$-172 to inhibit these responses further supports its CFTR specificity. Additionally, the FIS assay of this individual's 3D-organoids also showed residual CFTR function with just Fsk (Figure 4.16).

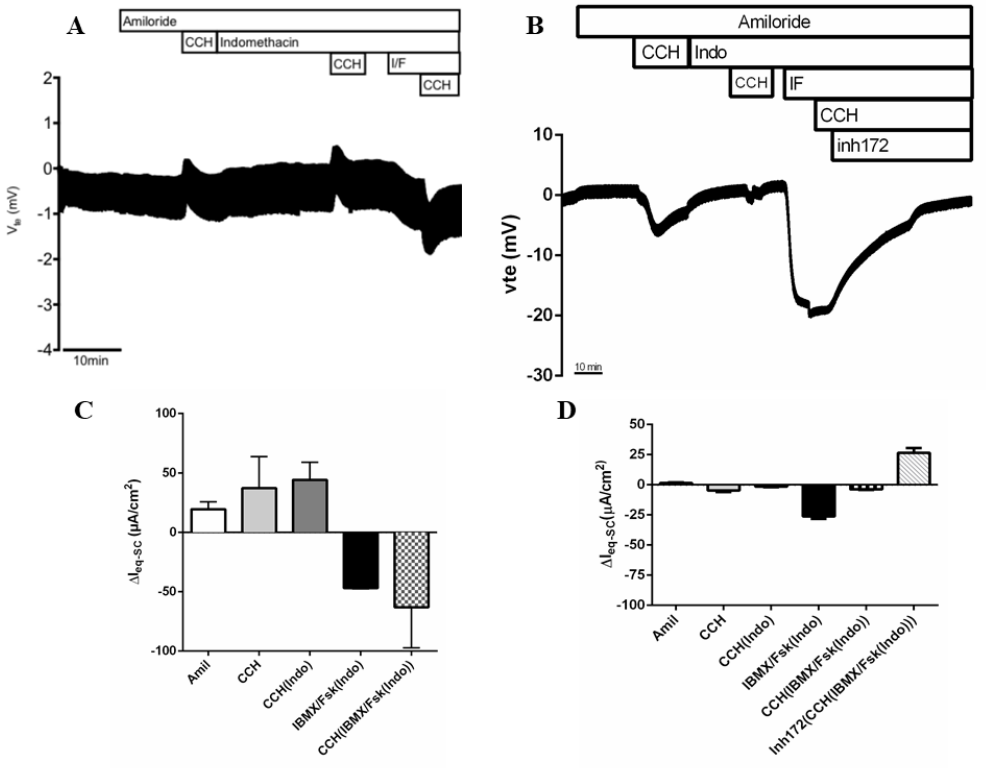

Figure 4.6 – Results from Ussing chamber measurements in rectal biopsies and 2D-monolayers from individual CFL59 (F508del/S995P genotype). Representative original recording of the effects of cholinergic (CCH, 100 µM, basolateral) and cAMP-dependent (IBMX/Fsk, 100µM/2µM, basolateral) activation on transepithelial voltage (Vte) in CFL59 (F508del/S995P genotype): (A) Rectal biopsies; (B) Undifferentiated 2D intestinal monolayers. Experiments were performed in the presence of Amiloride (Amil, 20 µM, apical) and/or Amiloride + Indomethacin (Indo, 10 µM, basolateral), as indicated in the figure. (C) and (D) Summary of activated equivalent short-circuit currents (ΔIeq-sc) for Amil (ΔIeq-sc,Amil), basal CCH (ΔIeq-sc,CCH), CCH + Indo (ΔIeq-sc,CCH(Indo)), IBMX/Fsk + Indo (ΔIeq-sc,IBMX/Fsk(Indo)), CCH following IBMX/Fsk application (ΔIeq-sc,CCH(IBMX/Fsk(Indo))) and Inh172 following CCH/IBMX/Fsk application (ΔIeq-sc, Inh172 (CCH(IBMX/Fsk(Indo)))), in the 2D intestinal monolayers; data represent the mean of measurements of 4 rectal biopsies and 3 monolayers ± SD. [Ussing chamber measurements in the rectal biopsies were performed by Raquel Centeio and used with permission]

4.4.2.2 F508del/R347P

Another individual analyzed was CFL54 who had the F508del/R347P genotype. Ussing chamber recordings and quantification of the rectal biopsies and 2D-monolayers were analyzed (Figure 4.7).

The original Ussing chamber tracings for rectal biopsies from individual CFL54 (Figure 4.7A) show two positive deflections upon the first two CCH stimulations that imply only net K^+ secretion, a small negative voltage change in response to IBMX/Fsk administration and a biphasic type response (Figure 1.6B) upon the final CCH stimulation indicating some cAMP-stimulated Cl^- secretion. This tracing suggests that the individual has low residual function that should result in a mild CF phenotype. Indeed, this IBMX/Fsk response is also demonstrated with the 2D-monolayers (Figure 4.7 B), were there is a large negative voltage change in response to IBMX/Fsk stimulation, suggesting cAMP-generated CFTR-mediated Cl^- currents, that are further enhanced by CCH addition. In comparison to the previous

individual, results show that both rectal biopsies and 2D-monolayers from CFL59 evidence larger CFTR residual activity than those of CFL54. So, both models indicate that there is residual CFTR activity in the CFL54 individual, thus being expected to have a non-classic CF phenotype (Table 4.1). Moreover, the FIS assay in 3D-organoids of this individual also demonstrates swelling with just Fsk (Figure 4.14), reinforcing these results.

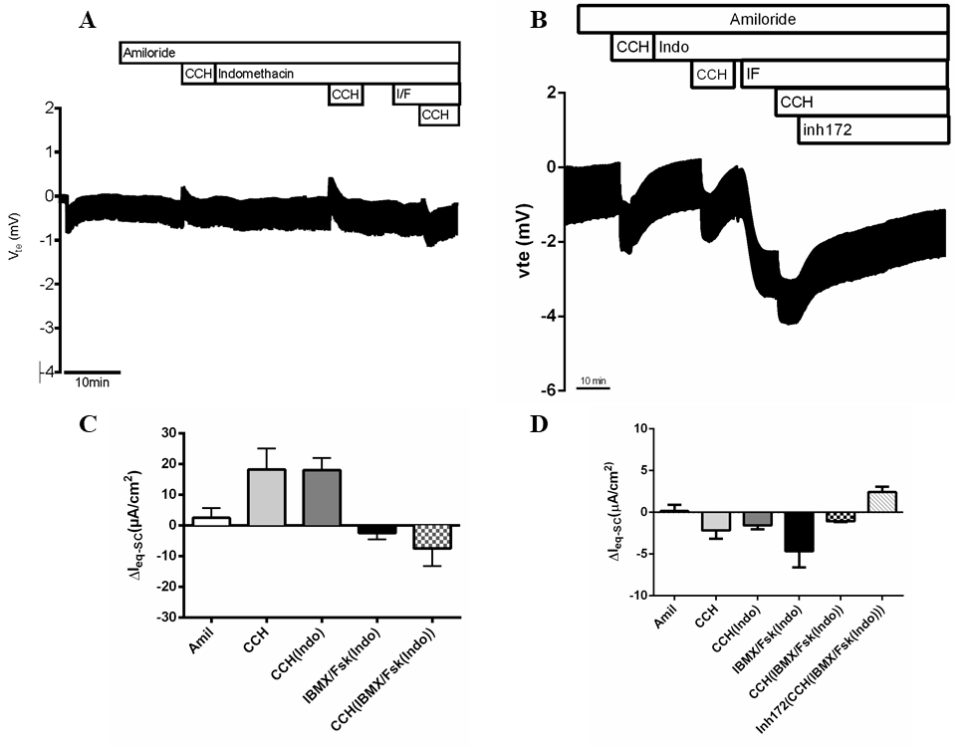

Figure 4.7 – Results from Ussing chamber measurements in rectal biopsies and 2D-monolayers from individual CFL54 (F508del/R347P genotype). Representative original recording of the effects of cholinergic (CCH, 100 µM, basolateral) and cAMP-dependent (IBMX/Fsk, 100µM/2µM, basolateral) activation on transepithelial voltage (Vte) in CFL54 (F508del/R347P genotype): (A) Rectal biopsies; (B) Undifferentiated 2D intestinal monolayers. Experiments were performed in the presence of Amiloride (Amil, 20 µM, apical) and/or Amiloride + Indomethacin (Indo, 10 µM, basolateral), as indicated in the figure. (C) and (D) Summary of activated equivalent short-circuit currents (ΔIeq-sc) for Amil (ΔIeq-sc,Amil), basal CCH (ΔIeq-sc,CCH), CCH + Indo (ΔIeq-sc,CCH(Indo)), IBMX/Fsk + Indo (ΔIeq-sc,IBMX/Fsk(Indo)), CCH following IBMX/Fsk application (ΔIeq-sc,CCH(IBMX/Fsk(Indo))) and Inh172 following CCH/IBMX/Fsk application (ΔIeq-sc, Inh172 (CCH(IBMX/Fsk(Indo)))), in the 2D intestinal monolayers; data represent the mean of measurements of 4 rectal biopsies and 3 monolayers ± SD. [Ussing chamber measurements in the rectal biopsies were performed by Raquel Centeio and used with permission]

4.4.2.3 F508del/R334W

CFL75 has the F508del/R334W genotype, being R334W a class IV mutation that allows for normal processing but severely reduced Cl^- secretion[114,115]. So, in this individual's rectal biopsies (Figure 4.8A) there are two positive deflections upon CCH stimulation, which indicate that there is K^+ exit but no Cl^- currents, consistent with a diagnosis of CF. However, after IBMX/Fsk stimulation there is a negative deflection that suggests cAMP-activated CFTR-mediated Cl^- secretion. However, after adding the final CCH solution, we see a positive deflection in a monophasic manner, indicating that the low CFTR activity

in the tissue from this individual is not enough to compensate for the K^+ exit from the cell. Therefore, individual CFL75 should have some low residual CFTR activity but not in a magnitude that would allow detection of a biphasic response upon CCH stimulation in the presence of IBMX/Fsk.

Similar results were found in the 2D-intestinal monolayer analysis (Figure 4.8B), where there was a clear negative deflection in response to IBMX/Fsk and further potentiated by CCH addition. These overall results reinforce the conclusion that individual CFL75 seems to have residual CFTR function, which was also observed in the FIS assay (Figure 4.18).

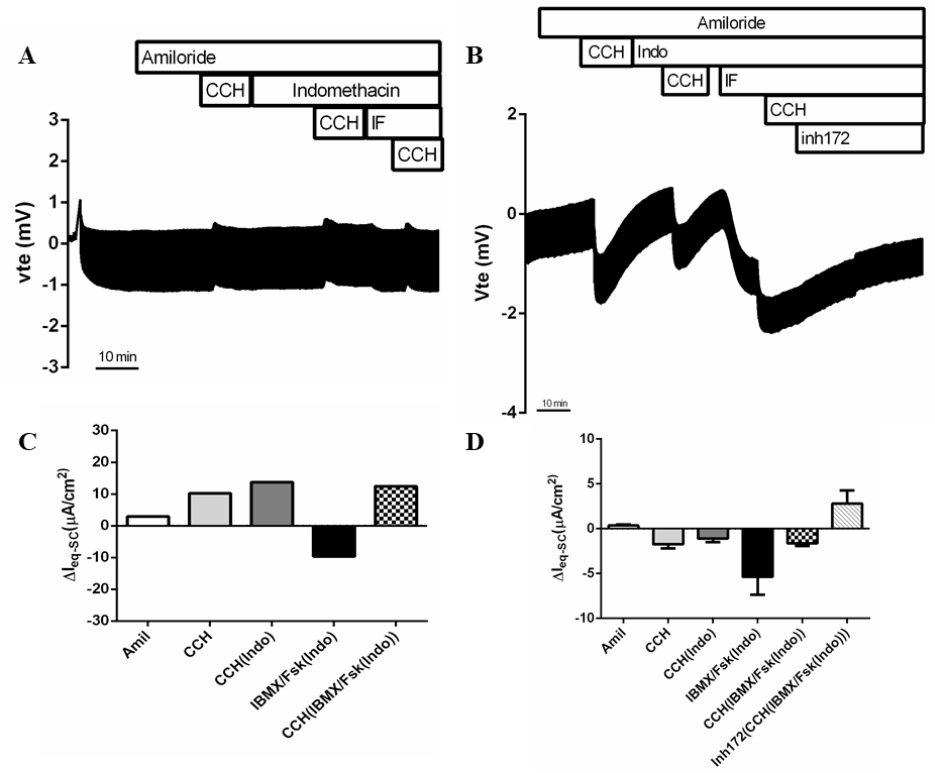

Figure 4.8 – Results from Ussing chamber measurements in rectal biopsies and 2D-monolayers from individual CFL75 (F508del/R334W genotype). Representative original recording of the effects of cholinergic (CCH, 100 µM, basolateral) and cAMP-dependent (IBMX/Fsk, 100µM/2µM, basolateral) activation on transepithelial voltage (Vte) in CFL75 (F508del/R334W genotype): (A) Rectal biopsies; (B) Undifferentiated 2D intestinal monolayers. Experiments were performed in the presence of Amiloride (Amil, 20 µM, apical) and/or Amiloride + Indomethacin (Indo, 10 µM, basolateral), as indicated in the figure. (C) and (D) Summary of activated equivalent short-circuit currents (ΔIeq-sc) for Amil (ΔIeq-sc,Amil), basal CCH (ΔIeq-sc,CCH), CCH + Indo (ΔIeq-sc,CCH(Indo)), IBMX/Fsk + Indo (ΔIeq-sc,IBMX/Fsk(Indo)), CCH following IBMX/Fsk application (ΔIeq-sc,CCH(IBMX/Fsk(Indo))) and Inh172 following CCH/IBMX/Fsk application (ΔIeq-sc, Inh172 (CCH(IBMX/Fsk(Indo)))), in the 2D intestinal monolayers; data represent the mean of measurements of 1 rectal biopsy and 3 monolayers ± SD.

4.4.3 Severe CFTR Mutations

4.4.3.1 F508del/G542X

To determine whether CFTR activity in these 2D-monolayers was consistently dependent on the CFTR residual activity observed in the rectal biopsies, we analyzed samples from a severe CF genotype namely, rectal biopsies and 2D-intestinal cell monolayers from individual CFL61's (F508del/G542X genotype) in the Ussing chamber.

The Ussing chamber recordings in the rectal biopsies (Figure 4.9A) show three positive deflections upon CCH stimulation and no response to IBMX/Fsk stimulation. This demonstrates that there is no CFTR-mediated Cl^- secretion and only a net positive current from luminal K^+ secretion. This is a hallmark response of an individual with CF with a severe phenotype[75] (see Figure 1.6C).

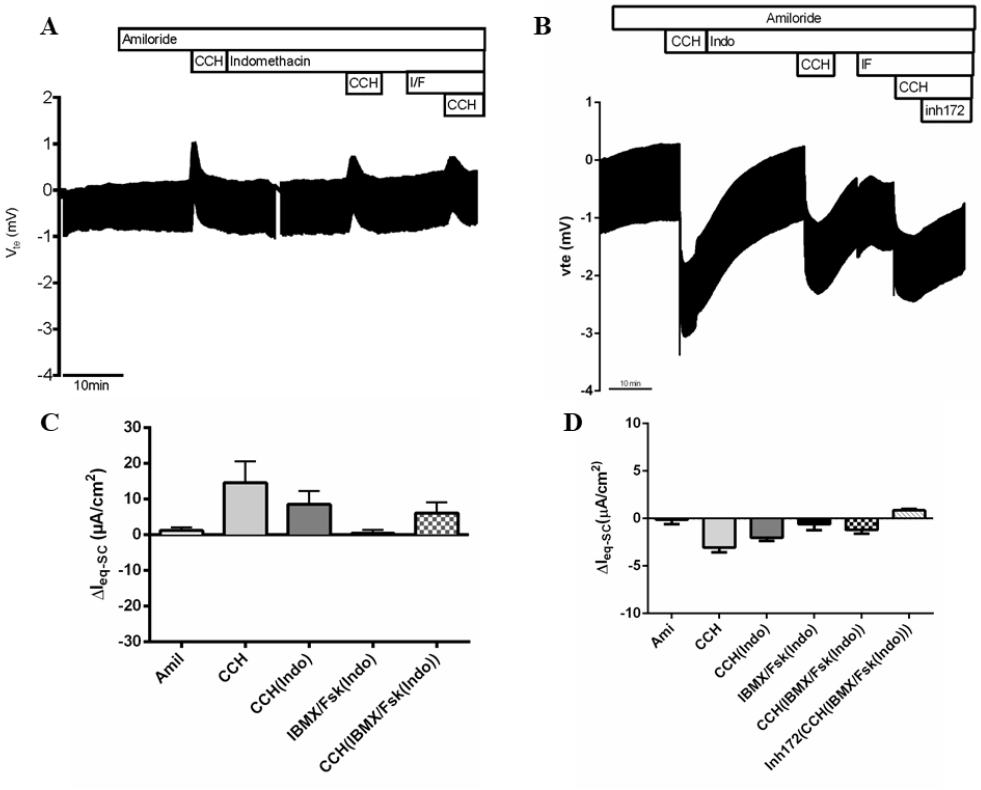

Figure 4.9 – Results from Ussing chamber measurements in rectal biopsies and 2D-monolayers from individual CFL61 (F508del/G542X genotype). Representative original recording of the effects of cholinergic (CCH, 100 µM, basolateral) and cAMP-dependent (IBMX/Fsk, 100µM/2µM, basolateral) activation on transepithelial voltage (Vte) in CFL61 (F508del/G542X genotype): (A) Rectal biopsies; (B) Undifferentiated 2D intestinal monolayers. Experiments were performed in the presence of Amiloride (Amil, 20 µM, apical) and/or Amiloride + Indomethacin (Indo, 10 µM, basolateral), as indicated in the figure. (C) and (D) Summary of activated equivalent short-circuit currents (ΔIeq-sc) for Amil (ΔIeq-sc,Amil), basal CCH (ΔIeq-sc,CCH), CCH + Indo (ΔIeq-sc,CCH(Indo)), IBMX/Fsk + Indo (ΔIeq-sc,IBMX/Fsk(Indo)), CCH following IBMX/Fsk application (ΔIeq-sc,CCH(IBMX/Fsk(Indo))) and Inh172 following CCH/IBMX/Fsk application (ΔIeq-sc, Inh172 (CCH(IBMX/Fsk(Indo)))), in the 2D intestinal monolayers; data represent the mean of measurements of 4 rectal biopsies and 3 monolayers ± SD. [Ussing chamber measurements in the rectal biopsies were performed by Raquel Centeio and used with permission]

The recordings in the 2D-intestinal monolayer (Figure 4.9B) show three negative deflections upon CCH stimulation and a much smaller IBMX/Fsk-stimulated voltage change when compared to either wt/wt cells (Figure 4.4) or those with high residual function (Figure 4.6). These results suggest that there is no detectable Cl^- secretion involved and the negative voltage deflections are the result of net negative currents derived from basolateral K^+ exit. Therefore, we suggest that this should be considered a typical 2D-monolayer tracing for an individual with classical CF.

4.4.3.2 F508del/F508del

Another individual analyzed was CFL65 who had the F508del/F508del genotype, the most common CF genotype. This mutation results in a severe lack of CFTR function due to protein misfolding, which is evidenced by the three positive peaks resulting from CCH stimulation of the individual's rectal biopsies (Figure 4.10A), a classic CF Ussing chamber tracing. Nonetheless, there is a slight negative voltage variation in response to IBMX/Fsk stimulation, suggesting some basal CFTR activity, as also shown in the 3D-organoid swelling (Figure 4.21). This was previously reported to occur for a small number of individuals with the F508del/F508del genotype[74].

In the 2D-monolayers (Figure 4.10B), two negative peaks were observed in response to the first and second CCH stimulation and also a negative voltage shift when IBMX/Fsk is introduced to stimulate CFTR. This last response indicates that there is still some cAMP-mediated Cl^- secretion in cells from this individual which is in agreement with what was observed in this individual's rectal biopsies and 3D-organoids (Figure 4.20). It is of note that the IBMX/Fsk response reaches a negative peak and rapidly the voltage begins to increase, which can be due to CFTR membrane protein internalization and degradation, since the F508del-CFTR has low stability at the PM[116]. Further stimulation with CCH only caused a reduced negative deflection, suggesting that CFTR activity could not be further increased. Lastly, the addition of CFTR-Inh_{172} raised the voltage until the levels prior to the IBMX/Fsk stimulation, indicating that the current generated was CFTR-specific.

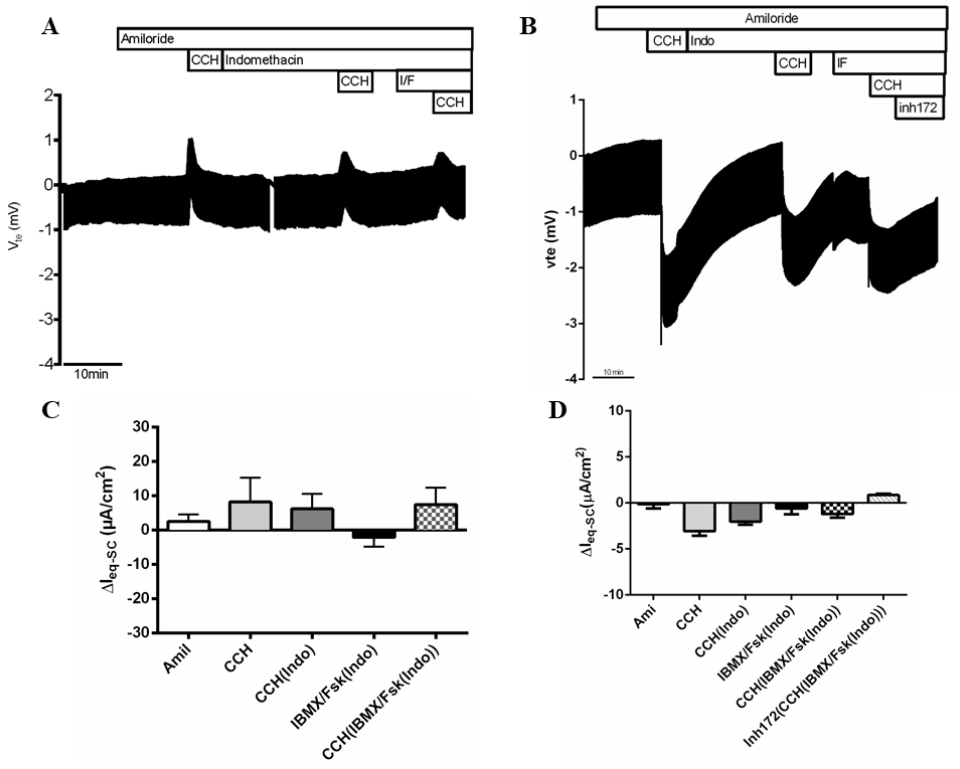

Figure 4.10 – Results from Ussing chamber measurements in rectal biopsies and 2D-monolayers from individual CFL65 (F508del/F508del genotype). Representative original recording of the effects of cholinergic (CCH, 100 µM, basolateral) and cAMP-dependent (IBMX/Fsk, 100µM/2µM, basolateral) activation on transepithelial voltage (Vte) in CFL65 (F508del/F508del genotype): (A) Rectal biopsies; (B) Undifferentiated 2D intestinal monolayers. Experiments were performed in the presence of Amiloride (Amil, 20 µM, apical) and/or Amiloride + Indomethacin (Indo, 10 µM, basolateral), as indicated in the figure. (C) and (D) Summary of activated equivalent short-circuit currents (ΔIeq-sc) for Amil (ΔIeq-sc,Amil), basal CCH (ΔIeq-sc,CCH), CCH + Indo (ΔIeq-sc,CCH(Indo)), IBMX/Fsk + Indo (ΔIeq-sc,IBMX/Fsk(Indo)), CCH following IBMX/Fsk application (ΔIeq-sc,CCH(IBMX/Fsk(Indo))) and Inh172 following CCH/IBMX/Fsk application (ΔIeq-sc, Inh172 (CCH(IBMX/Fsk(Indo)))), in the 2D intestinal monolayers; data represent the mean of measurements of 4 rectal biopsies and 3 monolayers ± SD. [Ussing chamber measurements in the rectal biopsies were performed by Raquel Centeio and used with permission]

Another individual with the F508del/F508del genotype - CFL80 - was analyzed (Figure 4.11). In the original representative tracing of the rectal biopsies (figure 4.11A) it is harder to distinguish the CCH-stimulated responses, because the biopsies were of lower quality. This is one of the problems that could be avoided in the analysis of the 2D-monolayers. Anyhow, there are three positive deflections present upon CCH stimulation that are consistent with a classical CF phenotype. Nonetheless, there is a small response to IBMX/Fsk that may indicate some basal CFTR activity, like it was evidenced in the FIS assay (Figure 4.23).

Next, 2D intestinal monolayers from the CFL80 individual were also analyzed in the Ussing chamber (Figure 4.11B). Again, there are two negative deflections in response to the first and second CCH stimulation and an IBMX/Fsk response that indicates that there is some cAMP-stimulated Cl^- secretion like in the rectal biopsies and 3D-organoids from this individual. Comparable with the CFL65 IBMX/Fsk response, cells from this individual also evidenced an increase in voltage in the second half of the IBMX/Fsk stimulation and further stimulation with CCH decreased the voltage, which suggests an

increase in CFTR activity. In the end, application of CFTR-Inh_{172} ablated both these last currents, indicating that they were CFTR specific. Overall, albeit the response in cells from individual CFL80 was smaller than those in cells from CFL65, both tracings are comparable for these two F508del/F508del genotypes.

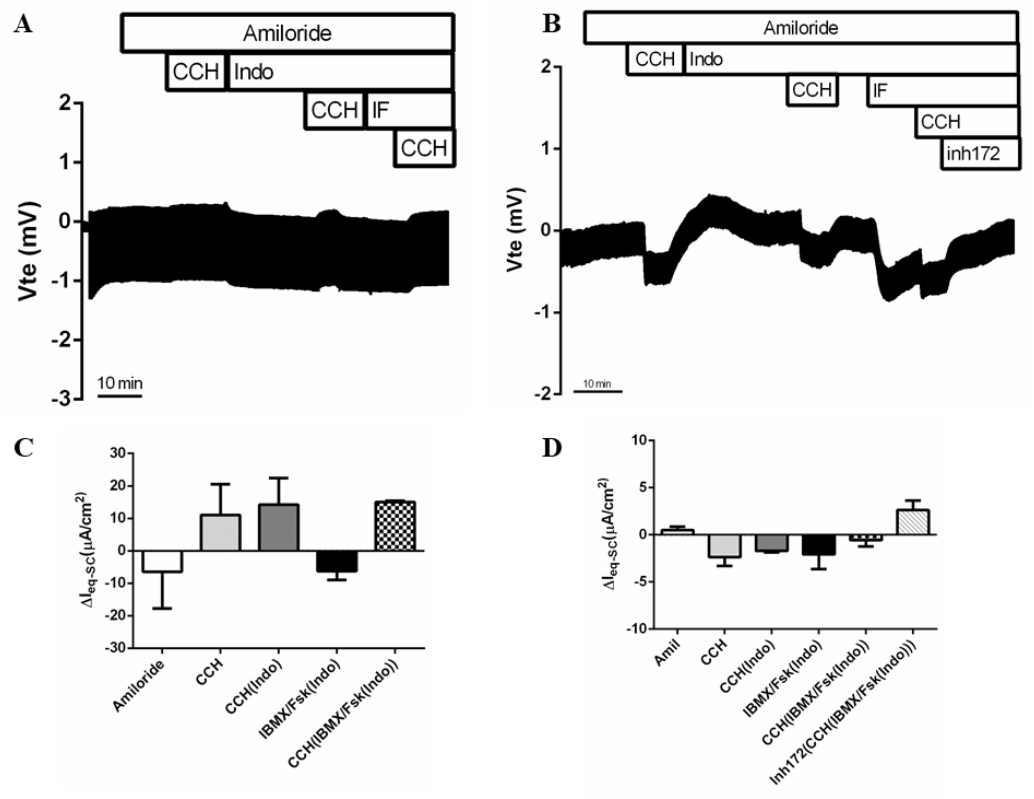

Figure 4.11 – Results from Ussing chamber measurements in rectal biopsies and 2D-monolayers from individual CFL80 (F508del/F508del genotype). Representative original recording of the effects of cholinergic (CCH, 100 µM, basolateral) and cAMP-dependent (IBMX/Fsk, 100µM/2µM, basolateral) activation on transepithelial voltage (Vte) in CFL80 (F508del/F508del genotype): (A) Rectal biopsies; (B) Undifferentiated 2D intestinal monolayers. Experiments were performed in the presence of Amiloride (Amil, 20 µM, apical) and/or Amiloride + Indomethacin (Indo, 10 µM, basolateral), as indicated in the figure. (C) and (D) Summary of activated equivalent short-circuit currents (ΔIeq-sc) for Amil (ΔIeq-sc,Amil), basal CCH (ΔIeq-sc,CCH), CCH + Indo (ΔIeq-sc,CCH(Indo)), IBMX/Fsk + Indo (ΔIeq-sc,IBMX/Fsk(Indo)), CCH following IBMX/Fsk application (ΔIeq-sc,CCH(IBMX/Fsk(Indo))) and Inh172 following CCH/IBMX/Fsk application (ΔIeq-sc, Inh172 (CCH(IBMX/Fsk(Indo)))), in the 2D intestinal monolayers; data represent the mean of measurements of 3 rectal biopsies and 3 monolayers ± SD.

Afterwards, the intestinal 2D-monolayers of patient CFL80 were cultured in differentiating conditions and analyzed in the Ussing chamber. The results are in Figure 4.12.

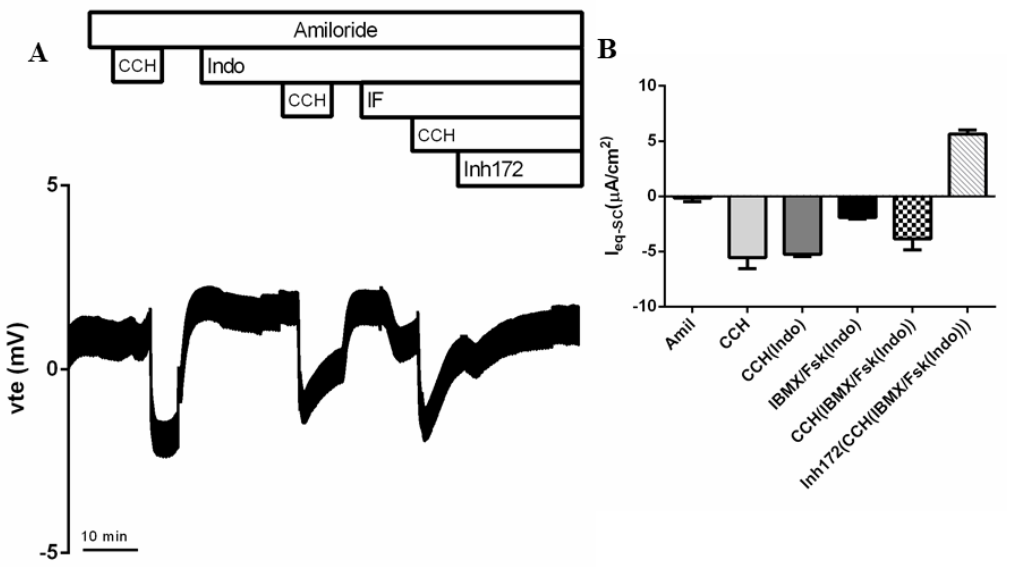

Figure 4.12 - Results from Ussing chamber measurements in differentiated 2D-monolayers from individual CFL80 (F508del/F508del genotype). Representative original recording of the effects of cholinergic (CCH, 100 µM, basolateral) and cAMP-dependent (IBMX/Fsk, 100µM/2µM, basolateral) activation on transepithelial voltage (Vte) in CFL80 (F508del/F508del): (A) differentiated intestinal epithelial monolayers. Experiments were performed in the presence of Amiloride (Amil, 20 µM, apical) and/or Amiloride + Indomethacin (Indo, 10 µM, basolateral), as indicated in the figure. (B) Summary of activated equivalent short-circuit currents (ΔIeq-sc) for Amil (ΔIeq-sc,Amil), basal CCH (ΔIeq-sc,CCH), CCH + Indo (ΔIeq-sc,CCH(Indo)), IBMX/Fsk + Indo (ΔIeq-sc,IBMX/Fsk(Indo)), CCH following IBMX/Fsk application (ΔIeq-sc,CCH(IBMX/Fsk(Indo))) and Inh172 following CCH/IBMX/Fsk (ΔIeq-sc, Inh172 (CCH(IBMX/Fsk(Indo))) application; data represent the mean of measurements of 3 replicates ± SD.

In the differentiated intestinal 2D-monolayers we can observe stronger CCH currents (Figure 4.12 B) than in the undifferentiated intestinal 2D-monolayers (Figure 4.11 D). This could be due to higher activity of Ca^{2+}-activated K^+ channels. There is a similar IBMX/Fsk response in both undifferentiated and differentiated 2D-monolayers that is abolished by the use of $CFTR_{inh}172$, even though the differentiated 2D-monolayers have much lower levels of CFTR protein expression. This current could be originated from the activity of other cAMP-activated ion channels, since there have been reports that the $CFTR_{inh}172$ is not CFTR-specific and also affects the activity of other membrane proteins[113].

4.4.3.3 F508del/A561E

For individual CFL70, who had the F508del/A561E genotype, rectal biopsies and 2D-intestinal cell monolayers were analyzed in the Ussing chamber (Figure 4.13). A561E is a class II mutation that causes protein trafficking impairment. Indeed, observing the representative Ussing chamber recording from the rectal biopsies (Figure 4.13A), the three positive deflections after CCH addition, characteristic of a classical CF phenotype, are present, as well as the lack of negative deflection after IBMX/Fsk stimulation, indicating that there is no cAMP-activated Cl^- secretion, and therefore no CFTR activity. However, the same is not represented in the 2D-monolayer analysis (Figure 4.13B), where there is a small

negative deflection associated with IBMX/Fsk addition, suggesting some residual CFTR activity. There were also three distinctive negative peaks upon CCH stimulation, being the first CCH addition (without Indo) the more negative one, which may indicate Cl^- secretion summed with K^+ channels-derived currents. The FIS assay of this individual also revealed some swelling with just Fsk (Figure 4.24), meaning that there might be some CFTR function measured in the 2D-monolayers and in 3D-organoids, which is not detected in the rectal biopsies. This may be due to a lower sensitivity of the rectal biopsy readout compared to the 2D-monolayers or to bad tissue quality, also reinforced by the very small responses. However, one way to test if there is some CFTR protein in the PM that could be active is to perform a WB analysis of cell lysates from cells from individual CFL70 and look for the presence of CFTR band C. This will be addressed in the future.

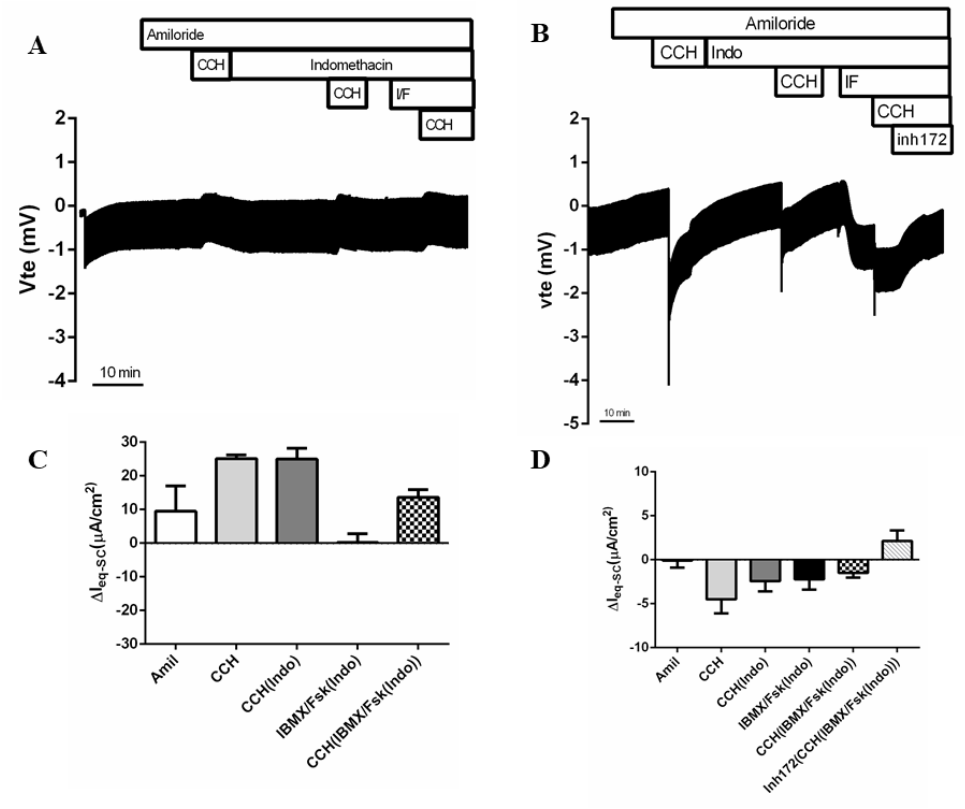

Figure 4.13 – Results from Ussing chamber measurements in rectal biopsies and 2D-monolayers from individual CFL70 (F508del/A561E genotype). Representative original recording of the effects of cholinergic (CCH, 100 µM, basolateral) and cAMP-dependent (IBMX/Fsk, 100µM/2µM, basolateral) activation on transepithelial voltage (Vte) in CFL70 (F508del/A561E genotype): (A) Rectal biopsies; (B) Undifferentiated 2D intestinal monolayers. Experiments were performed in the presence of Amiloride (Amil, 20 µM, apical) and/or Amiloride + Indomethacin (Indo, 10 µM, basolateral), as indicated in the figure. (C) and (D) Summary of activated equivalent short-circuit currents (ΔIeq-sc) for Amil (ΔIeq-sc,Amil), basal CCH (ΔIeq-sc,CCH), CCH + Indo (ΔIeq-sc,CCH(Indo)), IBMX/Fsk + Indo (ΔIeq-sc,IBMX/Fsk(Indo)), CCH following IBMX/Fsk application (ΔIeq-sc,CCH(IBMX/Fsk(Indo))) and Inh172 following CCH/IBMX/Fsk application (ΔIeq-sc, Inh172 (CCH(IBMX/Fsk(Indo)))), in the 2D intestinal monolayers; data represent the mean of measurements of 3 rectal biopsies and 3 monolayers ± SD.

After the analysis and the comparison of the Ussing chamber readouts of the individuals' rectal biopsies and 2D-intestinal monolayers we can conclude that:

i) For the residual function and severe genotypes, the magnitude of the biopsy responses is higher than that in the 2D-monolayers;

ii) For both residual function and severe genotypes, the first two CCH stimulations are negative in the 2D-monolayers and positive in the rectal biopsies; and

iii) The last CCH stimulation is always negative in both models.

The reason for this last observation is yet to be clarified but it can be due to a change in overall ion channel expression and PM distribution (especially the K^+ channels). Indeed, fresh biopsies consist in a mixture of different cells and the 2D-monolayers have culture conditions specific to maintain the Cl^- secreting $LGR5^+$ stem cells from the bottom of the colonic crypts. However, in the 2D-monolayers, the tracings are distinguishable between the residual CFTR activity genotypes and the severe CF genotypes, indicating that these 2D-monolayer assays can distinguish between these two major phenotypes.

4.4 Comparison of CFTR Functional Rescue Between 2D and 3D Models

After the comparison of CFTR basal function assessment between rectal biopsies and 2D-intestinal epithelial monolayers, we aimed to compare the CFTR functional rescue with CFTR corrector and potentiator drugs in this novel 2D model (using Ussing chamber experiments) with the already established and validated 3D intestinal organoid model (using FIS assay).

4.4.1 Residual CFTR Function Mutations

4.4.1.1 F508del/R347P

One of the individuals with CF analyzed in this project is CFL54 who has the F508del/R347P genotype (Table 4.2). As mentioned before, F508del is a class II trafficking mutation that results in the lack of mature protein in the membrane. R347P is a mutation localized in TMD6 and was firstly described as a class IV conductance mutation that allows for protein maturation but results in poor Cl^- conductance in the membrane, having been associated with milder CF phenotypes, sometimes with some residual function. This was seen in Fisher Rat Thyroid cells expressing mutant R347P-CFTR analyzed by the whole-cell patch-clamp technique[114]. Nevertheless, recently the hypothesis of R347P not being a 'pure' class IV mutation has been proposed. In assays using patient-derived materials it was reported that R347P causes a folding defect similar to other class II mutations and that this mutant only matures to ~15% of WT levels. So, it is possible that the R347P not only has a conductance deficiency like class IV mutations but also a trafficking deficit similar to class II mutations[115].

CFTR function was assessed in the 3D-intestinal organoids derived from this individual's rectal biopsies (Figure 4.14). In the FIS assay, Fsk raises the intracellular cAMP concentration, which in turn activates CFTR and allows for CFTR-dependent fluid secretion to the lumen of the organoid. So, if CFTR is functional the organoid swells. In this assay, CF114 organoids (with S1251N/F508del genotype) were

used as a positive control. S1251N is a class III gating mutation for which the potentiator VX-770 was already shown to be effective and approved for clinical use[85]. Thus, S1251N/F508del organoids are suitable reference controls to compare the responses of organoids with unknown responses[45]. Therefore, as the control organoids only swell at 0.8 µM of Fsk, we analyzed the drug response of CFL54's organoids at this concentration (Figure 4.14).

Statistical analysis of the data by one-way ANOVA using Dunnet's multiple comparison test showed that there is no significant differences between Fsk alone and Fsk + VX-770 or Fsk + VX-661, but there is a statistically difference with VX-661/770 treatment. This means that VX-770 alone is not sufficient to correct the diminished Cl^- conductance caused by these two mutations (F508del/R347P) in this individual but to observe rescue it required the combined action of the corrector VX-661 and potentiator VX-770. This may be due to the fact that, R347P may not be a classic class IV mutation since it also impairs protein trafficking due to folding defects, and it was observed that it requires a corrector to either increase traffic to the cell membrane or function at this location[115]. However, it may also be due to the presence of F508del, which is classical Class II mutation.

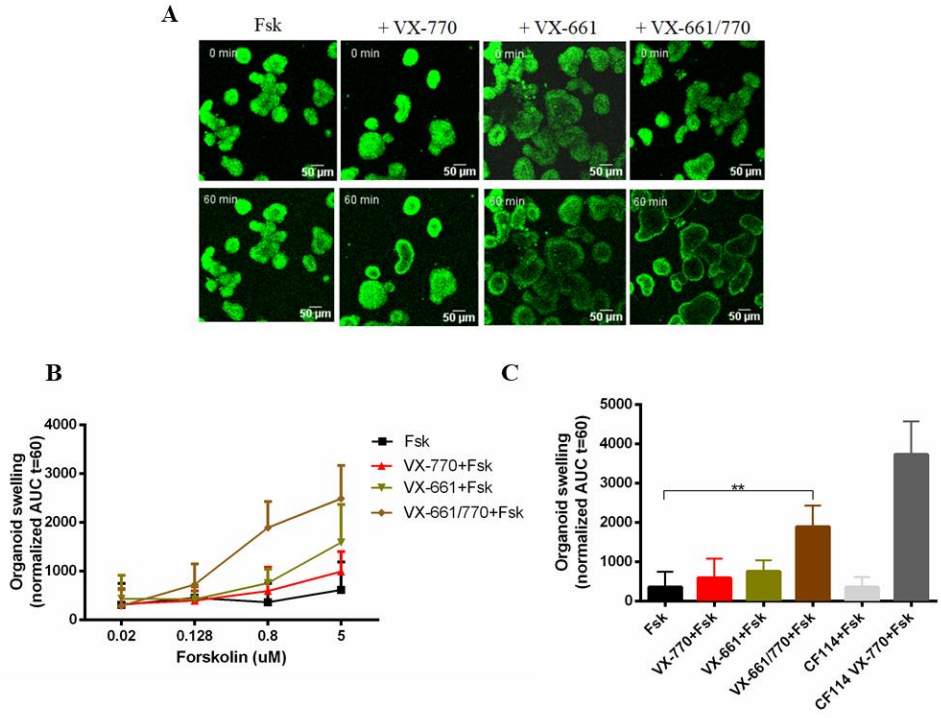

Figure 4.14 – Results from the FIS assay on 3D-intestinal organoids from individual CFL54 (F508del/R347P genotype). (A) Representative original confocal microscopy images of 3D intestinal organoids from individual CFL54 (F508del/R347P genotype) at times 0 and 60 min of incubation with the following treatments: Forskolin (Fsk) alone at the concentration of 0.8 µM, VX-770 (3 µM) + Fsk, VX-661 (3 µM) + Fsk and VX-661/770 + Fsk. (B) Quantification of FIS in organoids for all treatments at Fsk concentrations 0.02, 0.128, 0.8 and 5 µM, expressed as the area under the curve (AUC) of organoid surface area increase (baseline = 100%, t = 60 min). (C) Quantification of CFL54 organoid swelling for all treatments at [Fsk] = 0.8 µM. Control organoids CF114 (S1251N/F508del genotype) were used as reference. (B) and (C) data represent the mean of measurements on 3-4 replicates for condition ± SD. Asterisks (*) represent the degree of significance calculated by an unpaired one-way ANOVA using Dunnet's test, ** indicate a *p*-value<0.01. [Experiments were performed in collaboration with Iris Silva and included with permission].

Next, 2D-monolayers were generated from the 3D-organoids from this individual and tested in the Ussing chamber. The results are in Figure 4.15. The monolayers were incubated with Amil to inhibit any ENaC current and then stimulated with IF to elicit cAMP-mediated CFTR-derived Cl^- currents, which were further potentiated by the use of VX-770. Lastly, the Inh_{172} was added to block CFTR currents. Results show a negative voltage response for IF in the 2D-monolayers treated with DMSO, suggesting some residual activity at this Fsk concentration (0.8 µM) that was further potentiated by the addition of VX-770 (although not significant). The corrector VX-661 response alone generated an increase in the IF current greater than the VX-770 alone, reinforcing the conclusion that the R347P mutation is also a class II mutation, as discussed previously. At last, the combination therapy, VX-661/VX-770, creates a significant increase in the CFTR-derived Cl^- currents, which shows that, for this individual with CF, the CFTR rescue measured in the FIS assay using 3D intestinal organoids and in the Ussing chamber using 2D monolayers are in agreement for the therapy that this individual with CF would benefit the most.

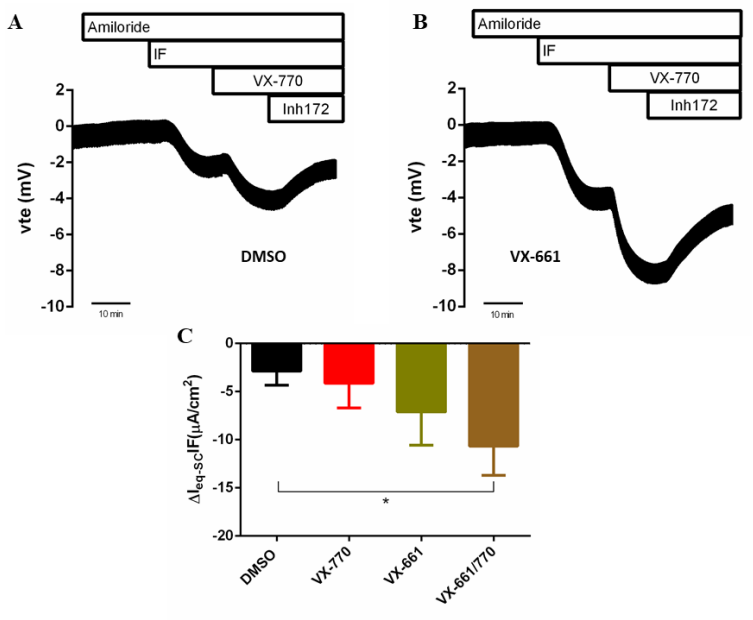

Figure 4.15 – Results from Ussing chamber measurements in 2D-intestinal monolayers from individual CFL54 (F508del/R347P genotype). Representative original recordings of the effects of cAMP-dependent (IBMX/Fsk (IF), 100µM/0.8µM, apical) activation, CFTR potentiation (VX-770, 3 µM, apical) and CFTR-specific inhibition (CFTRinh-172 (Inh172), 30µM, apical) on transepithelial voltage (Vte) in 2D intestinal epithelial monolayers from individual CFL54 (F508del/R347P genotype). Experiments were performed in the presence of Amiloride (20 µM, apical) for: (A) 0.05% DMSO; (B) 3µM VX-661. (C) Summary of activated equivalent short-circuit currents in the presence of IBMX/Fsk (IF, 100 µM/0.8µM). Data represent the mean of measurements on 3 replicates per condition ± SD. Asterisks (*) represent the degree of significance calculated by an unpaired one-way ANOVA using Dunnet's test, * indicate a *p*-value<0.05.

4.4.1.2 F508del/S955P

Individual CFL59 studied in this project had a F508del/S955P genotype. The S955P is a new and uncharacterized *CFTR* variant. There are no reports of individuals with this mutation in the literature or in common CF databases. It is located in the intracytoplasmic loop 4, connecting the RD to TMD7.

CFTR function was assessed in the individual's 3D organoids (Figure 4.16) and with only 0.128 µM of Fsk organoid swelling was already observed, suggesting a residual CFTR function (Figure 4.16 B-C, black). At the same concentration, organoid swelling with the combination treatments VX-809/770 and VX-661/770 was significantly different from control and above the threshold for medium clinical benefit (Figure 4.16 B-C, blue and green). Due to the presence of an F508del-allele and the lack of information about S955P, it is hard to predict the effect of these CFTR modulators in S955P. Further cellular and functional effect and drug response characterization should be done in a relevant cell line, such as Cystic Fibrosis Bronchial Epithelial cell line. Nonetheless, we predict that this individual will benefit from both combination treatments.

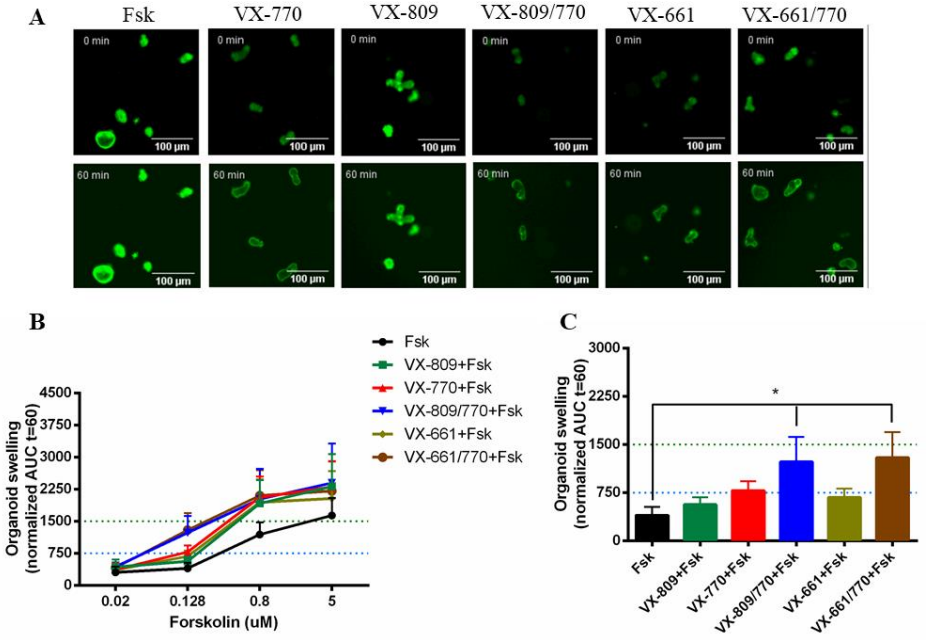

Figure 4.16 – Results from the FIS assay on 3D-intestinal organoids from individual CFL59 (F508del/S995P genotype). (A) Representative original wide-field microscopy images of 3D intestinal organoids from individual CFL59 (F508del/S995P genotype) at times 0 and 60 min of incubation with the following treatments: Forskolin (Fsk) alone at the concentration of 0.128 µM, VX-770 (3 µM) + Fsk, VX-809 (3µM) + Fsk, VX-809/770 + Fsk, VX-661 (5 µM) + Fsk and VX-661/770 + Fsk. (B) Quantification of FIS in organoids for all treatments at Fsk concentrations of 0.02, 0.128, 0.8 and 5 µM, expressed as the area under the curve (AUC) of organoid surface area increase (baseline = 100%, t = 60 min). (C) Quantification of organoid swelling for all treatments at [Fsk] = 0.128 µM. The dashed blue and green line represent the established thresholds for medium and high clinical benefit potential for treatments, respectively. (B) and (C) data represent the mean of measurements on 3-4 replicates for condition ± SD. Asterisks (*) indicate degree of significant difference calculated by unpaired one-way ANOVA using Fisher's LSD test, * indicate a *p*-value<0.05. [Experiments were performed by Raquel Centeio and used with permission].

As for the previous individual, CFL59's 2D-intestinal monolayers were generated from its 3D-organoids and functional rescue of CFTR with approved modulators was assessed in the Ussing chamber (Figure 4.17). An IBMX/Fsk response (Figure 4.17 A,C) generating a large negative current could be observed, suggesting high residual CFTR activity. In fact, an unpaired one-way ANOVA using Dunnet's multiple comparisons test showed that none of the three treatments (VX-770, VX-661 and VX-661/770) evidenced a statistically significant difference in relation to the control DMSO. This may be because of the high concentration of Fsk used in this experiment (2 µM), which by itself stimulated CFTR to an extent that a possible further effect by modulators could not occur. This experiment should be repeated in the future with lower concentration of Fsk to better evaluate the modulators effects.

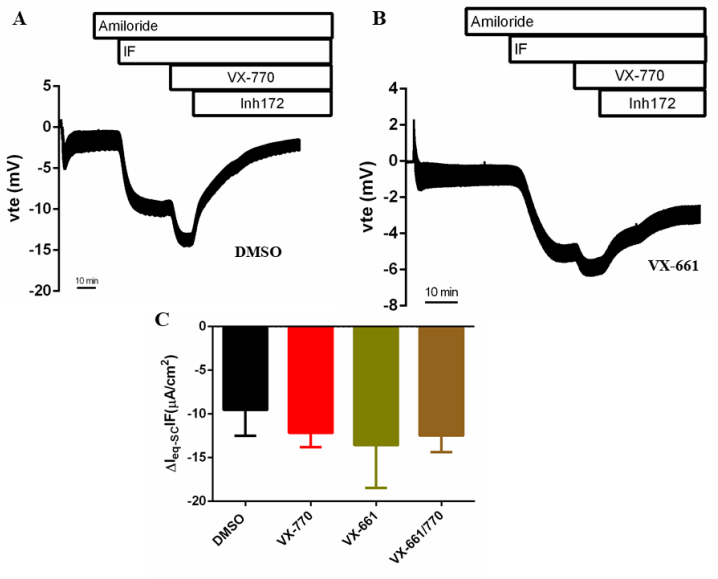

Figure 4.17 – Results from Ussing chamber measurements in 2D-intestinal monolayers from individual CFL59 (F508del/S995P genotype). Representative original recordings of the effects of cAMP-dependent (IBMX/Fsk (IF), 100µM/0.8µM, apical) activation, CFTR potentiation (VX-770, 3 µM, apical) and CFTR-specific inhibition (CFTRinh-172 (Inh172), 30µM, apical) on transepithelial voltage (Vte) in 2D intestinal epithelial monolayers from individual CFL59 (F508del/S995P genotype). Experiments were performed in the presence of Amiloride (20 µM, apical) for: (A) 0.05% DMSO; (B) 3µM VX-661. (C) Summary of activated equivalent short-circuit currents in the presence of IBMX/Fsk (IF, 100 µM/0.8µM). Data represent the mean of measurements on 3 replicates per condition ± SD.

4.4.1.3 F508del/R334W

Individual CFL75 who has an F508del/R334W genotype was also analyzed. R334W is a CF-causing mutation located in the TMD6 and classified as class IV due to a high level of protein processing (98% of WT)[45] but some groups showed that CFTR bearing this mutation has a very low conductance and a severely reduced open probability[114].

3D-intestinal organoids from individual CFL75 were generated and CFTR function was assessed by the FIS assay (Figure 4.18). CF114 (S1251N/F508del genotype) was used as control since the S1251N is a class III gating mutation that is functionally rescued by VX-770 and R334W mutation, although is a class IV mutation, results in a CFTR protein with low open probability, and should also benefit from VX-

770 alone. Since CF114's organoids swelled at 0.8 µM of Fsk, that concentration was used to evaluate CFL75's organoids swelling. The results show that, at this concentration of Fsk, there is already organoid swelling only with Fsk (Figure 4.18 A-C, black). Also, a positive effect on CFTR activity under potentiator VX-770, as well as with the VX-661/VX-770 combination was observed (Figure. 4.17B and C). These results were expected since R334W-CFTR traffics to the membrane in a manner that resembles WT-CFTR but, being a class IV mutation, has lower conductance[114]. Unfortunately, none of the therapies used significantly rescues CFTR function, so the results show that the probability of this individual with CF to benefit from any of the approved modulators tested in this experiment is low. Notwithstanding, the lack of additional swelling by modulators could be due to the fact that there is already considerable 'basal' pre-swelling as a consequence of the residual function associated with the R334W mutation.

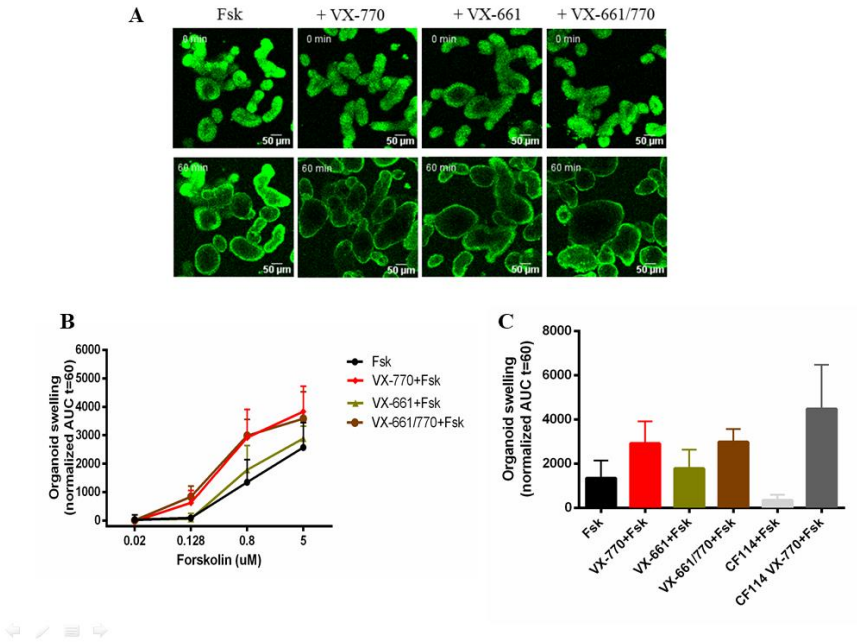

Figure 4.18 – Results from the FIS assay on 3D-intestinal organoids from individual CFL75 (F508del/R334W genotype). (A) Representative original confocal microscopy images of 3D intestinal organoids from individual CFL75 (F508del/R334W genotype) at times 0 and 60 min of incubation with the following treatments: Forskolin (Fsk) alone at the concentration of 0.8 µM, VX-770 (3 µM) + Fsk, VX-661 (3 µM) + Fsk and VX-661/770 + Fsk. (B) Quantification of FIS in organoids for all treatments at Fsk concentrations 0.02, 0.128, 0.8 and 5 µM, expressed as the area under the curve (AUC) of organoid surface area increase (baseline = 100%, t = 60 min). (C) Quantification of CFL75 organoid swelling for all treatments at [Fsk] = 0.8 µM. Control organoids CF114 (S1251N/F508del genotype) were used as reference. (B) and (C) data represent the mean of measurements on 3-4 replicates for condition ± SD. [Experiments were performed in collaboration with Iris Silva and included with permission].

Sequentially to the FIS assay, 2D-intestinal cell monolayers derived from this individual's organoids were generated and analyzed in the Ussing chamber at the same concentration of Fsk (0.8 µM) (Figure 4.19). We can observe a large IBMX/Fsk response in the control monolayers (Figure 4.19 A, C), indicating residual CFTR function for this patient, as it was determined in the FIS assay (Figure 4.18). Nevertheless, contrary to what was observed in the FIS assay of the 3D-organoids, there is no potentiator VX-770 response in the 2D-intestinal monolayers, but there is a significant difference in the IBMX/Fsk current in the monolayers treated with VX-661 with the control monolayers. This can be due to the fact

that, in the Ussing chamber analysis for the control and treated 2D-monolayers, the IBMX/Fsk stimulation elicits a maximal CFTR activation, so there is no detectable further effect by the stimulation with potentiator VX-770 on CFTR activity. Moreover, corrector VX-661 might assist in the correction of the molecular defect caused by F580del (the second mutation in this individual) and perhaps also with some effect on R334W-CFTR. Nonetheless, more 2D-intestinal monolayers should be tested in the Ussing chamber before making any assumption regarding the response of this individual with CF to the modulators tested.

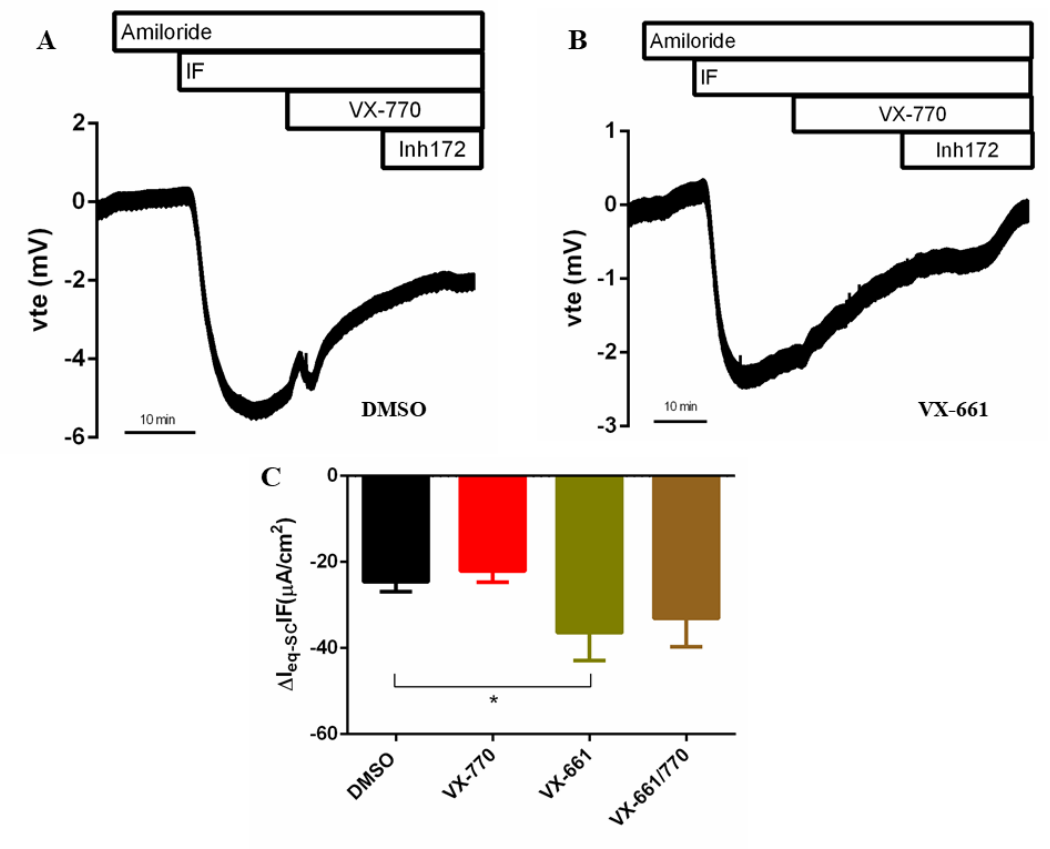

Figure 4.19 – Results from Ussing chamber measurements in 2D-intestinal monolayers from individual CFL75 (F508del/R334W genotype). Representative original recordings of the effects of cAMP-dependent (IBMX/Fsk (IF), 100µM/0.8µM, apical) activation, CFTR potentiation (VX-770, 3 µM, apical) and CFTR-specific inhibition (CFTRinh-172 (Inh172), 30µM, apical) on transepithelial voltage (Vte) in 2D intestinal epithelial monolayers from individual CFL75 (F508del/R334W genotype). Experiments were performed in the presence of Amiloride (20 µM, apical) for: (A) 0.05% DMSO; (B) 3µM VX-661. (C) Summary of activated equivalent short-circuit currents in the presence of IBMX/Fsk (IF, 100 µM/0.8µM). Data represent the mean of measurements on 3 replicates per condition ± SD. Asterisks (*) represent the degree of significance calculated by an unpaired one-way ANOVA using Dunnet's test, * indicate a *p*-value<0.05.

4.4.2 Severe CFTR Mutations

4.4.2.1 F508del/G542X

Individual CFL61 analyzed in this project has the F508del/G542X genotype. G542X is a nonsense mutation localized in NBD1, which generates a premature stop codon (PTC) and has been demonstrated to severely reduce the levels of CFTR mRNA in nasal epithelial cells[117]. 2D-monolayers were generated for this individual and response to approved modulators was assessed (Figure 4.20).

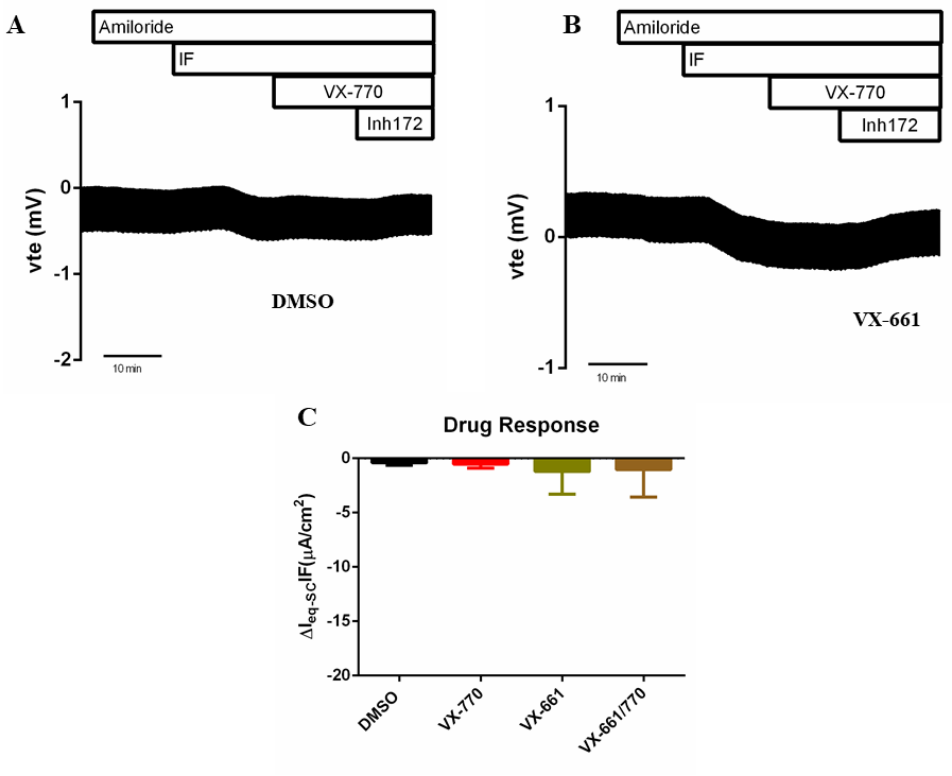

Figure 4.20 – Results from Ussing chamber measurements in 2D-intestinal monolayers from individual CFL61 (F508del/G542X genotype). Representative original recordings of the effects of cAMP-dependent (IBMX/Fsk (IF), 100µM/0.8µM, apical) activation, CFTR potentiation (VX-770, 3 µM, apical) and CFTR-specific inhibition (CFTRinh-172 (Inh172), 30µM, apical) on transepithelial voltage (Vte) in 2D intestinal epithelial monolayers from individual CFL61 (F508del/G542X genotype). Experiments were performed in the presence of Amiloride (20 µM, apical) for: (A) 0.05% DMSO; (B) 3µM VX-661. (C) Summary of activated equivalent short-circuit currents in the presence of IBMX/Fsk (IF, 100 µM/0.8µM). Data represent the mean of measurements on 3 replicates per condition ± SD.

In the control DMSO 2D-monolayers the results show no IBMX/Fsk response, implying that neither the truncated protein produced from the G542X allele nor the unfolded protein from the F508del allele have any residual function and this individual patient is expected to have a classical CF phenotype, which is in fact the case (Table 4.1). None of the approved CFTR modulators tested produced any

significant CFTR rescue when compared to the DMSO, so we hypothesize that the individuals with CF will not benefit from any of these therapies. Recently, it has been observed in HBE cells homozygous for the G542X mutation that the treatment with a combination of a read-through compound (G418) and the modulators VX-809/770 rescues some CFTR function[118]. Moreover, an Eloxx compound, ELX-02, is currently under Phase I trial (healthy subjects) and aims to correct genetic diseases causes by PTC mutations acting as a read-though compound[119]. Unfortunately, there are no approved read-through compounds that could eventually be tested in this individual's organoids but it could be interesting for a future experiment to treat the 2D-intestinal monolayers with any read-through compound available and see if we could rescue the PTC so as to detect CFTR function.

4.4.2.2 F508del/F508del

Individual CFL65 has the F508del/F508del CFTR genotype, which is the most common one. CFTR function was assessed in the 3D-intestinal organoids of the individual CFL65 by the FIS assay (Figure 4.21).

Even at low concentrations of Fsk there is already some swelling only with Fsk (Figure 4.21 B, black line), suggesting that there is some basal CFTR activity in this individual. At 0.8 μM of Fsk, both combination therapies (VX-809/770 and VX-661/770) rescue CFTR function to a significant extent (Figure 4.21B and C). This is in agreement to what was expected since these therapies have been approved for individuals with the F508del/F508del genotype[46,47]. So, from these results, we conclude that this individual should benefit from the administration of VX-809/770 or VX-661/770.

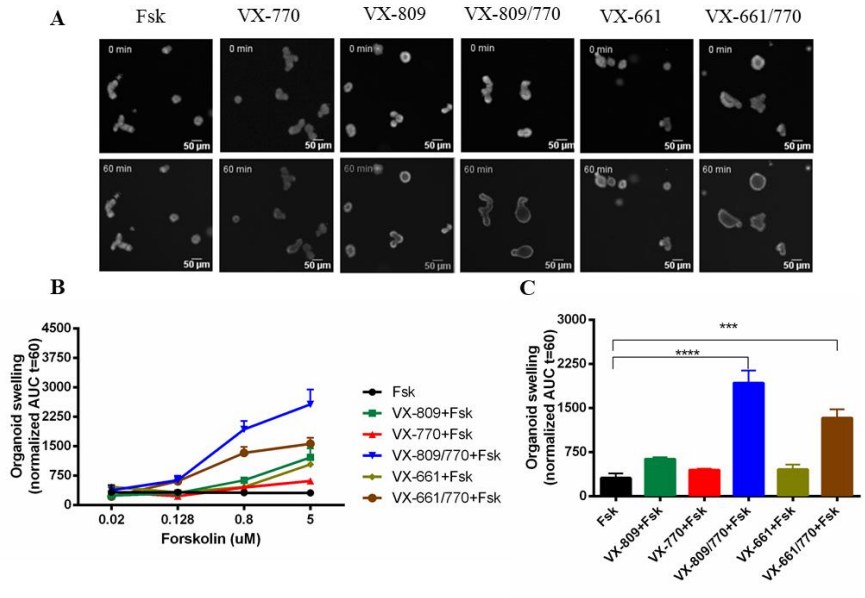

Figure 4.21 – Results from the FIS assay on 3D-intestinal organoids from individual CFL65 (F508del/F508del genotype). (A) Representative original wide-field microscopy images of 3D intestinal organoids from individual CFL65 (F508del/F508del genotype) at times 0 and 60 min of incubation with the following treatments: Forskolin (Fsk) alone at the concentration of 0.128 µM, VX-770 (3 µM) + Fsk, VX-809 (3µM) + Fsk, VX-809/770 + Fsk, VX-661 (5 µM) + Fsk and VX-661/770 + Fsk. (B) Quantification of FIS in organoids for all treatments at Fsk concentrations of 0.02, 0.128, 0.8 and 5 µM, expressed as the area under the curve (AUC) of organoid surface area increase (baseline = 100%, t = 60 min). (C) Quantification of organoid swelling for all treatments at [Fsk] = 0.8 µM. The dashed blue and green line represent the established thresholds for medium and high clinical benefit potential for treatments, respectively.. (B) and (C) data represent the mean of measurements on 3-4 replicates for condition ± SD. Asterisks (*) indicate degree of significant difference calculated by unpaired one-way ANOVA using Fisher's LSD test, *** indicate a *p*-value<0.001 and **** indicate a *p*-value<0.0001. [Experiments were performed by Raquel Centeio and used with permission].

Next, the 2D-monolayers derived from 3D-intestinal organoids from individual CFL65 were analyzed on the Ussing chamber for the effect of CFTR modulators (Figure 4.22). We can observe that the DMSO control has a small response to IF stimulation, suggesting some CFTR activity is detected as observed in the FIS assay (Figure 4.22), but with no further potentiation from VX-770. However, adding the corrector VX-661 leads to a clear increase in the IF-stimulated response that can be further potentiated by the use of the potentiator VX-770, demonstrating that there is rescue of this F508del-CFTR by the combination of these two modulators. This last current, the one generated by the combination VX-661/770, is significantly different from the IF current under the DMSO control, thus this individual should have clinical benefit from the combination therapy.

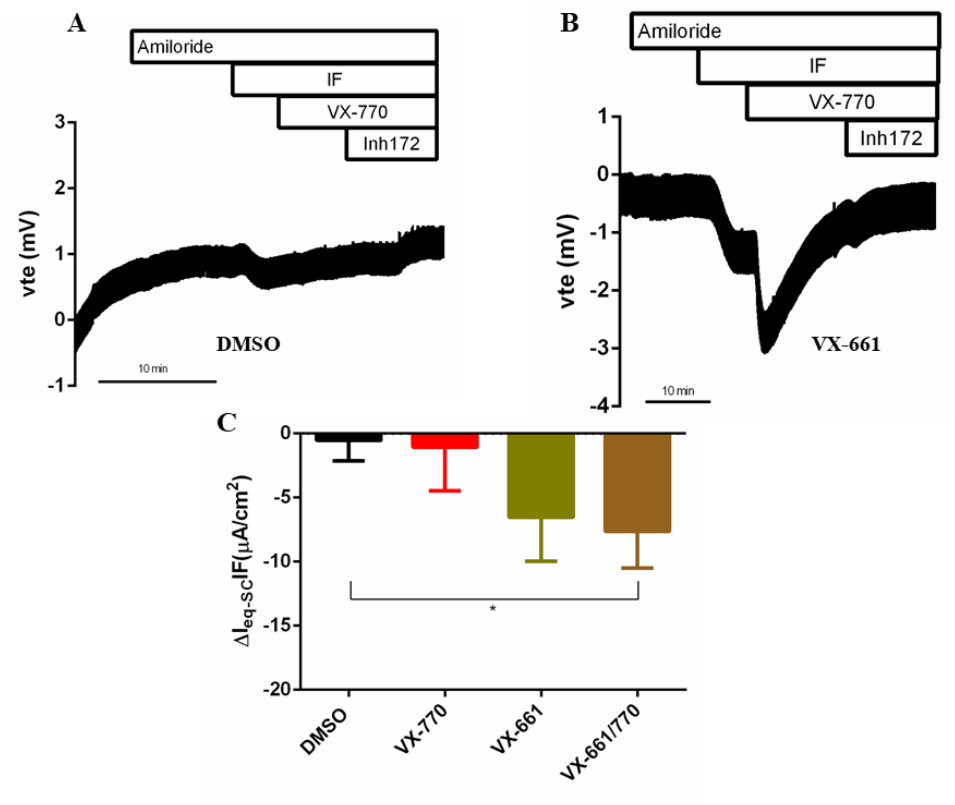

Figure 4.22 - Results from Ussing chamber measurements in 2D-intestinal monolayers from individual CFL65 (F508del/F508del genotype). Representative original recordings of the effects of cAMP-dependent (IBMX/Fsk (IF), 100μM/0.8μM, apical) activation, CFTR potentiation (VX-770, 3 μM, apical) and CFTR-specific inhibition (CFTRinh-172 (Inh172), 30μM, apical) on transepithelial voltage (Vte) in 2D intestinal epithelial monolayers from individual CFL65 (F508del/F508del genotype). Experiments were performed in the presence of Amiloride (20 μM, apical) for: (A) 0.05% DMSO; (B) 3μM VX-661. (C) Summary of activated equivalent short-circuit currents in the presence of IBMX/Fsk (IF, 100 μM/0.8μM). Data represent the mean of measurements on 3 replicates per condition ± SD. Asterisks (*) represent the degree of significance calculated by an unpaired one-way ANOVA using Dunnet's test, * indicate a *p*-value<0.05.

Similarly to CFL65, individual CFL80 has the F508del/F508del genotype and FIS assay was performed to evaluate CFTR functional rescue with the approved modulators (Figure 4.23).

Identical to CFL65, 3D-organoids from CFL80 evidence some swelling with just Fsk at 0.8 μM, suggesting that, again, there is already some F508del-CFTR in the PM. At the same concentration of Fsk, there is a significant difference between the swelling of the combination VX-661/770 and the Fsk control. Nevertheless, this is a small swelling response when compared to that of the CF114 control. So, we predict that this individual could have a modest clinical benefit with the administration of the combination therapy VX-661/770, which was firstly designed for this genotype.

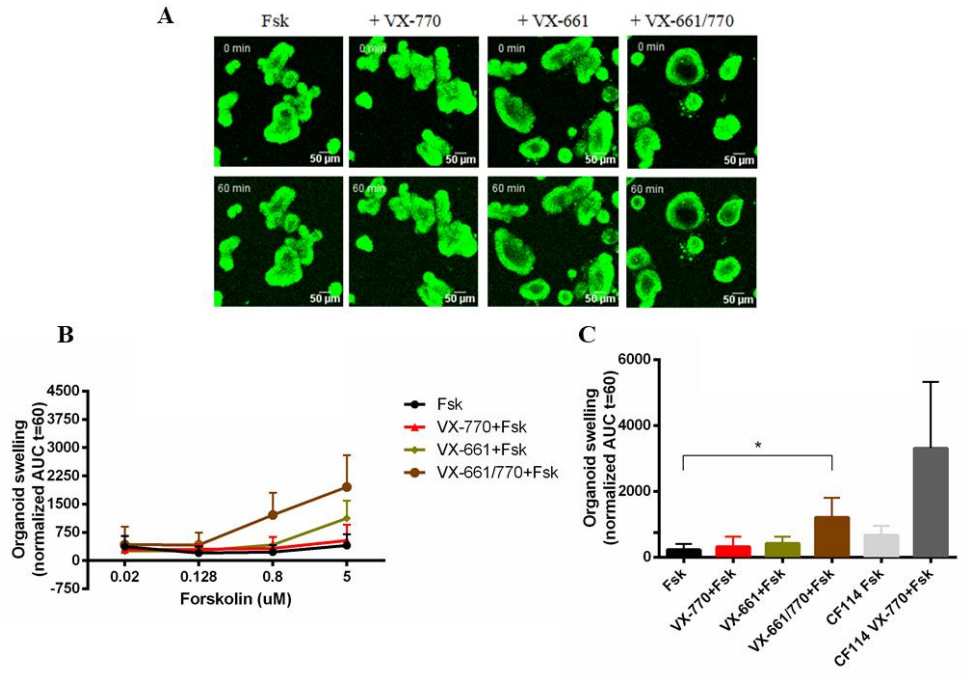

Figure 4.23 – Results from the FIS assay on 3D intestinal organoids from individual CFL80 (F508del/F508del genotype). (A) Representative original confocal microscopy images of 3D intestinal organoids from individual CFL80 (F508del/F508del genotype) at times 0 and 60 min of incubation with the following treatments: Forskolin (Fsk) alone at the concentration of 0.8 µM, VX-770 (3 µM) + Fsk, VX-661 (3 µM) + Fsk and VX-661/770 + Fsk. (B) Quantification of FIS in organoids for all treatments at Fsk concentrations 0.02, 0.128, 0.8 and 5 µM, expressed as the area under the curve (AUC) of organoid surface area increase (baseline = 100%, t = 60 min). (C) Quantification of CFL80 organoid swelling for all treatments at [Fsk] = 0.8 µM. Control organoids CF114 (S1251N/F508del genotype) were used as reference. (B) and (C) data represent the mean of measurements on 3-4 replicates for condition ± SD. Asterisks (*) represent the degree of significance calculated by an unpaired one-way ANOVA using Dunnet's test, * indicate a *p*-value<0.05.

The individual's intestinal 2D-epithelial cell monolayers were also analyzed for drug response in the Ussing chamber (Figure 4.24). We can observe that under DMSO (Figure 4.24 A, C), there is cAMP-generated Cl^- secretion upon IBMX/Fsk stimulation that can be further potentiated with the use of VX-770). Nevertheless, in the monolayers treated with the corrector VX-661, there is no potentiator response following the IBMX/Fsk stimulation, unlike what was observed in the FIS assay. This can be explained by the maximal activation of CFTR in the treated monolayers with just IBMX/Fsk, which was at high concentration. Moreover, during the IBMX/Fsk stimulation there is a steady increase in voltage. This may be explained by CFTR internalization and degradation since F508del-CFTR is not stable at the PM[116]. For the modulator response, there is no significant difference between the treated monolayers and the control monolayers; unlike it was seen in the FIS assay where the swelling with the combination VX-661/770 was significantly different from the Fsk alone. So, from the 2D-intestinal monolayer analysis, we could not predict whether this individual would get any clinical benefit from the CFTR modulators tested.

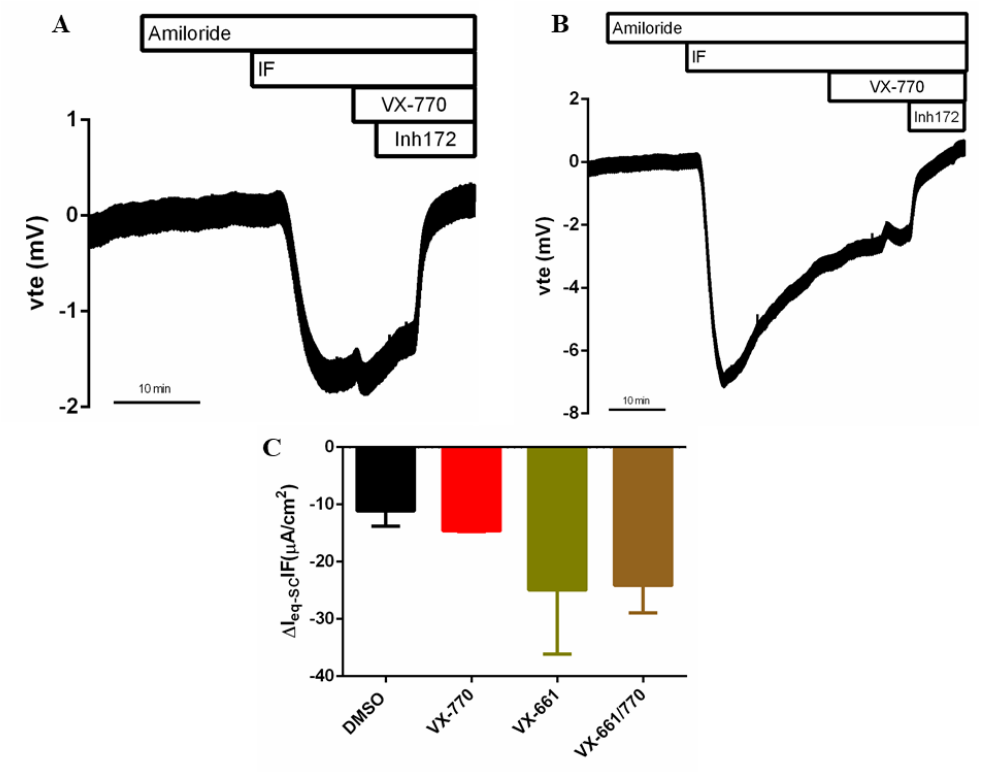

Figure 4.24 - Results from Ussing chamber measurements in 2D-intestinal monolayers from individual CFL80 (F508del/F508del genotype). Representative original recordings of the effects of cAMP-dependent (IBMX/Fsk (IF), 100µM/0.8µM, apical) activation, CFTR potentiation (VX-770, 3 µM, apical) and CFTR-specific inhibition (CFTRinh-172 (Inh172), 30µM, apical) on transepithelial voltage (Vte) in 2D intestinal epithelial monolayers from individual CFL80 (F508del/F508del genotype). Experiments were performed in the presence of Amiloride (20 µM, apical) for: (A) 0.05% DMSO; (B) 3µM VX-661. (C) Summary of activated equivalent short-circuit currents in the presence of IBMX/Fsk (IF, 100 µM/0.8µM). Data represent the mean of measurements on 3 replicates per condition ± SD.

4.4.2.3 F508del/A561E

Individual CFL70 has the F508del/A561E genotype. A561E is a missense mutation which, like F508del, is located in the NBD1 of the CFTR protein, and previously shown to impair folding and processing, causing a trafficking defect to the PM, much like the F508del mutation. Therefore, like F508del, A561E is considered a class II mutation[120].

CFTR activity was measured in the 3D-organoids derived from this individual using the FIS assay (Figure 4.25). Similarly to CFL65, organoids from the CFL70 individual evidenced some organoid swelling at low Fsk concentrations (Figure 4.25 B, black line), indicative of some CFTR activity. Potentiator VX-770 or corrector VX-661 alone did not rescue CFRT function at [Fsk] = 0.8µM but the VX-661/VX-770 combination elicited a significant increase in the organoids swelling (Figure 4.25, orange). Therefore, our results show that this individual might benefit from the combination treatment. However, when compared to the CF114 control organoids, we predict that the clinical benefit would be modest. Authors have reported previously that the combined use of CFTR correctors and potentiators

partially rescue A561E-CFTR function[121] and, as A561E presents a folding/traffic defect similar to that of F508del-CFTR (class II), the use of correctors might be expected to increase folding efficiency and membrane trafficking. Indeed, Ussing chamber recordings done in primary HBECs with a A561E/A561E genotype treated with VX-809 showed a rescue of CFTR activity similar to the rescue observed in HBECs with a F508del/F508del genotype[77].

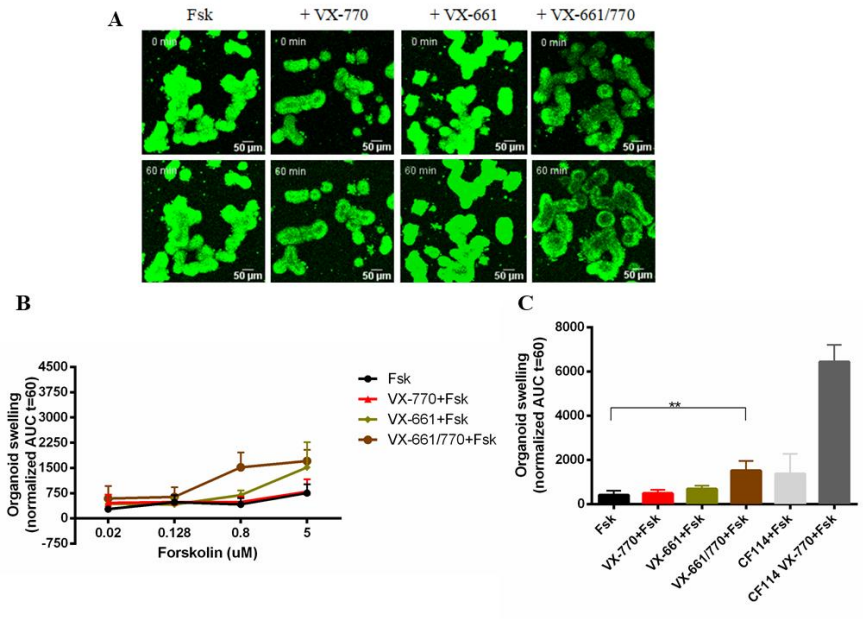

Figure 4.25 - Results from the FIS assay on 3D-intestinal organoids from individual CFL70 (F508del/A561E genotype). (A) Representative original confocal microscopy images of 3D intestinal organoids from individual CFL70 (F508del/A561E genotype) at times 0 and 60 min of incubation with the following treatments: Forskolin (Fsk) alone at the concentration of 0.8 µM, VX-770 (3 µM) + Fsk, VX-661 (3 µM) + Fsk and VX-661/770 + Fsk. (B) Quantification of FIS in organoids for all treatments at Fsk concentrations 0.02, 0.128, 0.8 and 5 µM, expressed as the area under the curve (AUC) of organoid surface area increase (baseline = 100%, t = 60 min). (C) Quantification of CFL70 organoid swelling for all treatments at [Fsk] = 0.8 µM. Control organoids CF114 (S1251N/F508del genotype) were used as reference. (B) and (C) data represent the mean of measurements on 3-4 replicates for condition ± SD. Asterisks (*) represent the degree of significance calculated by an unpaired one-way ANOVA using Dunnet's test, ** indicate a *p*-value<0.01.

As for the analysis of 2D-monolayers in the Ussing chamber (Figure 4.26), the results show that in the presence of IBMX/Fsk there is only some very low CFTR-mediated Cl^- current in the DMSO control (Figure 4.26A, C), which is in agreement with the FIS assay in the 3D-organoids. Also in agreement with the 3D-organoids data is the fact that in the 2D-monolayers only the combination treatment significantly rescued CFTR function.

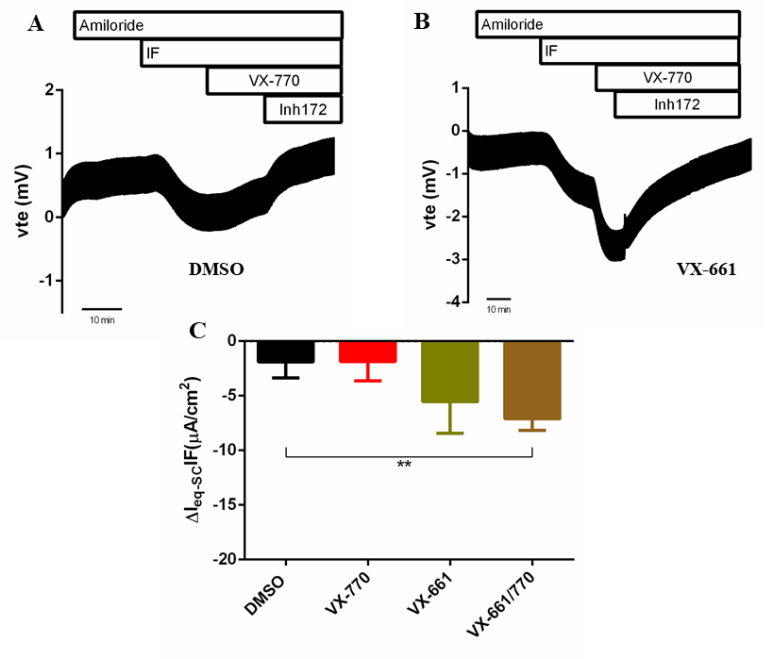

Figure 4.26 - Results from Ussing chamber measurements in 2D-intestinal monolayers from individual CFL70 (F508del/A561E genotype). Representative original recordings of the effects of cAMP-dependent (IBMX/Fsk (IF), 100μM/0.8μM, apical) activation, CFTR potentiation (VX-770, 3 μM, apical) and CFTR-specific inhibition (CFTRinh-172 (Inh172), 30μM, apical) on transepithelial voltage (Vte) in 2D intestinal epithelial monolayers from individual CFL70 (F508del/A561E genotype). Experiments were performed in the presence of Amiloride (20 μM, apical) for: (A) 0.05% DMSO; (B) 3μM VX-661. (C) Summary of activated equivalent short-circuit currents in the presence of IBMX/Fsk (IF, 100 μM/0.8μM). Data represent the mean of measurements on 3 replicates per condition ± SD. Asterisks (*) represent the degree of significance calculated by an unpaired one-way ANOVA using Dunnet's test, ** indicate a *p*-value<0.05.

The data obtained for all individuals with CF from both analyses from the 3D-organoids and 2D-monolayers with the approved CFTR modulators are summarized in Table 4.2.

Table 4.2 – Summary of 3D intestinal organoids and 2D intestinal monolayer analyses for all individuals studied. *CFTR* genotypes, individual codes, CFTR rescued observed in 3D organoids and 2D monolayers for all individuals studied at [Fsk] = 0.8 μM. Asterisks (*) indicate the of statistical significant differences when compared to control, * indicate a *p*-value<0.05, ** indicate a *p*-value<0.01 and *** indicate a *p*-value<0.001. ns = not significant. NA = not available.

***CFTR* Genotype**		**Individual Code**	**CFTR Rescue (3D organoids)**			**CFTR Rescue (2D monolayers)**		
			VX-770	VX-661	VX-661/770	VX-770	VX-661	VX-661/770
Mild CF	F508del/R347P	CFL54	ns	ns	**	ns	ns	*
	F508del/S955P	CFL59	ns	ns	*	ns	ns	ns
	F508del/R334W	CFL75	ns	ns	ns	ns	*	ns
Severe CF	F508del/F508del	CFL65	ns	ns	***	ns	ns	*
	F508del/A561E	CFL70	ns	ns	**	ns	ns	**
	F508del/G542X	CFL61	NA	NA	NA	ns	ns	ns
	F508del/F508del	CFL80	ns	ns	*	ns	ns	ns

For all the individuals analyzed, the response observed in the 3D-organoids was compared with that in the 2D-monolayers. For 3 out of 7 individuals analyzed (CFL54, CFL65, CFL70), there was agreement between the FIS assay in the 3D-organoids and the Ussing chamber assay for the 2D-monolayers because both analyses demonstrated significant difference between the combination VX-661/770 and the DMSO control, meaning that there is rescue of CFTR function. For individual CFL75, we concluded that there is no rescue of CFTR function with the approved modulators in the FIS assay but the in 2D-monolayers there was significant rescue with just VX-661. For individual CFL80, there was a significant rescue of CFTR function with the combination VX-661/770 but no rescue was observed with the modulators in the 2D-monolayers. For individual CFL61 it is not possible to make the comparison since we did not obtain FIS data for this individual and for individual CFL59 the 2D-monolayer assay should be repeated with a lower concentration of Fsk.

In conclusion, we obtained mixed results regarding the correlations between drug response in 3D-organoids and 2D-monolayers. Thus, more analyses from individuals with different mutations should be analyzed to test the validity of the 2D-monolayer assay to predict drug response and some of the ones already done here should be repeated under different conditions (e.g., lower Fsk concentrations, better washout of VX-770 from plastic tubes).

Lastly, to assess if the CFTR function parameters measured in these 2D-monolayers can be used to assess CFTR function, in the next subsection correlation studies were made between the 2D-monolayer data and the data from the rectal biopsies, 3D-organoids and clinical biomarkers.

4.5 Correlations of CFTR Function Parameters and Clinical Data among Fresh tissue, 3D and 2D models

To establish the validity of the 2D model to assess CFTR function, correlations among fresh tissue, 3D- and 2D-models were calculated. The data used in these correlations are summarized in Table 4.3.

Table 4.3 – Summary of all data used for the correlation studies. Patient codes; *CFTR* genotype; activated short circuit currents measured in Ussing chamber analyses of 2D monolayers under CCH (2D ΔI_{sc-eq}CCH), IF + CCH (2D ΔI_{sc-eq}(max), inh172 following IF + CCH ((2D ΔI_{sc-eq}(inh172)); activated short circuit currents measured in Ussing chamber analyses of rectal biopsies under IF + CCH (Biopsy ΔI_{sc-eq}(max)); activated short circuit currents measured in Ussing chambers of control 2D monolayers under IF (2D ΔI_{sc-eq}IF(DMSO)) and treated 2D monolayers under IF + VX-770 (2D ΔI_{sc-eq}(661/770); sweat [Cl^-] (mmol/L); fecal elastase E1 (FEE, µg/g stool; forced expiratory volume in 1 sec (FEV_1, %); AUC values measured in FIS assay at just [Fsk] = 0.02, 0.128, 0.8 e 5 µM (AUC [Fsk] = 0.02, 0.128, 0.8, 5) and with VX-661/770 (AUC 661/770 [Fsk] = 0.02, 0,128, 0,8, 5; for all individuals studied. NA = Not Available.

Patient code	2D ΔI_{sc-eq} (CCH)	2D ΔIsc-eq(IF)	2D ΔI_{sc-eq} (max)	2D ΔI_{sc-eq} (inh172)	Biopsy ΔI_{sc-eq} (max)	2D ΔI_{sc-eq} (IF (661/770))	[Sweat Cl^-]	FEE	FEV_1	AUC [Fsk] = 0.02	AUC [Fsk] = 0.128	AUC [Fsk] = 0.8	AUC [Fsk] = 05	AUC 661/770 [Fsk] = 0.02	AUC 661/770 [Fsk] = 0.128	AUC 661/770 [Fsk] = 0.8	AUC 661/770 [Fsk] = 5
CFL54	-2,18	-4,65	-5,73	2,42	-9,98	-10,67	94,3	351	70	309,27	452,93	361,21	616,57	288,85	725,30	1892,67	2489,33
CFL59	-4,67	-26,13	-29,93	26,59	-34,59	NA	56,5	500	99	221,44	512,67	1394,90	1875,07	NA	NA	NA	NA
CFL61	-3,06	-0,60	-1,81	0,86	6,46	-1,03	82,7	1	95	NA	NA	NA	NA	NA	NA	NA	NA
CFL65	-4,18	-5,30	-5,32	2,31	5,31	-7,62	117	1	89	329,16	322,63	311,90	308,30	214,87	606,23	1330,33	1563,67
CFL70	-4,52	-2,22	-3,71	2,14	13,86	-7,11	112	30	101	277,63	480,23	416,77	752,27	592,77	638,33	1518,67	1708,00
CFL75	-1,74	-5,38	-7,02	2,80	2,88	-33,07	91	500	124	23,59	91,72	1347,60	2574,00	7,10	834,87	2982,67	3585,00
CFL80	-1,72	-2,08	-2,63	2,63	12,90	-18,27	125	1	61	373,60	202,83	227,90	404,26	425,39	417,53	1211,10	1956,33

4.5.1 Correlations between 2D Model and Fresh Tissue

One of the main objectives of the present work was to assess if the 2D-intestinal epithelial monolayers could be used to measure CFTR basal activity to possibly replace CFTR function analysis of fresh rectal biopsies. Therefore, correlation analyses among different CFTR function parameters used, namely the cAMP (I/F)- and cholinergic (CCH)-mediated activated short-circuit currents (I_{sc-eq} IF+CCH) measured in the Ussing chamber on both 2D-monolayers and fresh tissue, were established. The results show a significant correlation between Biopsy ΔI_{sc-eq} (max) vs 2D ΔI_{sc-eq} (max) ($p<0.05$) (Table 4.4).

Table 4.4 – Correlation data between activated short circuit currents measured in 2D-monolayers and rectal biopsies. Parameter 1 refers to the sum of activated short circuit currents measured *ex vivo* in rectal biopsies upon addition of IF and CCH (Biopsy ΔI_{sc-eq} (max)). Parameter 2 refers to the activated short circuit currents measured in 2D-monolayers in response to CCH without Indo (2D ΔI_{sc-eq} (CCH)), IBMX/Fsk (2D ΔIsc-eq(IF)), the sum of the last two currents (2D ΔI_{sc-eq} (max)) and inh172 addition after the last response (2D ΔI_{sc-eq} (inh172)). Pearson correlation coefficients (*r)*, Spearman correlation coefficients (ρ), respective *p* –value and sample number (n) are denoted. Significant *p* –values are highlighted in bold. NA – Not Aplicable.

Parameter 1	Parameter 2	Pearson *r*	Spearman ρ	*p* -value	n
Biopsy ΔI_{sc-eq} (max)	2D ΔI_{sc-eq}(CCH)	0.3119562	NA	0.4957952	7
	2D ΔI_{sc-eq}(IF)	NA	0.7500000	0.0521814	7
	2D ΔI_{sc-eq} (max)	NA	**0.8214286**	**0.0234488**	7
	2D ΔI_{sc-eq} (inh172)	NA	-0.6428571	0.1193924	7

The results indicate that there is a positive correlation between the cholinergic-mediated co-activated current measured in the 2D-monolayers and the same response measured *ex vivo* in the rectal biopsies (Figure 4.27). We can conclude that the maximal activation of CFTR function in the 2D-monolayers can predict the maximal activation of CFTR in the rectal biopsies, making the 2D-monolayers a good model to assess basal CFTR function.

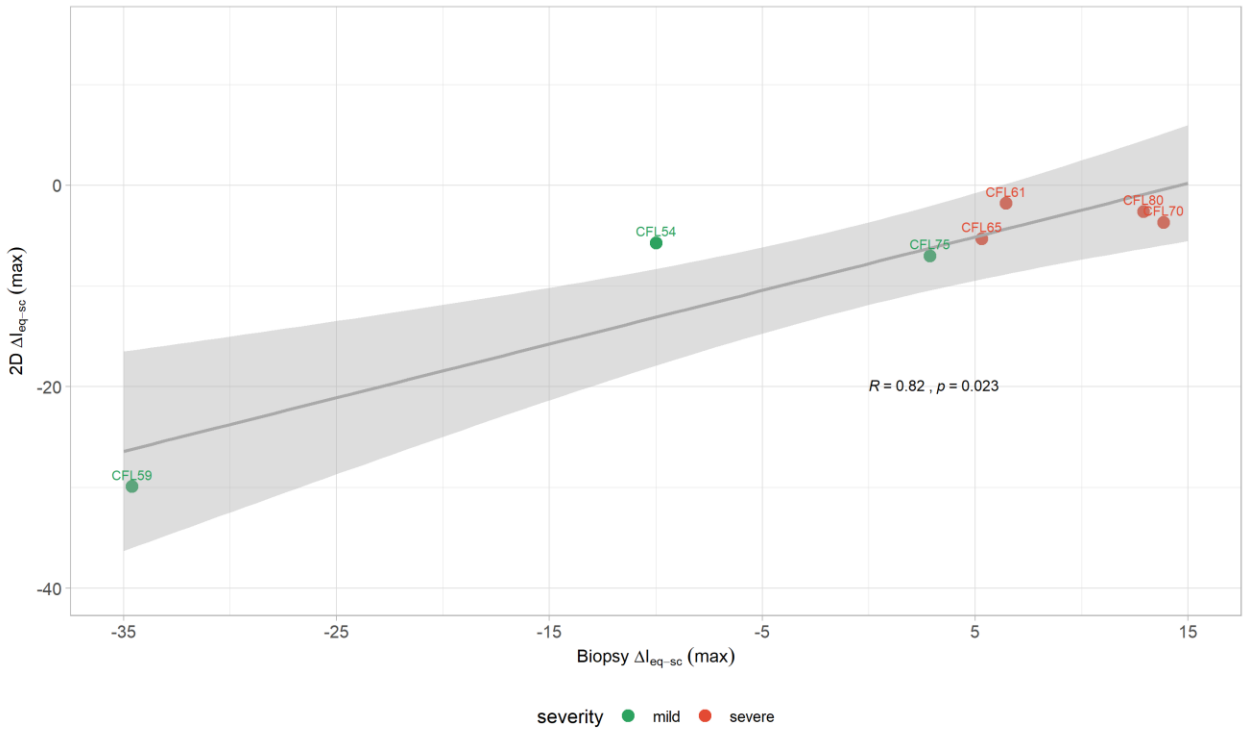

Figure 4.27 – Correlation between CCH-induced short circuit currents following IBMX/Fsk administration to 2D-monolayers and rectal biopsies. Plot of 2D $\Delta I_{sc\text{-}eq}$ (max) ($\mu A/cm^2$) determined in *in vitro* Ussing chamber measurements of 2D-monolayers and Biopsy $\Delta I_{sc\text{-}eq}$ (max) ($\mu A/cm^2$) determined in *ex vivo* measurements of rectal biopsies from individual with CF (Spearman $\rho = 0.82$, p –value = 0.023, n = 7). A degree of *CFTR* genotype severity was determined from previously proposed CF diagnosis from rectal biopsy analyzes as mild (green) and severe (red). Grey line represents the linear regression of the data. Grey area represents the 95% confidence interval.

4.5.2 Correlations between 2D- and 3D-models

As one of the objectives of this MSc thesis was to ascertain if the 2D-intestinal epithelial monolayers could be used to measure the level of CFTR functional rescue by the currently approved modulators, a correlation analysis with the already implemented FIS assay was established. Moreover, we aimed to determine if the basal CFTR activity measured with the condition of 'Fsk alone' in the FIS assay correlates with the basal CFTR activity measured in the 2D-monolayers. To that end, the activated short-circuit currents measured in the 2D-monolayers using the Ussing chamber were correlated with the AUC FIS assay measurements in the 3D-intestinal organoids. For this, data summarized in Table 4.3 were used and the correlation results are in Table 4.5. The strongest correlations were found between 2D $\Delta I_{sc\text{-}eq}$ (max) vs AUC [Fsk] = 0.8 (p<0.05) and $\Delta I_{sc\text{-}eq}$ (IF (661/770)) vs AUC 661/770 [Fsk] = 5.

Table 4.5 – Correlation analyzes between activated short circuit currents measured in 2D-monolayers and organoid swelling. Correlation analyses were established between parameters 1 and 2. Parameter 1 refers to the activated short circuit currents measured in 2D monolayers in response to CCH (2D $\Delta I_{sc\text{-}eq}$ (CCH)), IBMX/Fsk (2D ΔIsc-eq(IF)), the sum of the last two currents (2D $\Delta I_{sc\text{-}eq}$ (max)), inh172 addition after the last response (2D $\Delta I_{sc\text{-}eq}$ (inh172)), IF addition in the control DMSO monolayers, IF and VX-770 addition in monolayers treated with VX-661 ($\mu A/cm^2$). Parameter 2 refers to the organoid swelling expressed as the AUC of the organoid surface area increase (baseline = 100%; t = 60 min) at [Fsk] = 0.02, 0.128, 0.8, 5 µM in the control condition (Fsk only) and at [Fsk] = 0.8 µM for the organoids treated with VX-661/770. Pearson correlation coefficients (*r)*, Spearman correlation coefficients (ρ), respective *p* –value and sample number (n) are denoted. Significant *p* –values are highlighted in bold. NA – Not Aplicable

Parameter 1	Parameter 2	Pearson *r*	Spearman ρ	*p* -value	n
2D $\Delta I_{sc\text{-}eq}$ (CCH)	AUC [Fsk] = 0.02	0.1103930	NA	0.7330893	6
	AUC [Fsk] = 0.128	-0.7220648	NA	0.1051370	6
	AUC [Fsk] = 0.8	NA	-0.6000000	0.8350831	6
	AUC [Fsk] = 5	-0.1798806	NA	0.2080000	6
2D ΔIsc-eq(IF)	AUC [Fsk] = 0.02	0.2121227	NA	0.6865882	6
	AUC [Fsk] = 0.128	-0.4459038	NA	0.3754739	6
	AUC [Fsk] = 0.8	NA	-0.7714286	0.0723965	6
	AUC [Fsk] = 5	-0.4740884	NA	0.3421455	6
2D $\Delta I_{sc\text{-}eq}$ (max)	AUC [Fsk] = 0.02	0.2434739	NA	0.6420057	6
	AUC [Fsk] = 0.128	-0.4495997	NA	0.3710414	6
	AUC [Fsk] = 0.8	NA	**-0.8285714**	**0.0415627**	6
	AUC [Fsk] = 5	-0.5056018	NA	0.3062217	6
2D $\Delta I_{sc\text{-}eq}$ (inh172)	AUC [Fsk] = 0.02	-0.1479237	NA	0.7797329	6
	AUC [Fsk] = 0.128	0.4704481	NA	0.3463880	6
	AUC [Fsk] = 0.8	NA	0.4857143	0.3287230	6
	AUC [Fsk] = 5	0.4325278	NA	0.3916671	6
2D $\Delta I_{sc\text{-}eq}$ (IF (661/770))	AUC 661/770 [Fsk] = 0.02	0.6813709	NA	0.2052722	5
	AUC 661/770 [Fsk] = 0.128	-0.3985623	NA	0.5063099	5
	AUC 661/770 [Fsk] = 0.8	-0.7951730	NA	0.1077953	5
	AUC 661/770 [Fsk] = 5	**-0.8825652**	NA	**0.0474490**	5

These results indicate that the cholinergic-mediated co-activated currents measured in the 2D-monolayers correlate well with the basal CFTR activity measured in the FIS assay at [Fsk] = 0.8 µM (Figure 4.28), in a negative trend meaning the more negative the current (i.e., more CFTR activity), more swelling is observed with basal CFTR activation.

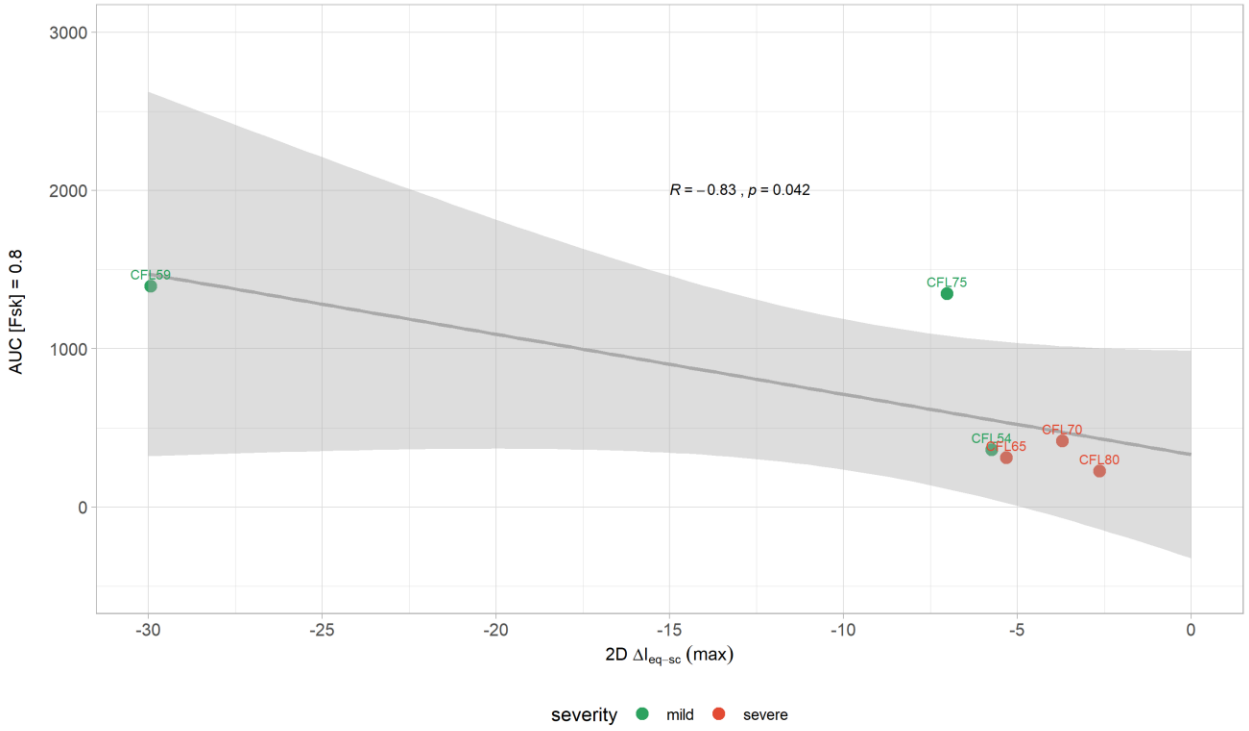

Figure 4.28 - Correlation between CCH-induced short circuit currents following IBMX/Fsk administration to 2D-monolayers and the AUC of organoid swelling at [Fsk] = 0.8 µM. Plot of 2D ΔI_{sc-eq} (max) (µA/cm^2) determined in *in vitro* Ussing chamber measurements of 2D-monolayers from individuals' 3D organoids and matched organoid swelling measurements in FIS assay expressed as AUC of organoid surface area increase (baseline = 100%, t = 60 min) for [Fsk] = 0.8 (Spearman ρ = -0.83, *p* –value = 0.042, n = 6). A degree of *CFTR* genotype severity was determined from previously proposed CF diagnosis from rectal biopsy analyzes as mild (green) and severe (red). Grey line represents the linear regression of data. Grey area represents de confidence interval of 95%.

For the drug tests in the 2D-monolayers, we could see a correlation between the effects of the combination VX-661/770 in monolayers stimulated with IF (100 µM, 0.8 µM) with the AUC of VX-661/770-treated organoid swelling at [Fsk] = 5 µM (Figure 4.29).

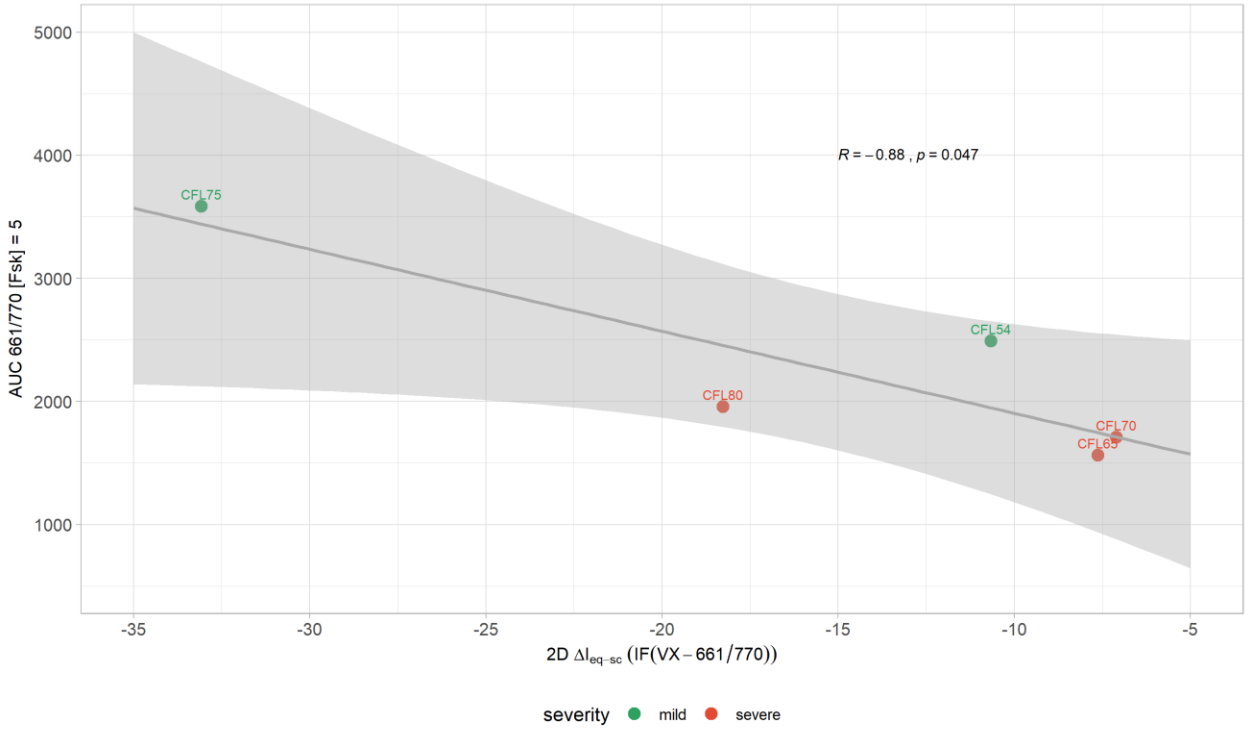

Figure 4.29 - Correlation between VX-770-induced short circuit currents following IBMX/Fsk in VX-661 treated 2D-monolayers and the AUC of VX-661/770-treated organoid swelling at [Fsk] = 5 µM. Plot of 2D $\Delta I_{sc\text{-}eq}$ (IF (DMSO)) (µA/cm^2) determined in *in vitro* Ussing chamber measurements of 2D-monolayers from individuals' 3D-organoids under IBMX/Fsk (100 µM, 0.8 µM) and matched organoid swelling measurements in FIS assay expressed as AUC of organoid surface area increase (baseline = 100%, t = 60 min) for [Fsk] = 0.128 (Pearson r = -0.88, p –value = 0.047, n = 5). A degree of *CFTR* genotype severity was determined from previously proposed CF diagnosis from rectal biopsy analyzes as mild (green) and severe (red). Grey line represents the linear regression of data. Grey area represents de confidence interval of 95%.

Overall, these results show that there are good correlations between the 2D- and the 3D-models for measurements of both basal CFTR activity and CFTR function rescue with approved CFTR modulators. So, in the future, there is a possibility to use these 2D-monolayers as a complement to the FIS assay in the prediction of individual-specific drug response.

4.5.3 Correlations between Different CFTR Function Parameters Measured in the 2D Monolayers with Clinical Data and Established CF Biomarkers

In order to assess if the 2D-model in study could be used to predict disease severity, correlation analyses were established between the short circuit-currents measured in the 2D-intestinal monolayers in the Ussing chamber and matched to the individual clinical data and values from other established CF biomarkers. Correlations were found between FEE vs 2D $\Delta Is_{c\text{-}eq}$(IF) (p<0.05) and between FEE vs 2D $\Delta I_{sc\text{-}eq}$ (max) (p<0.01), being the last one the strongest and most significant.

Table 4.6 – Correlation data between the activated short circuit currents measured in the 2D monolayers and the individuals' clinical data. Parameter 1 refers to the Sweat [Cl^-] (mmol/L), fecal elastase E1 (FEE, µg/g stool and forced expiratory volume in 1 sec (FEV_1, %). Parameter 2 refers to the activated short circuit currents measured in 2D monolayers in response to CCH (2D $\Delta I_{sc\text{-}eq}$ (CCH)), IBMX/Fsk (2D ΔIsc-eq(IF)), the sum of the last two currents (2D $\Delta I_{sc\text{-}eq}$ (max)), inh172 addition after the last response (2D $\Delta I_{sc\text{-}eq}$ (inh172)) and IF addition in the control DMSO monolayers. Pearson correlation coefficients (*r)*, Spearman correlation coefficients (ρ), respective *p* –value and sample number (n) are denoted. Significant *p* – values are highlighted in bold. NA – Not Aplicable

Parameter 1	Parameter 2	Pearson *r*	Spearman ρ	*p* -value	n
[Sweat Cl^-]	2D $\Delta I_{sc\text{-}eq}$(CCH)	0.2619717	NA	0.5703656	7
	2D $\Delta I_{sc\text{-}eq}$(IF)	NA	0.3571429	0.4316114	7
	2D $\Delta I_{sc\text{-}eq}$ (max)	NA	0.4285714	0.3373683	7
	2D $\Delta I_{sc\text{-}eq}$ (inh172)	NA	-0.2142857	0.6445116	7
FEE	2D $\Delta I_{sc\text{-}eq}$(CCH)	0.1315618	NA	0.7785816	7
	2D $\Delta I_{sc\text{-}eq}$(IF)	NA	**-0.7671932**	**0.0441075**	7
	2D $\Delta I_{sc\text{-}eq}$ (max)	NA	**-0.8794654**	**0.0090698**	7
	2D $\Delta I_{sc\text{-}eq}$ (inh172)	NA	0.6923451	0.0847243	7
FEV_1	2D $\Delta I_{sc\text{-}eq}$(CCH)	-0.2458050	NA	0.5951997	7
	2D $\Delta I_{sc\text{-}eq}$(IF)	NA	-0.4285714	0.3373683	7
	2D $\Delta I_{sc\text{-}eq}$ (max)	NA	-0.3928571	0.3833169	7
	2D $\Delta I_{sc\text{-}eq}$ (inh172)	NA	0.1071429	0.8191509	7

With these correlation analyses, the results show that the cAMP-activated currents and cholinergic co-activated currents measured in the 2D-monolayers could be good predictors of the individual's pancreatic status (Figure 4.30). The other clinical parameters did not produce significant correlations. However, to be sure about this lack of correlation an increased sample size would be needed.

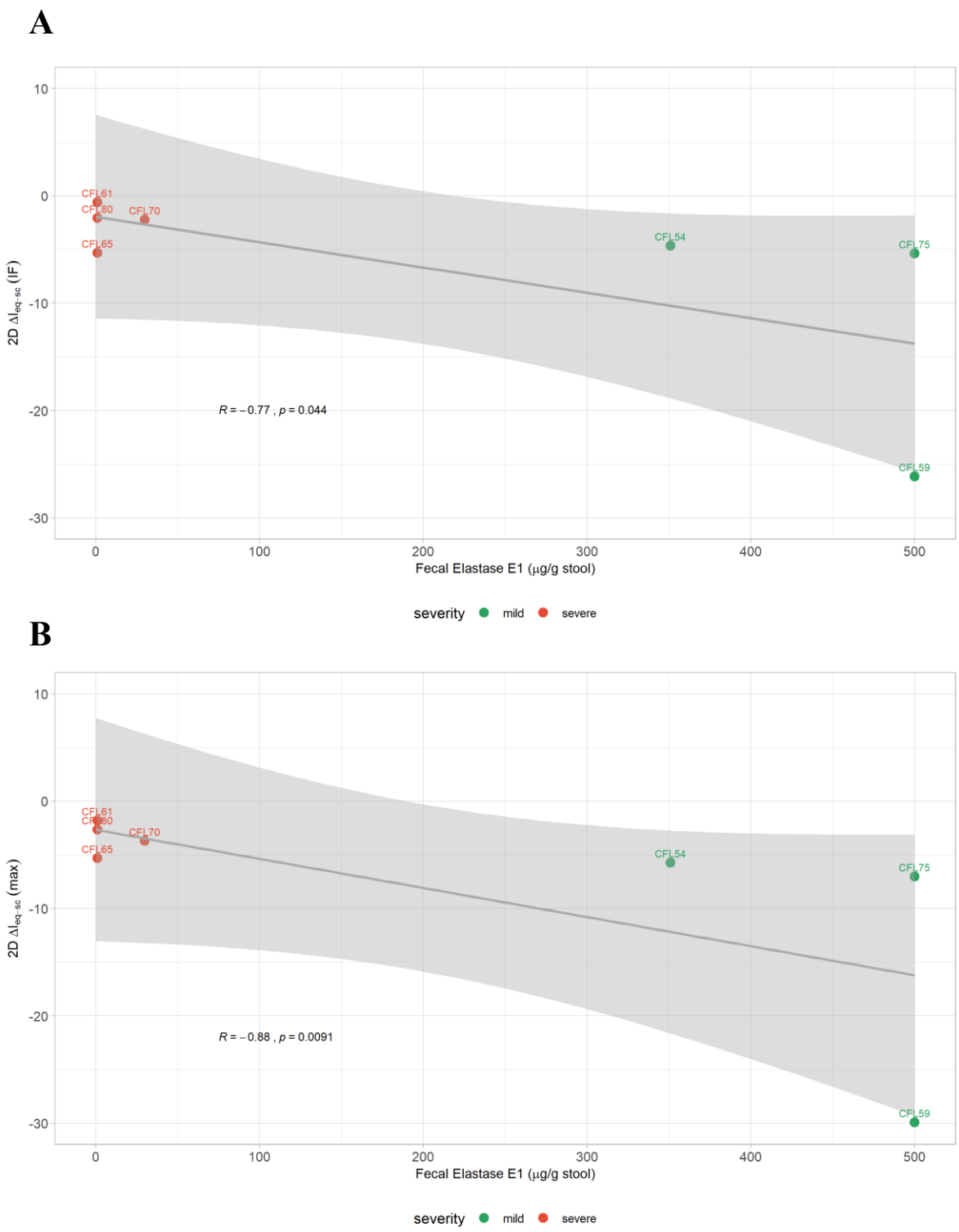

Figure 4.30 – Correlation among IBMX/Fsk-induced short circuit currents and CCH-induced short circuit current following IBMX/Fsk, and individuals' FEE values. Plot of the individuals' FEE measurements (µg/ g stool) and: **(A)** 2D ΔIsc-eq(IF) determined in Ussing chamber measurements of 2D monolayers under CCH (100 µM) following IBMX/Fsk stimulation (100 µM, 2 µM) (Spearman ρ = -0.88, *p* –value = 0.0091, n = 7); **(B)** 2D $\Delta I_{sc\text{-}eq}$ (max) determined in Ussing chamber measurements of 2D monolayers under IBMX/Fsk (100µM, 2 µM) (Spearman ρ = -0.77, *p* –value = 0.044, n = 7). A degree of *CFTR* genotype severity was determined from previously proposed CF diagnosis from rectal biopsy analyzes as mild (green) and severe (red). Grey line represents the linear regression of data. Grey area represents the 95% confidence interval.

5. Conclusion and Future Perspectives

In this MSc project, we explored a new and exciting *ex vivo* model that consists in growing 2D-monolayers of intestinal epithelial cells derived from 3D-intestinal organoids of individuals with CF and healthy non-CF controls. This is a versatile model, since it can remain in culture as a monolayer of undifferentiated stem cells or can be differentiated into several cell types of the colon epithelium. By assessing the differentiation process, we could conclude that these cells differentiate in a very short time, just 6 days in culture. However, the differentiation process results in a severe reduction of CFTR protein levels. Measuring the basal activity in wt/wt 2D-monolayers, we observed that cAMP-stimulated CFTR-mediated Cl^- secretion was diminished in differentiated monolayers. This means that, unexpectedly, the undifferentiated cells are the ones that have the higher capability to secrete CFTR-mediated Cl^- and fluid. Thus, for CFTR function studies using 2D-intestinal monolayers, the undifferentiated monolayers were used in subsequent studies to compare these cells with the rectal biopsies and the 3D-organoids, which are more established models to study CFTR function.

With the 3D-intestinal organoid model, CFTR function and rescue of function with approved modulators can be assessed by measuring the amount of organoid swelling when cAMP is increased, by using the so called FIS assay. The 2D-monolayers, for instance, can be used for the same CFTR function assay but, in this case, bioelectrical measurements are used resorting to micro-Ussing chambers. Therefore, CFTR functional rescue with the already approved modulators can be assessed through transepithelial electrical current measurements of Cl^- secretion, being a more direct and sensitive approach than the measurement of fluid secretion to the lumen of the organoids. Indeed, we could conclude that there was rescue of CFTR function with approved modulator drugs in materials from 4 out of 7 individuals with CF analyzed, which should be an incentive to expand this assay to more individuals with CF bearing different mutations.

A method to complement CF diagnosis and to measure basal CFTR activity in fresh tissue which is already implemented in specialized labs is the diagnosis protocol using rectal biopsies. In this assay, Cl^- secretion is evaluated through bioelectrical measures in micro-Ussing chambers of fresh rectal biopsies from individual with CF. This assay has its limitations, such as a short time limit (<6h) to perform the assay before the biopsies are degraded and the fact that not every biopsy has enough quality to generate electrical responses in the Ussing chamber. However, there is a high success rate for the generation of intestinal 3D-organoids from the biopsy even 24h post-collection. Thus, 2D-intestinal monolayers can be grown from these intestinal 3D-organoids and be used to perform the same basal CFTR activity measurements in the fresh biopsies in the Ussing chamber.

Correlation analyses between CFTR function parameters measured in the 2D-monolayers, with the ones measured in the 3D-organoids and fresh tissue showed that these are in fact well correlated. We observed that the 2D-monolayers can predict the maximal activation of CFTR function in the rectal biopsies, making the 2D-model a good one to replace or complement the rectal biopsy assay for diagnosis/prognosis of CF. Moreover, the basal CFTR activity measured in the 3D-organoids with the FIS assay also correlates with basal CFTR activity measurements in the 2D-models. Additionally, Ussing chamber measurements of CFTR function rescue with the combination VX-661/770 in 2D-monolayers correlate well with the FIS assay of matched individuals' 3D organoids with the same treatment. This is

very important since 2D-monolayers can, thus, be used to complement individual-specific drug response measured with the FIS assay. Accordingly, we can use the 2D-model to deliver a personalized medicine/theranostics approach to provide each individual with CF with the right drug. Lastly, to assess the relevance of the 2D-model in predicting clinical outcomes, correlations with clinical parameters and other established CF biomarkers were established. It was found that CFTR function parameters measured in the 2D-monolayers correlate significantly with FEE values of the individuals with CF studied here, thus making the 2D-monolayers a possible good model to predict disease severity, i.e. CF prognosis. Overall, the results can be perceived as an incentive for the further study of these 2D-monolayers and their use in the CF field. For this purpose, the numbers of samples from individual with CF should be increased, so as to establish better correlations to further validate this 2D-model for the assessment of CFTR function and assist in providing a personalized therapy for all individuals with CF.

6. References

1. De Boeck, K. & Amaral, M. D. Progress in therapies for cystic fibrosis. *Lancet Respir. Med.* **4**, 662–674 (2016).
2. Bell, S. C., Boeck, K. De & Amaral, M. D. Pharmacology & Therapeutics New pharmacological approaches for cystic fibrosis : Promises, progress, pitfalls. *Pharmacol. Ther.* **145**, 19–34 (2015).
3. ECFS Patient Registry Annual Data Report. (2014).
4. Riordan, J. R. CFTR Function and Prospects for Therapy. *Annu. Rev. Biochem.* **77**, 701–727 (2008).
5. Cohen, T. S. & Prince, A. Cystic fibrosis: a mucosal immunodeficiency syndrome. *Nat Med* **18**, 509–519 (2013).
6. Riordan, J. R. *et al.* Identification the Cystic Fibrosis Gene : Cloning and Characterization of Complementary DNA. *Science.* **245**, 1066–1073 (1989).
7. Fernandez, E. F. *et al.* CFTR dysfunction in cystic fibrosis and chronic obstructive pulmonary disease. *Expert Rev. Respir. Med.* (2018).
8. Cantin, A. M., Hartl, D., Konstan, M. W. & Chmiel, J. F. Inflammation in cystic fibrosis lung disease : Pathogenesis and therapy. *J. Cyst. Fibros.* **14**, 419–430 (2015).
9. Reddy, M. M., Light, M. J. & Quinton, P. M. Activation of the epithelial Na+ channel (ENaC) requires CFTR Cl- channel function. *Nature* **402**, 301–304 (1999).
10. Stoltz, D. A. *et al.* Origins of Cystic Fibrosis Lung Disease. *N Engl J Med* **372**, 351–362 (2015).
11. Button, B. *et al.* Periciliary Brush Promotes the Lung Health by Separating the Mucus Layer from Airway Epithelia. *Science.* **337**, 937–941 (2012).
12. Henderson, A. G. *et al.* Cystic fibrosis airway secretions exhibit mucin hyperconcentration and increased osmotic pressure. *J Clin Invest* **125**, 3047–3060 (2014).
13. Collawn, J. F. & Matalon, S. CFTR and lung homeostasis. *Am J Physiol Lung Cell Mol Physiol* **307**, 1917–1923 (2014).
14. Quinton, P. M. Cystic fibrosis : impaired bicarbonate secretion and mucoviscidosis. *Lancet* **372**, 415–417 (2008).
15. Quinton, P. M. Role of epithelial HCO3- transport in mucin secretion : lessons from cystic fibrosis. *Am J Physiol Cell Physiol* **299**, 1222–1233 (2010).
16. Hoegger, M. J. *et al.* Impaired Mucus Detachment Disrupts Mucociliary Transport in a Piglet Model of Cystic Fibrosis. *Science.* **345**, 818–822 (2014).
17. Tang, X. X. *et al.* Acidic pH increases airway surface liquid viscosity in cystic fibrosis. *J Clin Invest* **126**, 879–891 (2016).
18. Keiser, N. W. *et al.* Defective Innate Immunity and Hyperinflammation in Newborn Cystic Fibrosis Transmembrane Conductance Regulator-Knockout Ferret Lungs. *Am J Respir Cell Mol Biol* **52**, 683–694 (2015).
19. Gaspar, M. C., Couet, W. & Olivier, J. Pseudomonas aeruginosa infection in cystic fibrosis lung disease and new perspectives of treatment : a review. *Eur J Clin Microbiol Infect Dis* **32**, 1231–1252 (2013).
20. Hug, M. J., Tamada, T. & Bridges, R. J. CFTR and Bicarbonate Secretion to Epithelial Cells. *News Physiol Sci* **12**, 38–42 (2003).
21. Zhan, X., Wang, F., Bi, Y. & Ji, B. Animal models of gastrointestinal and liver diseases. Animal models of acute and chronic pancreatitis. *Am J Physiol Gastrointest Liver Physiol* **311**, 343–355 (2016).
22. Haller, W. *et al.* Cystic fibrosis: An update for clinicians. Part 1: Nutrition and gastrointestinal complications. *J. Gastroenterol. Hepathology* **29**, 1344–1355 (2014).
23. Ledder, O., Haller, W., Couper, R. T. L., Lewindon, P. & Oliver, M. Cystic fibrosis : An update for clinicians. Part 2: Hepatobiliary and pancreatic manifestations. *J. Gastroenterol. Hepathology* **29**, 1954–1962 (2014).

24. Somaraju, U. R. & Solis-Moya, A. Pancreatic enzyme replacement therapy for people with cystic fibrosis (Review). *Cochrane Database Syst. Rev.* (2014).
25. Lisle, R. C. De & Borowitz, D. The Cystic Fibrosis Intestine. *Cold Spring Harb Perspect Med* **3**, (2013).
26. Courtney, J. M. *et al.* Predictors of Mortality in Adults With Cystic Fibrosis. *Pediatr. Pulmonol.* **42**, 525–532 (2007).
27. Stallings, V. A., Stark, L. J., Robinson, K. A., Feranchak, A. P. & Quinton, H. Evidence-Based Practice Recommendations for Nutrition-Related Management of Children and Adults with Cystic Fibrosis and Pancreatic Insufficiency: Results of a Systematic Review. *Am J Diet Assoc* **108**, 832–839 (2008).
28. Andersen, D. H. Cystic Fibrosis of the Pancreas and its Relation to Celiac Disease. *Prog. Pediatr.* (1938).
29. Dodge, J. A., Lewis, P. A., Stanton, M. & Wilsher, J. Cystic fibrosis mortality and survival in the UK: 1947–2003. *Eur. Respir. J.* 522–526 (2006).
30. Dean, M. & Allikmets, R. Complete Characterization of the Human ABC Gene Family. *J. Bioenerg. Biomembr.* **33**, 475–479 (2001).
31. Gadsby, D. C., Vergani, P. & Csanády, L. The ABC protein turned chloride channel whose failure causes cystic fibrosis. *Nature* **440**, 447–483 (2006).
32. Liu, F., Zhang, Z., Gadsby, D. C. & Chen, J. Molecular Structure of the Human CFTR Ion Channel. *Cell* **169**, 85–95 (2017).
33. Cheng, S. I. *et al.* Phosphorylation of the R Domain by CAMP-Dependent Protein Kinase Regulates the CFTR Chloride Channel. *Cell* **66**, 1027–1036 (1991).
34. Hunt, J. F., Wang, C. & Ford, R. C. Cystic Fibrosis Transmembrane Conductance Regulator (ABCC7) Structure. *Cold Spring Harb Perspect Med* **3**, (2012).
35. Cant, N., Pollock, N. & Ford, R. C. CFTR structure and cystic fibrosis. *Int. J. Biochem. Cell Biol.* **52**, 15–25 (2014).
36. Csanády, L. *et al.* Severed Channels Probe Regulation of Gating of Cystic Fibrosis Transmembrane Conductance Regulator by Its Cytoplasmic Domains. *J. Gen. Physiol.* **116**, 477–500 (2000).
37. Li, C. *et al.* ATPase Activity of the Cystic Fibrosis Transmembrane Conductance Regulator. *J. Biol. Chem.* **271**, 28463–28468 (1996).
38. Lu, Y. *et al.* Co- and Posttranslational Translocation Mechanisms Direct Cystic Fibrosis Transmembrane Conductance Regulator N Terminus Transmembrane Assembly. *J. Biol. Chem.* **273**, 568–576 (1998).
39. Jensen, T. J. *et al.* Multiple Proteolytic Systems, Including the Proteasome, Contribute to CFTR Processing. *Cell* **83**, 129–135 (1995).
40. Pindsgr, S., Riordansbii, J. R. & Williamsss, D. B. Participation of the Endoplasmic Reticulum Chaperone Calnexin (p88, IP90) in the Biogenesis of the Cystic Fibrosis Transmembrane Conductance Regulator. *J. Biol. Chem.* **269**, 12784–12788 (1994).
41. Gentzsch, M. *et al.* Endocytic Trafficking Routes of Wild Type and ⌬F508 Cystic FIbrosis Transmembrane Conductance Regulator. *Mol. Biol. Cell* **15**, 2684–2696 (2004).
42. Kopito, R. O. N. R. Biosynthesis and Degradation of CFTR. *Physiol. Rev.* **79**, 167–173 (1999).
43. Ramsey, B. W. . et al. A CFTR Potentiator in Patients with Cystic Fibrosis and the G551D Mutation. *N. Engl. J. Med.* **365**, 1663–1672 (2011).
44. Boeck, K. De *et al.* Efficacy and safety of ivacaftor in patients with cystic fibrosis and a non-G551D gating mutation. *J. Cyst. Fibros.* **13**, 674–680 (2014).
45. Goor, F. Van, Yu, H., Burton, B. & Hoffman, B. J. Effect of ivacaftor on CFTR forms with missense mutations associated with defects in protein processing or function. *J. Cyst. Fibros.* **13**, 29–36 (2014).
46. Wainright, C. E. *et al.* Lumacaftor–Ivacaftor in Patients with Cystic Fibrosis Homozygous for

Phe508del. *N. Engl. J. Med.* **373**, 220–231 (2015).
47. Taylor-Cousar, J. L. *et al.* Tezacaftor-Ivacaftor in Patients with Cystic Fibrosis Homozygous for Phe508del. *N. Engl. J. Med.* **377**, 2013–2023 (2017).
48. Sala, M. & Jain, M. Tezacaftor for the treatment of cystic fibrosis. *Expert Rev. Respir. Med.* (2018).
49. Rowe, S. M. *et al.* Tezacaftor–Ivacaftor in Residual-Function Heterozygotes with Cystic Fibrosis. *N. Engl. J. Med.* **377**, 2024–2035 (2017).
50. Larson, J. E. *et al.* CFTR modulates lung secretory cell proliferation and differentiation. *Am. J. Physiol. - Lung Cell. Mol. Physiol.* **279**, 333–341 (2000).
51. Hajj, R., Lesimple, P., Birembaut, P., Puchelle, E. & Coraux, C. Human airway surface epithelial regeneration is delayed and abnormal in cystic fibrosis. *J Pathol* **211**, 340–350 (2007).
52. Lesimple, P., Liao, J., Robert, R., Gruenert, D. C. & Hanrahan, J. W. Cystic fibrosis transmembrane conductance regulator trafficking modulates the barrier function of airway epithelial cell monolayers. *J Physiol* **588**, 1195–1209 (2010).
53. Ruan, Y. C. *et al.* CFTR interacts with ZO-1 to regulate tight junction assembly and epithelial differentiation through the ZONAB pathway. *J. Cell Sci.* **127**, 4396–4408 (2014).
54. Molina, X. S. A. *et al.* Junctional abnormalities in human airway epithelial cells expressing F508del CFTR. *Am J Physiol Lung Cell Mol Physiol* **309**, 475–487 (2015).
55. Puchelle, E., Zahm, J.-M., Tournier, J.-M. & Coraux, C. Airway Epithelial Repair, Regeneration, and Remodeling after Injury in Chronic Obstructive Pulmonary Disease. *Proc. Am. Thorac. Soc.* **3**, 726–733 (2006).
56. Willis, B. C. & Borok, Z. TGF-β -induced EMT : mechanisms and implications for fibrotic lung disease. *Am J Physiol Lung Cell Mol Physiol* **293**, 525–534 (2007).
57. Rout-pitt, N., Farrow, N., Parsons, D. & Donnelley, M. Epithelial mesenchymal transition (EMT): a universal process in lung diseases with implications for cystic fibrosis pathophysiology. *Respir. Res.* **19**, 1–10 (2018).
58. Accurso, F. J. *et al.* Sweat Chloride as a Biomarker of CFTR Activity: Proof of Concept and Ivacaftor Clinical Trial Data. *J. Cyst. Fibros.* **13**, 139–147 (2014).
59. Wallis, C., Frcpch, M. & Dch, F. C. P. *50 - Diagnosis and Presentation of Cystic Fibrosis*. *Kendig's Disorders of the Respiratory Tract in Children* (Elsevier Inc., 2019).
60. Langen, A. V., Dompeling, E., Loeber, G. & Dankert-roelse, J. Clinical evaluation of the Nanoduct sweat test system in the diagnosis of cystic fibrosis after newborn screening. *Eur. J. Pediatr.* **174**, 1025–1034 (2015).
61. Farrell, P. M. *et al.* Diagnosis of Cystic Fibrosis: Consensus Guidelines from the Cystic Fibrosis Foundation. *J. Pediatr.* **181**, S4–S16 (2017).
62. De Boeck, K. *et al.* Cystic fibrosis : terminology and diagnostic algorithms. *Thorax* **61**, 627–635 (2006).
63. Sermet-gaudelus, I. *et al.* Clinical Phenotype and Genotype of Children with Borderline Sweat Test and Abnormal Nasal Epithelial Chloride Transport. *Am J Respir Crit Care Med* **182**, 929–936 (2010).
64. Mastella, G., Cesare, G. Di, Borruso, A., Menin, L. & Zanolla, L. Reliability of sweat-testing by the Macroduct collection method combined with conductivity analysis in comparison with the classic Gibson and Cooke technique. *Acta Pediatr.* **89**, 933–937 (2000).
65. Middleton, P. G., Geddes, D. M. & Alton, E. W. F. W. Protocols for in vivo measurement of the ion transport defects in cystic fibrosis nasal epithelium. *Eur. Respir. J.* **7**, 2050–2056 (1994).
66. Schu, D. *et al.* Basic protocol for transepithelial nasal potential difference measurements. *J. Cyst. Fibros.* **3**, 151–155 (2004).
67. Standaert, T. A. *et al.* Standardized Procedure for Measurement of Nasal Potential Difference: An Outcome Measure in Multicenter Cystic Fibrosis Clinical Trials. *Pediactric Pulmonol.* **37**, 389–392 (2004).
68. Castellani, C. *et al.* European best practice guidelines for cystic fibrosis neonatal screening. *J. Cyst.*

Fibros. **8**, 153–173 (2009).
69. Crossley, R., Smith, P. A., Edgar, B. W., Gluckman, P. D. & Elliott, R. B. Neonatal screening for cystic fibrosis, using immunoreactive trypsin assay in dried blood spots. *Clin. Chim. Acta* **113**, 111–121 (1981).
70. Sontag, M. K., Lee, R., Bs, D. W., Freedenberg, D. & Sagel, S. D. Improving the Sensitivity and Positive Predictive Value in a Cystic Fibrosis Newborn Screening Program Using a Repeat Immunoreactive Trypsinogen and Genetic Analysis. *J. Pediatr.* **175**, 150–158 (2016).
71. Kay, D. M. *et al.* Screening for cystic fibrosis in New York State: considerations for algorithm improvements. *Eur. J. Pediatr.* **175**, 181–193 (2016).
72. Borowitz, D. *et al.* Cystic Fibrosis Foundation Practice Guidelines for the Management of Infants with Cystic Fibrosis Transmembrane Conductance Regulator-Related Metabolic Syndrome during the First Two Years of Life and Beyond. *J. Pediatr.* **155**, 106–116 (2009).
73. Mall, M., Hirtz, S., Gonska, T. & Kunzelmann, K. Assessment of CFTR function in rectal biopsies for the diagnosis of cystic fibrosis. *J. Cyst. Fibros.* **3**, 165–169 (2004).
74. Hirtz, S. *et al.* CFTR Cl-channel function in native human colon correlates with the genotype and phenotype in cystic fibrosis. *Gastroenterology* **127**, 1085–1095 (2004).
75. Sousa, M. *et al.* Measurements of CFTR-Mediated Cl-Secretion in Human Rectal Biopsies Constitute a Robust Biomarker for Cystic Fibrosis Diagnosis and Prognosis. *PLoS One* **7**, e47708 (2012).
76. Fulcher, M. L. & Randell, S. H. Human nasal and tracheo-bronchial respiratory epihelial cell culture. *Methods Mol. Biol.* **945**, 109–121 (2013).
77. Awatade, N. T. *et al.* Measurements of Functional Responses in Human Primary Lung Cells as a Basis for Personalized Therapy for Cystic Fibrosis. *EBioMedicine* **2**, 147–153 (2015).
78. Pranke, I. M. *et al.* Correction of CFTR function in nasal epithelial cells from cystic fibrosis patients predicts improvement of respiratory function by CFTR modulators. *Sci. Rep.* **7**, 1–11 (2017).
79. Guimbellot, J. S. *et al.* Nasospheroids permit measurements of CFTR-dependent fluid transport. *JCI Insight* **2**, 1–11 (2017).
80. Brewington, J. J. *et al.* Detection of CFTR function and modulation in primary human nasal cell spheroids. *J. Cyst. Fibros.* (2017).
81. Dekkers, J. F. *et al.* A functional CFTR assay using primary cystic fibrosis intestinal organoids. *Nat. Med.* **19**, 939–945 (2013).
82. Barker, N. *et al.* Identification of stem cells in small intestine and colon by marker gene Lgr5. *Nature* **449**, 1003–1008 (2007).
83. Field, M. Intestinal ion transport and the pathophysiology of diarrhea. *JCI* **111**, 931–943 (2003).
84. Dekkers, J. F., van der Ent, C. K. & Beekman, J. M. Novel opportunities for CFTR-targeting drug development using organoids. *Rare Dis.* **1**, e27112 (2013).
85. Dekkers, J. F. *et al.* Potentiator synergy in rectal organoids carrying S1251N , G551D , or F508del CFTR mutations. *J. Cyst. Fibros.* **15**, 568–578 (2016).
86. Dekkers, J. F. *et al.* Optimal correction of distinct CFTR folding mutants in rectal cystic fibrosis organoids. *Eur. Respir. J.* **48**, 451–458 (2016).
87. Dekkers, J. F. *et al.* Characterizing responses to CFTR-modulating drugs using rectal organoids derived from subjects with cystic fibrosis. *Sci. Transl. Med.* **8**, 344ra84 (2016).
88. Paul, J. *et al.* CFTR modulator theratyping: Current status, gaps and future directions. *J. Cyst. Fibros.* **18**, 22–34 (2019).
89. Zomer-van Ommen, D. D. *et al.* Comparison of ex vivo and in vitro intestinal cystic fibrosis models to measure CFTR-dependent ion channel activity. *J. Cyst. Fibros.* **17**, 316–324 (2018).
90. Sato, T., Stange, D. E., Ferrante, M., Vries, R. G. J. & Es, J. H. V. A. N. Long-term Expansion of Epithelial Organoids From Human Colon, Adenoma, Adenocarcinoma, and Barrett's Epithelium. *Gastroenterology* **141**, 1762–1772 (2011).
91. Stewart, A. P., Haerteis, S., Diakov, A., Korbmacher, C. & Edwardson, J. M. Atomic Force

Microscopy Reveals the Architecture of the Epithelial Sodium Channel (ENaC). *J. Biol. Chem.* **286**, 31944–31952 (2011).
92. Stokes, J. B., Sigmund, R. D., John, B. & Sigmund, R. D. Regulation of rENaC mRNA by dietary NaCl and steroids: organ, tissue, and steroid heterogeneity. *Am J Physiol* **274**, 1699–1707 (1998).
93. Frizzell, R. A. & Hanrahan, J. W. Physiology of Epithelial Chloride and Fluid Secretion. *Cold Spring Harb Perspect Med* **2**, 1–20 (2012).
94. Dharmsathaphorn, K. & Pandol, S. J. Mechanism of chloride secretion induced by carbachol in a colonic epithelial cell line. *J Clin Invest* **77**, 348–354 (1986).
95. Lomax, R. B., Warhurst, G. & Sandle, G. I. Characteristics of two basolateral potassium channel populations in human colonic crypts. *Gut* **38**, 243–247 (1996).
96. Sandle, G. I. *et al.* Altered cryptal expression of luminal potassium (BK) channels in ulcerative colitis. *J Pathol* **212**, 66–73 (2007).
97. Chang, M. *et al.* Slc26a9 Is Inhibited by the R-region of the Cystic Fibrosis Transmembrane Conductance Regulator via the STAS Domain. *J. Biol. Chem.* **284**, 28306–28318 (2009).
98. Bertrand, C. A., Zhang, R., Pilewski, J. M. & Frizzell, R. A. SLC26A9 is a constitutively active , CFTR-regulated anion conductance in human bronchial epithelia. *J. Gen. Physiol.* **133**, 421–438 (2009).
99. Miller, M. R. *et al.* Variants in Solute Carrier SLC26A9 Modify Prenatal Exocrine Pancreatic Damage in Cystic Fibrosis. *J. Pediatr.* **166**, 1152–1157 (2015).
100. Sun, L. *et al.* Multiple apical plasma membrane constituents are associated with susceptibility to meconium ileus in individuals with cystic fibrosis. *Nat. Genet.* **44**, 562–569 (2012).
101. Ko, S. B. H. *et al.* A molecular mechanism for aberrant CFTR-dependent HCO3- transport in cystic fibrosis. *EMBO J.* **21**, 5662–5672 (2002).
102. Alimperti, S. & Andreadis, S. T. CDH2 and CDH11 as Regulators of Stem Cell Fate Decisions. *Stem Cell Res.* **14**, 270–282 (2015).
103. Toi, M., Elisa, M. & Elisa, M. Detection of epithelial cell death in the body by cytokeratin 18 measurement. *Biomed. Pharmacother.* **59**, 359–362 (2005).
104. Gerdes, J., Schwab, U., Lemke, H. & Stein, H. Production of a mouse monoclonal antibody reactive with a human nuclear antigen associated with cell proliferation. *Int. J. Cancer* **31**, 13–20 (1983).
105. Gerdes, J. *et al.* Cell cycle analysis of a cell proliferation-associated human nuclear antigen defined by the monoclonal antibody Ki-67. *J. Immunol.* **133**, 1710–1715 (1984).
106. Farinha, C. M. *et al.* Biochemical methods to assess CFTR expression and membrane localization. *J. Cyst. Fibros.* **3**, 73–77 (2004).
107. Doucet, L. *et al.* Applicability of Different Antibodies for the Immunohistochemical Localization of CFTR In Respiratory and Intestinal Tissues of Human and Murine Origin. *J. Histochem. Cytochem.* **51**, 1191–1199 (2003).
108. Jakab, R. L., Collaco, A. M. & Ameen, N. A. Physiological relevance of cell-specific distribution patterns of CFTR, NKCC1, NBCe1, and NHE3 along the crypt-villus axis in the intestine. *Am J Physiol Gastrointest Liver Physiol* **300**, 82–98 (2011).
109. Rogers, C. S. *et al.* Disruption of the CFTR Gene Produces a Model of Cystic Fibrosis in Newborn Pigs. *Science.* **321**, 1837–1841 (2008).
110. Odes, H. S. *et al.* Cystic fibrosis transmembrane conductance regulator and Na + channel subunits mRNA transcripts , and Cl - efflux , show a different distribution in rat duodenum and colon. *Acta Physiol Scand* **178**, 231–240 (2003).
111. Hong, J. H., Park, S., Shcheynikov, N. & Muallem, S. Mechanism and synergism in epithelial fluid and electrolyte secretion. *Pflugers Arch - Eur J Physiol* **466**, 1487–1499 (2014).
112. Rajendran, V. M., Schulzke, J. & Seidler, U. E. *Ion Channels of the Gastrointestinal Epithelial Cells*. *Physiology of the Gastrointestinal Tract* (Elsevier Inc., 2018).
113. Melis, N. *et al.* Revisiting CFTR inhibition: a comparative study of CFTRinh -172 and GlyH-101 inhibitors. *Br. J. Pharmacol.* **171**, 3716–3727 (2014).

114. Sheppard, D. N. *et al.* Mutations inf CFTR associated with mild-disease-form Cl- channels with altered pore properties. *Nature* **362**, 160–164 (1993).
115. Willigen, M. Van *et al.* Folding – function relationship of the most common cystic fibrosis – causing CFTR conductance mutants. *Life Sci. Alliance* **2**, 1–14 (2019).
116. Meng, X., Clews, J., Kargas, V., Wang, X. & Ford, R. C. The cystic fibrosis transmembrane conductance regulator (CFTR) and its stability. *Cell. Mol. Life Sci.* **74**, 23–38 (2017).
117. Hamosh, A., Rosenstein, B. J. & Cutting, G. R. CFTR nonsense mutations G542X and W1282X associated with severe reduction of CFTR mRNA in nasal epithelial cells. *Hum. Mol. Genet.* **1**, 542–544 (1992).
118. Xue, X. *et al.* Identification of the amino acids inserted during suppression of CFTR nonsense mutations and determination of their functional consequences. *Hum. Mol. Genet.* **26**, 3116–3129 (2017).
119. Leubitz, A., Frydman-marom, A., Sharpe, N., Duzer, J. Van & Campbell, K. C. M. Safety, Tolerability and Pharmacokinetics of Single Ascending Doses of ELX-02, a Potential Treatment for Genetic Disorders Caused by Nonsense Mutations, in Healthy Volunteers. *Clin. Pharmacol. Drug Dev.* (2019). doi:10.1002/cpdd.647
120. Mendes, F. *et al.* Unusually common cystic fibrosis mutation in Portugal encodes a misprocessed protein. *Biochem. Byophysical Res. Commun.* **311**, 665–671 (2003).
121. Wang, Y. *et al.* CFTR potentiators partially restore channel function to A561E-CFTR , a cystic fibrosis mutant with a similar mechanism of dysfunction as F508del-CFTR. *Br. J. Pharmacol.* **171**, 4490–4503 (2014).